ENDOCYTIC RECYCLING IN *CAENORHABDITIS ELEGANS*

by

ADENRELE MADELINE GLEASON

A dissertation submitted to the

Graduate School-New Brunswick

Rutgers, The State University of New Jersey

and

The Graduate School of Biomedical Sciences

In partial fulfillment of the requirements

For a degree of

Doctor of Philosophy

Graduate Program in Cell and Developmental Biology

Written under the direction of

Barth D. Grant

And approved by

_____

_____

_____

_____

New Brunswick, New Jersey

OCTOBER 2016

ABSTRACT OF THE DISSERTATION

Endocytic Recycling in *Caenorhabditis Elegans*

By ADENRELE MADELINE GLEASON

Dissertation Director

Dr. Barth D. Grant

The power of conservation is exemplified in the *C. elegans* intestinal epithelia. As a model to study endocytic recycling, molecular transport regulators have been characterized in this genetically tractable system. In this dissertation, I describe the molecular requirements for Syndpin/SDPN-1 *in vivo.* Proteoliposome assays confirm that full-length SDPN-1 is capable of tubulating acidic liposomes in vitro. As a likely accessory protein, SDPN-1 coordinates the exit of recycling cargo from the early endosome. I propose that Syndapin/SDPN-1 facilitates this transport step through the localized recruitment of actin to early endosomes. In addition, the worm intestine provides a lucid understanding of the endosomal determinates that coordinate TGFβ signaling. We report TGFβ signaling and internalization require Clathrin-Dependent Endocytosis (CDE). Furthermore, post internalization of the receptors result in the sorting of the type I and the type II receptors into distinct molecular sorting complexes. Mutants defective in retromer-dependent recycling missort their type I SMA-6 to the

lysosome and impair signaling. Alternatively, the type II receptor, DAF-4 (dauer formation defective-4) is returned through the ARF-6 (ADP-ribosylation factor-6) dependent recycling pathway.

ACKNOWLEDGEMENTS

I would first like to thank my thesis advisor Barth D. Grant whose mentorship and guidance has strengthened my autonomy as a scientist. In addition, I would also like to thank Dr. Richard Padgett for his scientific guidance and words of encouragement throughout my tenure as a graduate student. Together, your patience and open door policy created an environment where good science makes it into a publication.

My undergraduate experience at Douglass College planted the research bug and I am forever grateful. It all started with Dr. Lori A. White and the Douglass Project. Thank you for taking me under your wing and showing me that 'women can do science'. Her enthusiasm and patience fostered my desire to obtain a PhD. I would also like to thank Drs. Jerome Langer and Beatrice Haimovich for cheering me on when the finish line seemed to move further away. I would also like to convey my gratitude to Dr. Kamal Khan for making me a part of the ODASIS program and believing in my talents.

Thanks you to all the past and present lab members of the Grant Lab, Drs. Saumya Pant, Anbing Shi, Ou Liu, Zhyiong Bai, Anne Norris, and Lin Sun. All of you have played an active role in my scientific growth. I would also like to take a moment and applaud Peter Schweinsberg, you really do keep the lab going. I will miss solving the world's problems in the midst of bombardments and protein biochemistry.

I would also like to thank my committee members Drs. Monica Driscoll, Maureen Barr and Peter Lobel. Every committee meeting brought me closer to my PhD. Together you guys conveyed that reproducible science is all you can ask for. This is a lesson that I value dearly and will take with me in the future. In addition, I would like to extend my gratitude to the Driscoll Lab. You guys balance scientific excellence with good ol' fashion fun. I have enjoyed being your neighbor and hope to remain connected in the future. It has been a pleasure to be a part of the *C. elegans* community at Rutgers. My PhD experience has been strengthened by great science and fruitful discussion.

My mom, Pauline Angela Walks MD, has dedicated her medical talents to making sure that the children of communities who are struggling have access to affordable health care. Her craft though valiant, does not make it to the news. I consider her a silent hero who has spent 30 years fighting to make our communities a better place. I would like to thank my brother Mark Adetomi Akintobi, who has followed in our mother's footsteps by ensuring that all children, despite their socioeconomic background, are deserving of a quality education. You both continue to inspire me and I am amazed at how you can tackle any storm with grace. I would also like to thank my father Sholademi Franklin Akintobi, for his insurmountable support over the years and never for a second doubting my abilities to excel in my craft.

To my friends Emerald and Ifeoma, thank you for providing over a decade of laughter and love. I must say these are the bear necessities in life. I would also like to thank Michelle (Mama J) and Terry (Pop) Jordan for your love and support. To my god-

daughter Kayla Amelia, nieces Ruby Mae and Iris Evon and nephew Jeremiah (J-bone) Ernest: Your brazen personalities and genuine curiosity are a joy to watch and I can't wait to see you make your mark in the world. I would like to thank my 4-legged children, the late Leonardo (Leo-nator), King Marlon, and the Sundance Kid, for bringing endless amounts of joy into a one-bedroom apartment. Regardless of the mounting experiments that lie before me in the lab...I am reminded everyday that 'food and water' come first!

And a special thank you to my dearest husband Ryan Joseph Gleason [:D] for encouraging me to live in the moment and 'enjoy the day'. Your love and support is a true blessing and remains the cornerstone of my scientific success. We can both say that this rollercoaster has finally come to an end, and I am looking forward to the next ride…(How about a merry-go-round?!).

This section of my thesis is written with the upmost sincerity and gratitude. Thank you all for being the light in moments when it was difficult for me to find the switch.

Table of Contents

List of Figure

Chapter I

Chapter II

Chapter III

DEDICATION

To My Family

Ryan, Pauline (Mumstar), Mark (The AX), Jeremiah & Sholademi

Chapter I

Introduction

Endocytosis begins with the internalization of proteins and lipids from the plasma membrane. Upon entry into the cytoplasm, each route within the endosomal network is made up of a series of interconnected tubular vesicular membrane bound organelles. In order to thrive, a cell has an evolutionary requirement to sort and transfer content between these heterogeneous compartments. In particular, the uptake of material from the plasma membrane is balanced in part by endocytic recycling-the selective return of internalized macromolecules to the plasma membrane. The interplay between endocytic uptake and recycling is tightly regulated and plays an integral role in a diverse array of biological processes including signal transduction, cell adhesion and junction formation, cell migration, pathogenic infection, cytokinesis, and cell polarity.

The internalization of receptors can occur through Clathrin-Dependent Endocytosis (CDE) or Clathrin-Independent Endocytosis (CIE). CDE is the most well characterized mode of internalization. To begin, the cytoplasimc tails of clathrin dependent transmembrane proteins contain either an evolutionary conserved aromatic tyrosine based motif or dileucine-based motif. Adaptor protein-AP2 recognizes these consensus sequences and recruits clathrin to the inner-leaflet of the plasma membrane. The assembly of clathrin makes “cage like’ invaginations in the plasma membrane. These structures are best known as clathrin coated pit (CCP). In the final stages of maturation, the invaginated CCP pinch off into vesicles, uncoat, and fuse with early endosomes. Various internalization pathways converge at the early endosome where cargo is then transported to specific cellular destinations (Figure 1). The reduced pH 4 at the early endosome makes it favorable to disassemble of many ligand-receptor complexes. Cargo can be recycled directly through early endosomes or indirectly through the recycling

endosome (slow recycling). An alternative recycling route transports cargo to the trans-Golgi network before returning to the plasma membrane. Finally cargo that is destined for degradation is dispatched to the late endosomes and eventually lysosomes.

Over the past 20 years it has become clear that many membrane-associated proteins utilize other endocytic mechanisms to internalize into the cell other than clathrin (Grant and Donaldson, 2009). CIE mechanisms include pinocytosis, macropinocytosis, and phagocytosis. One hallmark pathway that has received great interest is the ADP-ribosylation factor-6 (Arf6) pathway. Arf6 is a small monomeric GTPase that affects both vesicular transport and cytoskeletal dynamics (Radhakrishna and Donaldson, 1997). Although, the overall mechanism of internalization in this pathway remains unclear, this pathway mediates the internalization of well-known proteins such as MHC-1, and the interleukin-2 (IL-2) receptor alpha chain (Tac), as well as integrins, E-cadherins, and GPI linked proteins (Naslavsky *et al.*, 2004; Naslavsky *et al.*, 2009).

Endocytic trafficking in polarized cells

Ground breaking research in the late 1970s revealed that Madin-Darby canine kidney (MDCK) cells grown on a permeable substratum developed into an electrically tight polarized epithelial monolayer (Misfeldt *et al.*, 1976; Cereijido *et al.*, 1978). The complexity of this model system was revealed when it was shown that influenza virus buds from the apical surface and vesicular stomatitius virus (VSV) buds from the basolateral surface of these cells (Rodriguez Boulan and Sabatini, 1978). The experimental advantages of this system lead to the concept that the final localization and trafficking routes of apical and basolatoral cargo are governed by the epithelial architecture of a cell. This became the first *in vitro* model system to link endocytic

trafficking to the formation and/or maintenance of a polarized epithelium. This break-through became known as the 'flexible epithelial phenotype' (Rodriguez-Boulan and Powell, 1992). In any polaraized cell, trafficking was carried out by *tissue-specific vectorial transport.* The domains of any polarized epithelium had a programmed route characteristic to their apical and basal proteins. Subsequent discoveries in the 1990's identified some of the sorting compartments that direct the formation and morphogenesis of these polarized domains. Both apical and basolateral membranes initially deliver cargo to the early endosomes-basolateral early endosomes (Harterink *et al.*) and apical early endosomes (AEE).

To ensure proper recycling, both CIE and CDE cargo are transported to the early endosomes and then to the endocytic recycling compartment (ERC). The ERC is comprised of tubular (30-80nm) membrane organelles, which are thought to be active transport carriers facilitating endocytic recycling (Maxfield and McGraw, 2004b). The machinery used to mediate the formation of these transport carriers is just beginning to be elucidated. A central goal in the field is to understand how tubublar cargo carriers on the recycling endosome are formed and to identify proteins that control their formation.

Endocytic transport in the *C. elegans* intestine

The *C. elegans* intestine is a model system to analyze intracellular transport within polarized epithelia (Chen *et al.*, 2006). This system allows for genetic manipulation and imaging analysis in the context of an intact living epithelial tube. The worm intestine is comprised of 20 cells organized into a single layer, which form 9 donut-like rings, called

intestinal rings (Int 1-9) (Leung *et al.*, 1999b). The apical domain faces the lumen and is comprised of microvilli, with underlying terminal web and overlying glycocalyx. This domain is responsible for nutrient uptake from the environment. The basolateral surface faces the pseudocoelom (body cavity) and is responsible for the exchange of molecules between the intestine and the rest of the body.

The molecular players involved in membrane fission

Transport of vesicular cargo and organelle biogenesis require membrane fission. Many of the studies characterizing fission involve the formation of clathrin coated vesicle, which are severed from the plasma membrane. The efficiency of vesicle formation and release involves 1) Assembly, 2) Maturation, and 3) Scission from the donor compartment (Pucadyil and Schmid, 2009). The molecular requirements for membrane fission involve the actin cytoskeleton, BAR domain proteins, and mechanochemical pinchases. All three players will be discussed in this section of the proposal. The most well studied protein involved in membrane fission is the GTPase dynamin. Dynamin belongs to a family of mechanoenzymes - proteins that self-assemble around the membranes, constrict, and promote membrane fission (Danino and Hinshaw, 2001; Danino *et al.*, 2004). Initial studies in Drosophila *melanogaster* were the first to connect dynamin and endocytosis(Chen *et al.*, 1991; Chen *et al.*, 1992). In these studies, temperature sensitive mutant *shibire* flies were given short exposures to non-permissive temperatures. At the neuromuscular junctions, synaptic vesicles exocytose normally, but re-internalization is arrested at the stage of invaginated pits. Morphological studies from other tissues in the *shi* mutant revealed similar accumulation. The *shibire* cDNA is 80% similar to brain dynamin cDNA. It encodes a 100kDa protein comprised of a GTPase

domain, pleckstrin homology (Takei *et al.*) domain, an internal GAP exchange factor (Gedamu *et al.*) and proline rich domain (PRD) (Sever *et al.*, 2000).

Despite the accumulating evidence implicating dynamin in endocytosis, the precise mechanochemical mechanism that is responsible for vesicular budding has been controversial. At the neck of nascent tubules, dynamin oligomerizes into a helix to form what is defined collar-like structure (Sweitzer and Hinshaw, 1998) (Takei *et al.*, 1995). It was proposed that dynamin-GTP generates these collar structures to promote a high degree of curvature in the membrane, bringing lipids into close proximity across the bud neck. Presumably this contributes to the final steps in membrane fission. Consistent with this model, additional studies show that the GTP-bound state of dynamin assemble into tightly packed dynamin helices, while the GDP-bound state results in a more loosely 'uncoiled' helical structure. This conformational change during GTP hydrolysis is suspected to provide the mechanical force necessary to destabilize the neck and sever a budding vesicle from the donor compartment (Marks *et al.*, 2001) (Stowell *et al.*, 1999). Recent investigations have shown that it is the depolymerization of short assemblies of helical dynamin after GTP hydrolysis that facilitates membrane fission (Pucadyil and Schmid, 2008). Complimentary studies by Bashikirov *et al*, demonstrate that dynamin mediated fission is optimal with short membrane tubules creating high curvature on membranes (Bashkirov *et al.*, 2008). It is proposed that shorter tubules help create compact dynamin helices which provide optimal collar-structures to produce fission. Long tubules on the other hand promote long dynamin helices, which are less efficient for the fission process.

The actin cytoskeleton is a dynamic structure that plays multiple roles in endocytosis. Accumulating evidence suggests that the assembly of actin filaments provides mechanical force used to facilitate multiple steps in proper vesicle formation and release (Merrifield, 2004; Dawson *et al.*, 2006; Doherty and McMahon, 2009; Romer *et al.*, 2010). Actin participates in vesicle formation through at least two mechanisms: i. Localization of actin to sites of internalization may speed up the assembly of proteins necessary to complete endocytosis, and ii. actin may also provide stabilization forces necessary to deform membranes and drive vesiculation from donor membrane compartments. This model was first described in the cortical actin1 patches of *Saccharomyces cerevisiae*. In this study, Kakosen compared the spatio/temporal dynamics of pairs of actin binding proteins in CDE and revealed that the fundamental requirement for actin involves the recruitment of six cortical actin patch-protein (Kaksonen *et al.*, 2003; Dawson *et al.*, 2006). Surprisingly the recruitment of these proteins at the actin patches was sequential at sites of internalization. In the later stages, which involves step 3. Scission from the donor compartment, additional proteins were recruited and patches began to move slowly inward from the plasma membrane. Actin polymerization is described as the driving force that mediates successful vesiculation from the plasma membrane.

In mammalian cells, the transport of vesicular cargo and organelle biogenesis also requires actin to facilitate the geometric arrangement of lipid at the plasma membrane. Experiments have shown that down regulation of actin disrupts receptor-mediated endocytosis, with stronger or weaker effects depending upon cell type (Kessels and Qualmann, 2002b). To address the function that the actin cytoskeleton plays in

endocytosis in mammalian cells, live-cell imaging techniques recorded the recruitment of fluorescently labeled proteins to active sites of endocytosis. Evanescent field microscopy of live cells monitored actin-polymerizing proteins Arp2/3 complexes and nWasp associating with dynamin-mediated vesiculation (Merrifield *et al.*, 2002; Merrifield *et al.*, 2005). A short-lived burst of actin polymerization at clathrin-coated pits has been reported to coincide with recruitment of the Arp2/3 complex (Merrifield *et al.*, 2002; Merrifield *et al.*, 2005). Similar to the studies in yeast, there is a spatio/temporal coordination of the components of the endocytic machinery in mammalian cells. The stereotyped assembly of clathrin and dynamin is associated with actin polymerization to facilitate invaginations at the plasma membrane as well as vesiculation of clathrin-coated pits into clathrin-coated vesicles. As discussed later, proteins involved in the deformation of membranes i.e. BAR domain proteins also help to localize points of actin polymerization near the budding neck of clathrin coated pits.

BAR (Bin/Amphiphysin/Rvs) domain proteins are cytosolic proteins that bind and deform membranes (Gallop and McMahon, 2005; McMahon and Gallop, 2005). The banana shaped BAR dimer is composed of two-coiled-coil alpha helices that form a six-helix bundle around the dimer interface (Peter *et al.*, 2004). This interface contains a concave surface that contains positively charged residues, which electrostatically interact with the negative potential of the membrane. Upon dimerization, these proteins can oligomerize around membranes and form tubules both *in vitro* and *in vivo*. BAR domains are also proposed to be ‘sensors of curvature,’ able to distinguish and bind preferentially to a membrane with a preexisting particular degree of curvature. To address this hypothesis

in vitro experiments showed that BAR domain proteins were capable of preferential binding to artificial membranes of a particular diameter.

These same structural studies identified a subclass of domains called the N-BAR. A frequent addition associated with BAR domain proteins is an amphipathic helix at its N-terminus (N-BAR). During membrane remodeling, it is suggested that these helices insert into the local membrane bilayer to generate tubules of high curvature (30-50nm diameter). An interesting model defines this insertion mechanism as a way to drive and stabilize force to tubulate the membrane. This highly conserved N-Bar domain is found in a number of proteins including amphiphysin, endophilin, sorting nexins, arfaptins, and centaurins (McMahon and Gallop, 2005). One particular interesting model *in vivo*, suggests that these proteins can generate tubular extensions from endocytic compartments.

An additional feature of BAR domain proteins is the ability to recruit membrane modulating effectors through its src homology (SH3) domain (Gallop and McMahon, 2005) (Dawson *et al.*, 2006). The SH3 domain recognize proline-rich motifs of the PxxP type and their specificity is ensured by the residues flanking such motifs. Upon oligomerization, N-BAR domains will present multiple SH3 domains, thus having the potential to recruit many effector proteins. Collective evidence has revealed that the SH3 domain of N-BAR proteins can recruit the actin cytoskeleton, clathrin, and dynamin to localized sites of membrane deformation (Bauer *et al.*, 1993) (Takei *et al.*, 1999) (Wu *et al.*, 2010) (Itoh *et al.*, 2005).

F-BAR domain in membrane fission

The rapid expansion of the BAR domain superfamily has classified Fes/CIP4 proteins as new members (Ahmed *et al.*, 2010) (Frost *et al.*, 2007) (Dawson *et al.*, 2006). Present at the N-terminus, the F-BAR contains two previously separate domains: Fes/CIP4 and a coiled-coil region (Zwaagstra *et al.*). Initial bioinformatic studies confirmed that these two separate domains were in fact a larger BAR domain-related structure, which included a CC region (Dawson *et al.*, 2006) (Itoh *et al.*, 2005). F-BAR domain proteins are comprised of five subfamilies. Toca-1, **Subfamily 1** is characterized by the presence of a Cdc42 binding site. Some known proteins include FBP-17, CIP4 and Toca-1(FBP1). **Subfamily 2,** including Fer, a subfamily of non-receptor tyrosine kinase which do not tubulate membranes. Their F-BAR domain does not contain all the conserved lysine residues that are necessary for lipid interactions. **Subfamily 3** contains a Rho GTPase activating protein (Rho GA) domain. Synaptic dynamin associated proteins Syndapin-also known as pascins-make up the **Subfamily 4**. Unlike subfamily 1, they do not have a HR domain but instead have a SH3 homology domain present at the C terminus. Lastly, **Subfamily 5** is comprised of a physiologically diverse array some of which include FCH domain only 2, Norstrin and cell division cycle.

In comparison to its 'classical' N-BAR family members, the structure of the F-BAR domain is unique. It contains a shallow degree of curvature, which gives rise to wider tubules in diameter *in vitro* and *in vivo* (Itoh *et al.*, 2005) (Shimada *et al.*, 2007). Furthermore, F-BAR domain proteins contain five as opposed to three alpha helices and each monomer is not flanked at the N-terminus with amphipathic helices, which is thought to enhance the production of narrow membrane tubules by N-BARs. These

proteins bind and tubulate acidic liposomes, specifically those containing phosphatidylinositol 4,5P (PIP2) and phosphatidylinositol serine (Thompson *et al.*), *in vivo* and *in vitro*. When over-expressed in mammalian cells prominent tubules are observed (Itoh *et al.*, 2005).

Syndapin is one of the most recently studied members of the SH3 domain containing F-BAR proteins. Prevailing models in the field suggest that syndapin connects the actin cytoskeleton to endocytic vesicle formation. Intriguingly syndapin oligomers associate with dynamin and N-WASP through its SH3 domain (Kessels and Qualmann, 2002b) (Kessels and Qualmann, 2002a, 2004a, 2006a; Kessels and Qualmann, 2006b). Cross-linking studies, in HEK293 cells, show that over expressed syndapin results in homo and heterologous dimers. Interestingly, these homo and heterologous dimers give rise to higher ordered complexes that include dynamin and N-WASP. N-WASP is a potent activator of the Arp2/3 complex. Supporting evidence indicates that receptor-mediated endocytosis is also disrupted upon over expression of N-WASP. This phenotype can be rescued by syndapin co-overexpression of the SH3 domain. Similar results were observed with other F-BAR proteins such as CIP4 and FBP17 (Itoh *et al.*, 2005).

Recent structural studies have uncovered a unique activity, wherein the F-Bar domain of mammalian syndapin creates small tubules and tubule constrictions, along with the classically established ‘wide’ tubules for its subfamily (Wang, 2009 #111). Specifically, the tips of syndapin are bent away from the central body in a 61 degree angle giving the dimeric molecule a twisted S shape. This unique characteristic causes a second degree of curvature that is hypothesized to bind/stabilize membranes with higher curvature or

vesicular intermediates. Another distinguishing characteristic is a unique, 8-residue-long insertion in the helix 2 of syndapin. This forms a flexible loop that protrudes towards the membrane interaction surface. This flexible loop is located at the end of the 6-helix bundle close to the bending points of the tips. The length of the loop is approximately 12 angstroms containing two hydrophobic residues. This mechanism of constriction is called the wedge loop model wherein a small loop present in the concave membrane interaction domain inserts into the lipid bilayer to stabilize tubulation and membrane constriction.

In vitro, full-length mammalian syndapin is incapable of tubulating and deforming membrane (Rao *et al.*, 2010). It has been shown that the SH3 domain of syndapin is a regulatory region that serves as a docking site for fission machinery like dynamin and the actin cytoskeleton. A recent report on the crystal structure of full-length syndapin illustrates an auto-inhibitory mechanism for its SH3 domain (Wang *et al.*, 2009). The PxxP binding grooves of the mammalian syndapin SH3 domain are negatively charged. Upon dimerization, the negative residues of the SH3 domain serves as a molecular docking site for positively charged motif present on the F-BAR domain. Recall that SH3 domains recruit dynamin to sites of internalization. Intriguingly, this mechanism extends a putative role for dynamin. Rao *et al*, demonstrate that the PRD domain of dynamin can also compete for the SH3 domain of syndapin (Rao *et al.*, 2010). When the PRD domain of dynamin interacts with the SH3 domain of syndapin, the bound F-BAR domain is released and capable of tubulating membranes in vivo and *in vitro.* When comparing the primary mammalian sequence, the conserved residues that regulate the auto-inhibitory mechanism are not present in *C. elegans*. Chapter II illustrates that full length *C. elegans* syndapin (SDPN-I) is capable of tubulating lipids in vitro demonstrated a conserved

function across species. This suggests that the autoinhibition may not be an evolutionary conserved mechanism across species (Chapter II).

Molecular coordination at the plasma membrane

A functional partnership exists between amphiphysin-I and dynamin in clathrin-mediated endocytosis of the mammalian synapse (Takei *et al.*, 1999). Studies using cell-free based proteoliposome assay show that in direct collaboration with dynamin, amphiphysin generates compact dynamin helical structures along the tubular portion of liposomes (Takei *et al.*, 1999). This functional partnership supports the model that a complex of proteins work together at the neck of endocytic buds that invaginate from the plasma membrane. Ultimately, it is suggested that an intricate assembly of BAR-domain proteins and the actin cytoskeleton help to produce efficient dynamin-mediated fission. Further studies reveal that during pit maturation, BAR-domain proteins coordinate with the actin cytoskeleton to initiate and stabilize tubular invaginations from the plasma membrane (Ferguson *et al.*, 2009). In summary, a number of effectors work in collaboration to coordinate the biogenesis of tubular cargo carriers. This mechanism is seen throughout biology and best described as coincidence detection (Cullen, 2008). This is a driving force in defining membrane tubules and essential for the transport of cargo to specific destinations. The generation and maintenance of these tubules serve as an optimal template for dynamin to assemble and pinch off a budding vesicle from the plasma membrane.

Fission at the Recycling Endosome

Our understanding of the molecular requirements for fission at the recycling endosme is in its nascent stages. Although much of what is known about endocytic fission have

come from studies pertaining to the uptake of cargo from the plasma membrane, some of the lessons learned at the plasma membrane can also apply to the recycling endosome. An initial screen of proteins required for endocytosis in worm oocytes, identified RME-1(Grant *et al.*, 2001). RME-1 is the founding member of a conserved protein family that includes four mammalian proteins (**e**psin **h**omology **d**omain) EHD1-EHD4, some of which are now known to function in the exit of receptors and other membrane proteins from the ERC (Caplan *et al.*, 2002) (Grant and Caplan, 2008). Intriguingly, the structure of EHD 2 has been characterized and showed some structural similarities to dynamin, further suggesting the possibility that RME-1/EHD proteins are endosomal pinchases (Daumke *et al.*, 2007). Immuno-electron microscopy images have revealed that Ce-RME-1 associates with the neck of budding vesicles on endosomes. This led us to suggest that RME-1 may in fact mediate vesicle release from the recycling endosome.

There is a functional partnership between the N-BAR protein, amphiphysin AMPH-1 and RME-1 at the recycling endosome (Pant *et al.*, 2009). Like *rme-1, amph-1* mutants fail to recycle CIE or CDE cargo *in vivo*. Mechanistically, proper recycling is maintained through a physical interaction between the NPF sequence of AMPH-1 and the EH-domain of RME-1. *In vitro* studies revealed a biochemical mechanism where AMPH-1 regulates RME-1 spiral assembly to produce tighter and more compact helices. This is particularly exciting because short dynamin helical assembles are optimal intermediates for fission (Pucadyil and Schmid, 2008). We hypothesize that a cooperative partnership between worm AMPH-1 and RME-1 results in conformations that promote the release of tubular cargo carriers exiting the recycling endosome. In mammals, amphiphysin proteins also potentiate Wasp-mediated actin polymerization through its SH3 domain

(Yamada *et al.*, 2009). This is of particular interest because previous studies suggest that actin polymerization modulates the shape and function of the recycling endosome (Grant and Donaldson, 2009). It is plausible that actin is an additional effector that works with RME-1 and AMPH-1 to facilitate the biogenesis of transport intermediates from the recycling endosome.

The role of Syndapin/SDPN-1 in endosomal recycling

Mammals contain three syndapin genes encoding the F-BAR domain proteins: syndapin I, which is expressed in neuronal tissue, syndapin II which is expressed ubiquitously, syndapin III which is expressed in muscle and upregulated during adipocyte differentiation (Kessels and Qualmann, 2004b). Mammalian syndapin-2 functions with EHD1 to promote transport from recycling endosomes to the plasma membrane in cultured HeLa cells. Yeast-2-Hybrid screen and co-immunoprecipitation studies revealed that the EH domain of EHD1 binds to Syndapin through its NPF sequence (Braun *et al.*, 2005). *In vivo*, Syndapin and EHD1 colocalizes in Hela cells. Further, over-expression of the syndapin NPF sequence led to impaired recycling of fluorescent transferrin. As anticipated, over-expression of a NPV, mutated version of the NPF sequence, did not effect recycling (Braun *et al.*, 2005). Taken together, these results suggest over-expression of syndapin's NPF sequence results in the sequestration of endogenous EHD from the recycling complex and ultimately inhibits the return of transferrin to the plasma membrane, however there has not been an in-depth molecular analysis of CIE recycling in the absence of syndapin protein. Thus the precise requirement for syndapin must be handled with discretion.

Chapter II provides a comprehensive analysis of CIE and CDE recycling in the context of syndapin/SDPN-1 knockout experiments. *C.elegan's* syndapin (SDPN-1) lacks NPFs and this physical relationship is not observed, even though worm SDPN-1 colocalizes with RME-1 on basolateral recycling endosomes of the worm intestine. This is consistent with the dominant negative studies performed in mammalian cells. We concluded that SDPN-1 is enriched on early endosomes and is responsible for the dispatch of recycling cargo from the early endosome en route to the ERC.

Endosomal trafficking as intracellular signaling stations: an emerging role in signal transduction

In response to external cues, cells transmit the message through a cascade of intracellular events best described as signal transduction. The canonical module of signal transduction begins at the cell surface where transmembrane receptors bind an extracellular ligand and activate cytoplasmic messenger proteins. Consequently the intracellular cascade is transmitted to the nucleus where gene expression is regulated. Endosomal trafficking has been widely accepted as means to terminate signal by shuttling post-internalized ligand-receptor complexes to the lysosome for degradation. Over the years endocytic compartments have emerged as signaling stations, for various signal transduction pathways. As another layer of organization, the spatial and temporal compartmentalization of many signaling pathways is propagated on endosomal organelles. A block in CDE by the expression of Dynamin^{K24E} perpetuates EGFR activation but impairs the activity of downstream signaling molecules such as mitogen-activated protein kinases (MAPKs) ERK1/2 or the p85 subunit phosphatyidylinositol 3-kinase (PI3-K) (Miaczynska *et al.*, 2004). Similarly, the MAPK activation is also impaired when internalization of the β-adreneric receptor is blocked. Intriguingly, downstream

EGFR signaling components (mSOS, GRB2, SHC) are found on early endosomes as opposed to the plasma membrane (Miaczynska *et al.*, 2004). In collaboration, Chapter III delineates the endosomal sorting requirements that propagate transforming growth factor beta TGFβ signaling.

Overview on the transforming growth factor β (TGFβ) *signaling pathway*

The TGFβ consists of a super family of structurally related ligands, which include TGFβ, bone morphogenic proteins (BMP), growth, inhibins, activins, differentiation factors (GDF), and Mullerian inhibition substance (Di Guglielmo *et al.*). Over the past two decades, major accomplishments in the field have contributed to the general mechanism in which TGFβ transduce signal to its target genes. The TGFβ signaling pathway is highly conserved across metazoan biology. In *Drosophila*, the pathway plays a key role in the development of the body plan, including patterning of the wings and eyes while in human embroygenesis the pathway controls vascular development. To propagate signaling, TGFβ mediates its effects on cells by a heteromeric complex of two types of transmembrane serine/theonine kinase receptors. TGFβ signaling is a sequential mechanism in which the TGFβ ligand first binds directly to the type II receptor (TGFBR2) kinase and then recruits the type 1 receptor kinase. Upon recruitment the TGFBR2 activates the TGFBR1 and phosphorylates the GS box of the TGFBR1, a glycine-serine-rich region of the receptor. (Massague, 2000; Massague and Chen, 2000). Ultimately, the activated TGFBR1 propagates the signal by phosphorylating receptor-associated Smad2 and Smad3, which ultimately form complexes with Smad4 and translocate to the nucleus. Once activated Smad complexes enter the nucleus, co-activators and cell specific DNA-binding factors work together to regulate gene expression, which

coordinate cell cycle and tissue repair (Massague, 2000; Massague and Chen, 2000). Recent investigations document that TGFβ signals though the smad anchor for receptor activation, SARA and recruits Smad2 on early endosomes. This the first report of endosomes as a mediator in TGFβ signaling. Using *C. elegans* as a model to examine the nexus that exist between trafficking and signaling, we are the first to uncover that the type I and II of the TGFβ receptors are sorted to distinct molecular sorting complexes upon internalizaiton (Chapter III).

TGFβ signaling in *C. elegans*

Two distinct TGFβ signaling pathways exist in *C. elegans.* In particular the dauer signaling pathway controls an alternative developmental period in the third larval stage of nematode. As a mechanism of survival, the worm will 'hibernate' and maintain growth arrest in response to harsh environmental conditions. (Riddle and Albert 1997). The identification of *daf-1* and *daf-4*, which encode the type I and type II receptor respectively, control dauer formation. Interestingly, *daf-4* mutans also exhibited male tail abnormalities (Mab mutations) and small body size (Sma mutations). These phenotypes were not observed in dauer defective mutant animals. This phenotypic distinction is coined as the SMA/MAB pathway, which is ultimately responsible for body size, mail tail development, olfactory learning, and innate immunity (Patterson and Padgett, 2000; Kurz and Tan, 2004; Nicholas and Hodgkin, 2004). By exploiting the body size defect, an elegant screen was performed which identified the following components *dbl-1* (ligand)*, sma-2, sma-3 sma-4,* and *sma-6* (type I) (Savage *et al.*, 1996; Savage-Dunn *et al.*, 2003).

Figure 1. Clathrin dependent endocytosis (CDE) and endosomal transport.

Schematic representation of post internalization routes that occur in mammalian systems.

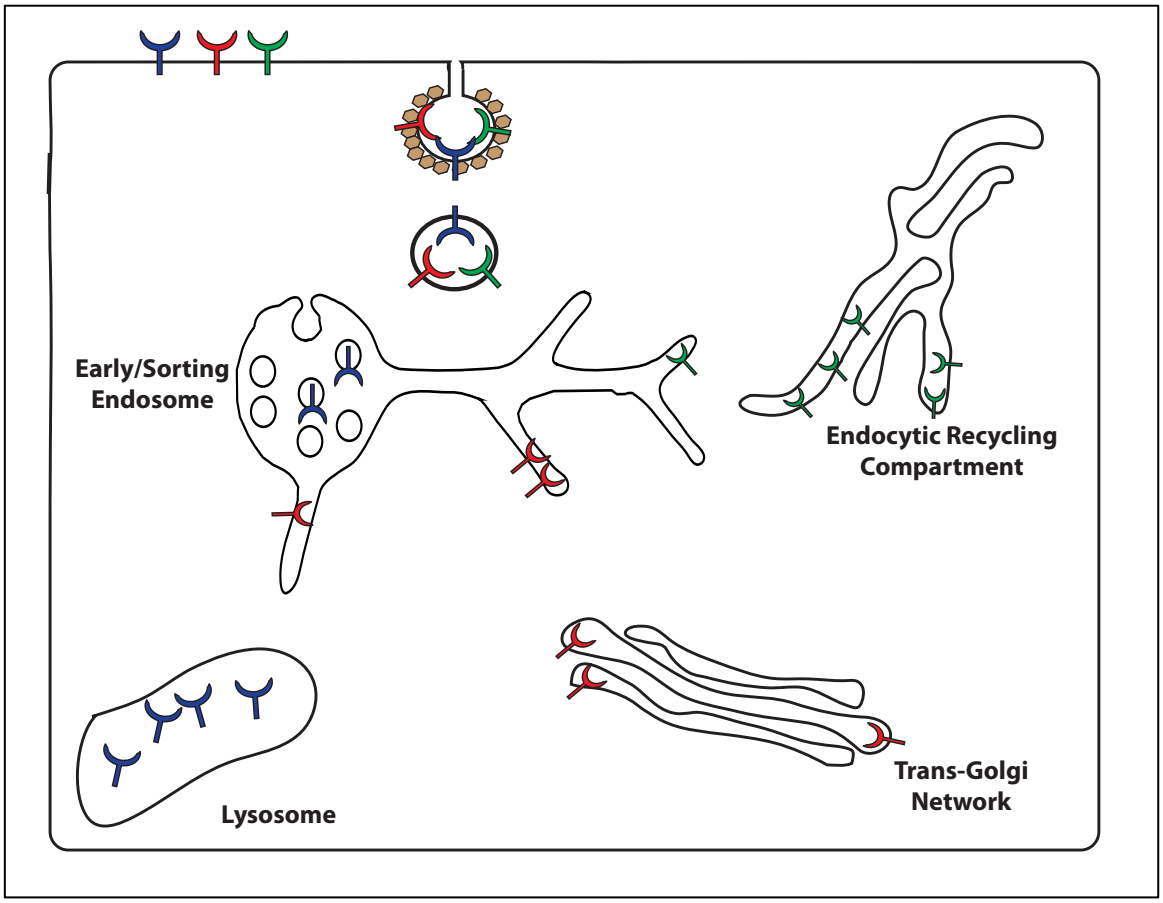

Figure 2. SH3 domain regulation of mammalian F-BAR
Hypothetical model for the role of PRD containing dynamin dissociating the intramolecular Bar-SH3 domain interaction (Rao 2009)

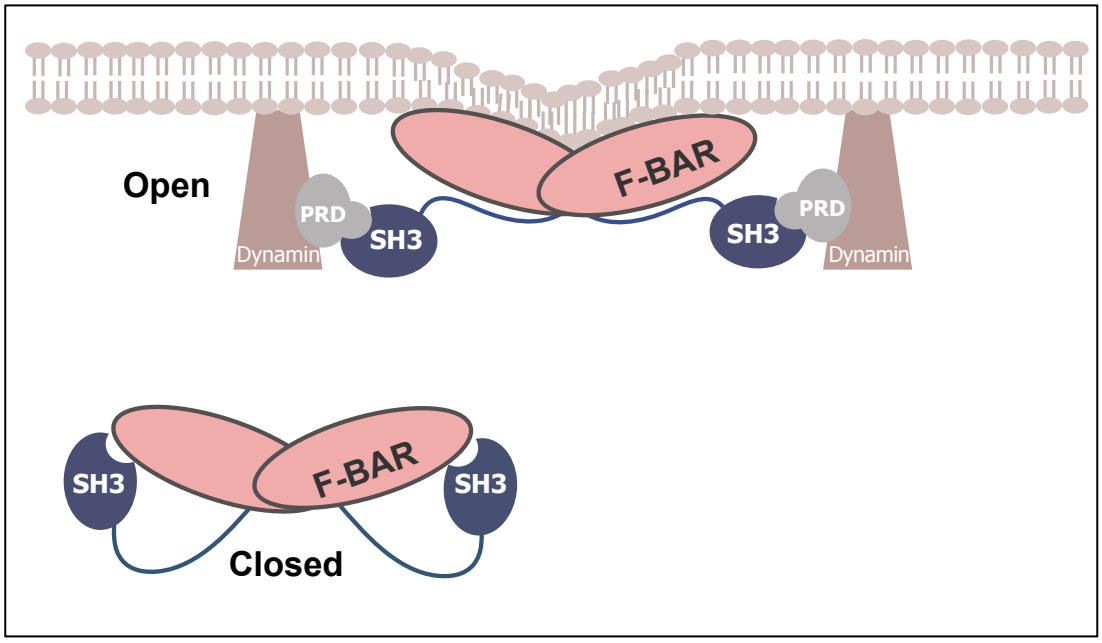

Figure 3. Canonical TGFβ signaling pathway

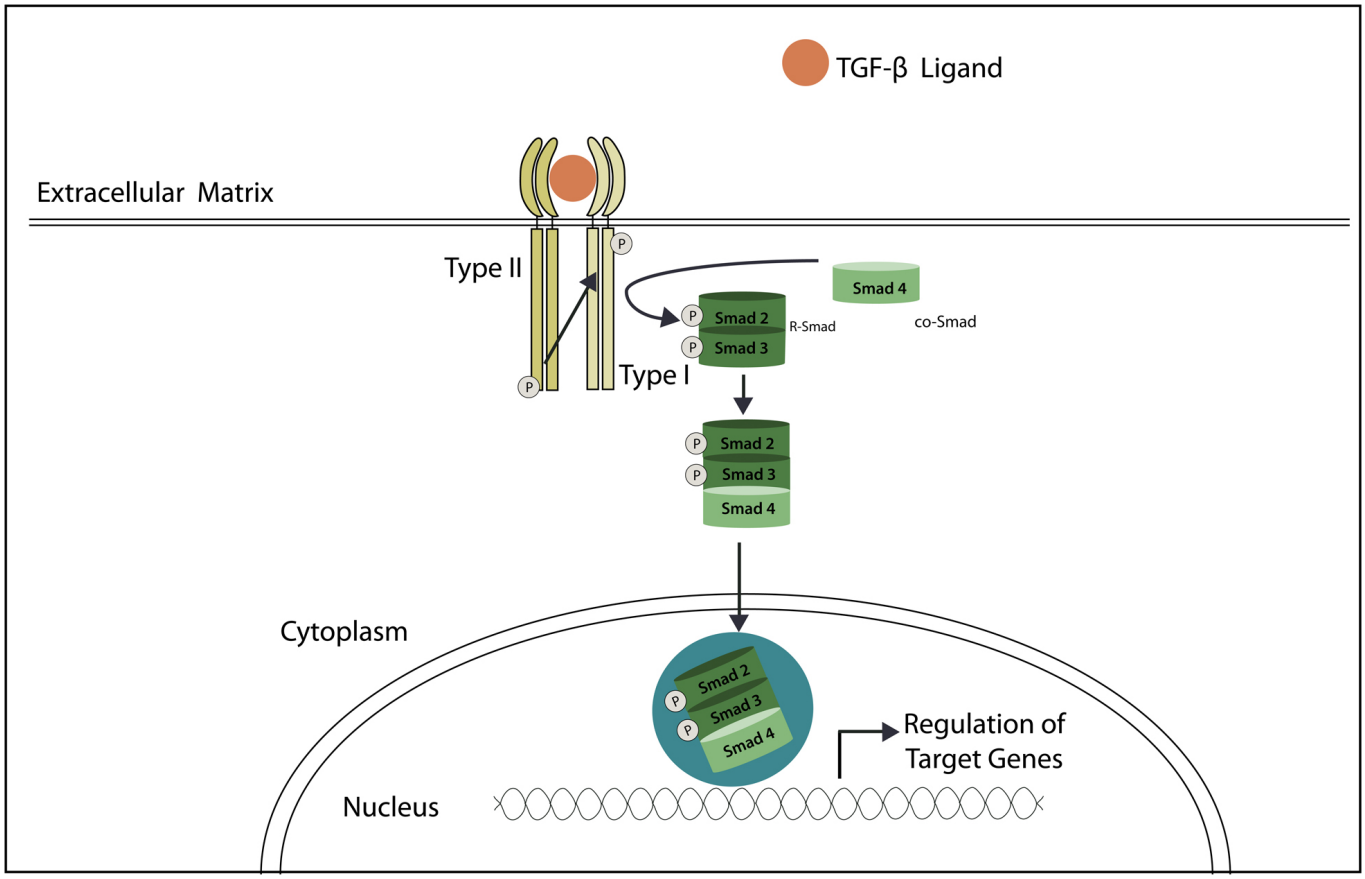

Chapter II

C. elegans Syndapin/SDPN-1 is required for endocytic recycling and endosomal actin polymerization

Introduction

Enclosed by a limiting membrane, cells establish and maintain their architecture in part through a process called endocytosis. Endocytosis is a highly conserved trafficking pathway that begins with the vesicle-mediated internalization of proteins and lipids from the plasma membrane. Cells internalize receptors through Clathrin Dependent Endocytosis (CDE) and Clathrin-Independent Endocytosis (CIE) pathways (Doherty and McMahon, 2009; Grant and Donaldson, 2009). In CDE, the adaptor protein 2 (AP2) can recognize motifs within the cytoplasmic tails of transmembrane proteins. Upon recognition, these adaptor proteins co-assemble with clathrin at the plasma membrane, forming cage like structures that produce plasma membrane coated pits. As the process continues, the invaginated clathrin coated pits (CCP) then pinch off into vesicles, uncoat, and fuse with one-another and pre-existing early endosomes (Gesbert *et al.*, 2004). Once in the early endosome, the reduced pH results in the dissociation of many ligand-receptor complexes. As fluid and membrane are added to the early endosome, membrane tubules begin to form and extend. At this point, many internalized receptors are recycled to the plasma membrane either directly (rapid recycling) or indirectly via the endocytic recycling compartment (ERC) (slow recycling) or Golgi (retrograde recycling). Membrane proteins and lumenal content that fail to recycle are transported to the late endosomes and eventually the lysosomes for degradation (Burke *et al.*, 2001; Doherty and McMahon, 2009).

Endocytic uptake and recycling are tightly regulated and function in a diverse array of biological processes, including cell adhesion and junction formation, cell migration, cytokinesis, cell polarity, and signal transduction (Maxfield and McGraw, 2004a; Grant and Donaldson, 2009). In mammalian fibroblasts the ERC is typically comprised of a

dense collection of juxtanuclear membrane tubules and vesicles that ultimately carry macromolecules back to the plasma membrane (Maxfield and McGraw, 2004a; Grant and Donaldson, 2009). Important aspects of the mechanisms that mediate the return of cargo molecules to the plasma membrane remain to be elucidated.

The *C. elegans* intestine, a polarized epithelium, is a powerful model system to characterize the molecular components required for endocytic recycling (Chen *et al.*, 2006). This system allows for genetic manipulation and imaging analysis in the context of an intact living epithelial tube. The worm intestine is surprisingly simple, comprised of 20 cells organized into a single layer, forming 9 donut like rings (Leung *et al.*, 1999a). The apical domain faces the lumen and is specialized for nutrient uptake, covered in dense microvilli. As in mammalian intestinal epithelia, the *C. elegans* intestinal lumen is supported by an underlying terminal web and overlying glycocalyx. The basolateral surface faces the pseudocoelom and is responsible for the exchange of molecules between the intestine and the rest of the body (McGhee, 2007).

A number of key, conserved recycling regulators were first discovered in *C. elegans*, including RAB-10 and RME-1(Grant *et al.*, 2001; Chen *et al.*, 2006). Animals lacking RME-1 accumulate gigantic endosomes that trap basolateral transmembrane recycling cargos (Grant *et al.*, 2001). These enlarged organelles are positive for ARF-6 and lack RAB-5, placing RME-1 function at a late step of endocytic recycling (Chen *et al.*, 2006; Shi *et al.*, 2009). Complimentary studies in mammalian cell culture demonstrated that loss of mRme-1/EHD-1, the mammalian homologue of RME-1, greatly slows the recycling of transferrin and major histocompatability class I protein (MHCI), trapping recycling cargo in the juxtanuclear ERC (Lin *et al.*, 2001a; Caplan *et al.*, 2002). While

recycling tubules are concentrated near the nucleus in cultured mammalian cells, in the *C. elegans* intestine RME-1 labels a network of tubular recycling endosomes, located just below the basolateral intestinal cortex (Lin *et al.*, 2001a; Caplan *et al.*, 2002). While superficially similar to the intestinal phenotype found in *rme-1* mutants, animals deficient in RAB-10 display an earlier block in basolateral recycling that is more cargo-specific. The grossly enlarged endosomes in *rab-10* mutants are positive for RAB-5 and ARF-6, and accumulate CIE α-cargo chain of the human IL-2 receptor TAC (hTAC) but not CDE cargo hTfR (Chen *et al.*, 2006; Shi *et al.*, 2010). RAB-10 appears to function just after the early endosome master regulator RAB-5, with feedback from RAB-10 acting to down-regulate RAB-5 as cargo recycles (Liu and Grant, 2015).

Little is known of recycling endosome biogenesis and its relationship to early endosomes. Given the tubular nature of the recycling network we sought to further analyze the role of BAR domain proteins in the sculpting of membrane tubules, potentially facilitating the biogenesis of recycling cargo carriers. One BAR domain protein family suggested to work in the endocytic recycling pathway is syndapin/pacsin. Mammals express three syndapin/pacsin genes encoding F-BAR domain membrane bending proteins (Dharmalingam *et al.*, 2009). Syndapin 1 is neuron-specific and is required for activity-dependent bulk endocytosis at pre-synaptic membranes, but not direct synaptic vesicle endocytosis via clathrin (CDE) (Anggono *et al.*, 2006). Syndapin 2 is ubiquitously expressed and has been variously reported to function in CDE (fibroblasts and apical membrane of epithelia), caveolae dynamics, Golgi traffic, endocytic recycling, actin dynamics, neuronal development, and cell migration (Ritter *et al.*, 1999; Meng *et al.*, 2011). The first work linking Syndapin 2 to endocytic recycling in mammalian cells

showed that NPF motifs in Syndapin 2 bind to the EH-domain of Ehd1/mRme-1, and that overexpression of the isolated NPF or EH domains interfered with transferrin recycling (Braun *et al.*, 2005). The syndapin 2 SH3-domain interacts with the recycling tubule protein MICAL-L1, further implicating it in recycling regulation (Giridharan *et al.*, 2013). Syndapin 3 expression is up-regulated during adipocyte differentiation and over-expression of syndapin 3, which lacks NPF sequences, increased the recycling of Arf6-dependent cargo GLUT1 in adipocytes (Roach and Plomann, 2007). Interestingly, previous reports from our laboratory show that loss of either basolateral recycling regulators RME-1 and AMPH-1 reduced the number of SDPN-1 labeled endosomes and display gross enlargement of the remaining SDPN-1 labeled structures in the *C. elegans* intestine (Pant *et al.*, 2009) Shi 2007). Collectively these results imply that loss of SDPN-1 protein leads to a defect in endocytic recycling. While suggestive, these studies do not definitively establish a role for syndapin in endocytic recycling.

Unlike syndapin 1, where mouse knockouts have been well utilized, many of the published studies on syndapin 2 and syndapin 3 must be interpreted with caution, since syndapin function in these studies was mainly tested by injection of anti-syndapin antibodies and/or overexpression of the full-length protein, or individual syndapin protein domains. In cases where syndapin 2 function has been studied after knockdown, analysis of its function in recycling has been hampered by its requirement in CDE. There is a general lack of Syndapin knockdown/knockout data analyzing the recycling of CIE cargo. Here we analyze the function of the *C. elegans* syndapin/pacsin-family protein SDPN-1, establishing its role in basolateral endocytic recycling in the context of the *C. elegans* intestine, a polarized epithelium. We further show that SDPN-1 is enriched on

both early and basolateral recycling endosomes, and loss of SDPN-1 appears to block recycling cargo in hybrid compartments containing either early or recycling markers. We propose that SDPN-1 coordinates a subdomain on early endosomes that connects to the late recycling endosome compartment, thus linking SDPN-1 to a very poorly understood transport step in recycling endosome maturation.

Results

Full-length recombinant SDPN-1 tubulates acidic membranes *in vitro*

In *C. elegans*, the only syndapin/pacsin family protein is called SDPN-1 (Figure 1A). Like its mammalian homologue, SDPN-1 contains one conserved N-terminal F-BAR domain and a single C-terminal SH3 domain (Figure 1B). Extensive reports show that syndapin is capable of tubulating/vesiculating membranes in vitro (Wang *et al.*, 2009; Rao *et al.*, 2010). To test conservation of function, we expressed and purified full-length recombinant SDPN-1 and examined its function *in vitro* when reconstituted with negatively charged liposomes. SDPN-1 protein created narrow membrane tubules with an average diameter around 40 nm (Figure 1D and E). These results are similar to those reported for the purified F-BAR domain of mammalian syndapin 2, indicating a conservation of molecular function (Wang *et al.*, 2009; Rao *et al.*, 2010). This is also the first demonstration of such activity in any full-length syndapin-family protein.

SDPN-1 is broadly expressed in multiple tissues

We characterized the expression pattern and subcellular localization of SDPN-1. We created low copy number integrated transgenic *C. elegans* lines expressing GFP fused to the C-terminus is SDPN-1 driven by *sdpn-1* promoter sequences (Supplemental Figure S1). We observed expression in the intestine, pharynx, and a neuron (Supplemental Figure S1). In the intestine, SDPN-1::GFP localized to distinct puncta near the basolateral cortex as well as on or near the apical intestinal membrane (Supplemental Figure S1B and C).

sdpn-1 mutants disrupt multiple transmembrane receptor cargo traveling from the early to recycling endosome

To test the cargo-trafficking requirements of SDPN-1, we assayed the effect of *sdpn-1* deletion mutation, *ok1667,* on a diverse panel of basolateral transmembrane cargo with well-characterized post-internalization trafficking routes expressed specifically in the *C. elegans* intestine (Chen *et al.*, 2006; Shi *et al.*, 2007; Shi *et al.*, 2010; Sun *et al.*, 2012; Sato *et al.*, 2014). The *ok1667* allele is missing sequences from within the second to eighth exon, deleting a substantial fraction of the F-BAR domain coding sequences, and producing a predicted frame-shift and premature stop codon predicted to remove the remainder of the protein (Fig. 1). Thus the *ok1667* mutant should not produce any functional SDPN-1 protein. The well-characterized basolateral cargos that we tested included GFP-tagged forms of hTAC (human IL-2 receptor α-chain TAC) DAF-4, a type II TGF-β receptor, hTFR (human transferrin receptor), MIG-14/Wntless (a transmembrane chaperone for WNT ligands), SMA-6 (a type I TGF-beta receptor) and CD4-dileucine (Chen *et al.*, 2006; Shi *et al.*, 2009; Gu *et al.*, 2013; Gleason *et al.*, 2014). hTAC and DAF-4 recycle via the recycling endosome in an ARF-6-dependent pathway (Shi *et al.*, 2012; Gleason *et al.*, 2014). MIG-14 and SMA-6 recycle via retrograde recycling in a retromer-dependent manner (Shi *et al.*, 2009; Gleason *et al.*, 2014). hTfR, MIG-14, SMA-6, and CD4-dileucine are clathrin-dependent in their endocytosis. hTAC is a clathrin-independent cargo. CD4-dileucine does not appear to recycle and appears to enter the degradative pathway after endocytosis (Figure 2J-L) (Gu *et al.*, 2013). hTAC::GFP, hTfR::GFP and DAF-4::GFP displayed dramatic accumulations at internal sites within the intestinal cells of *sdpn-1(ok1667)* mutants, and did not accumulate on the cell surface (Figure 2A-C, 2D-F, and Supplemental Figure 2A-C). The abnormal

accumulation of recycling cargo hTFR::GFP was rescued by intestinal specific expression of SDPN-1::tagRFP further indicating that the cargo transport defect is caused by loss of SDPN-1 (Supplemental Figure S3, A-C). The localization of MIG-14::GFP, SMA-6::GFP, and CD4-dileucine remained comparable to wild-type in *sdpn-1(ok1667)* mutants (Figure 2G-I and Supplemental Figure 2D-F). Taken together, these results indicate that SDPN-1 is not required for uptake from the basolateral plasma membrane or retrograde transport from endosomes to the Golgi. Rather, loss of SDPN-1 appears to specifically affect basolateral cargo proteins that recycle to the plasma membrane via the recycling endosome.

We also examined the apical intestinal plasma membrane protein PGP-1::GFP in *sdpn-1* mutant. PGP-1::GFP in *sdpn-1* mutants did not accumulate intracellularly and appeared normally localized to the apical membrane, suggesting that apical secretion/recycling does not depend upon SDPN-1. Intriguingly however, the PGP-1-GFP marker, and electron microcopy of unmarked strains, revealed that the intestinal lumen was grossly expanded in *sdpn-1* mutants, with an unusual convoluted structure (Supplemental Figure S4, B&D). Close inspection of electron micrographs suggested that although expanded, the apical membrane itself and the associated microvilli and terminal web appeared normal (Supplemental Figure S4, E&F). These results may indicate a role for SDPN-1 in apical endocytosis, as has been previously suggested in other systems (Da Costa *et al.*, 2003).

Loss of SDPN-1 function does not induce gonad migration defects but reduces fecundity

Interestingly, *sdpn-1* mutants display reduced fecundity, producing 95 (±10.5) eggs through day 2 as compared to wild-type 171(±21.5) [$p<0.001$ student t-test].

To determine a role in distal tip migration, we scored 30 L4 gonad arms in wild-type and *sdpn-1* mutant animals using Normaski microscopy. The U-shaped gonad arms of *sdpn-1* mutant animals remained comparable to wild-type. These results are expected because *sdpn-1* mutant animals failed to disrupt the trafficking of transmembrane cargo MIG-14, a known regulator in DTC migration.

SDPN-1 is required for endosomal morphology

The transmembrane cargo data above indicates a role for SDPN-1 in endocytic recycling. To further investigate these results, we also quantified the effects of SDPN-1 loss-of-function on endosomal morphology using a group of well-established molecular markers for specific endosome types. Collectively, such studies can help to determine the specific transport steps affected. We noted that the intensity of RAB-5 and RAB-7 labeled early (Figure 3, A-C) and late endosomes (Figure 3, D-F) increased drastically in *sdpn-1* mutants. This observation correlates to the increase in RAB-5 and RAB-7 endosomal size (Supplemental Figure 5,A&B). Further we observed the same abnormal accumulation of RAB-10-labeled basolateral recycling endosomes (BREs) (Figure 3G-I and Supplemental Figure 5C). RAB-10 resides on a subset of recycling endosomes that contribute to formation and/or maintenance of mature BREs. Interestingly, both the

number of RAB-5 and RAB-10 labeled endosomes were reduced in *sdpn-1* mutants, while RAB-7 labeled late endosome remained the same as wild- type. (Figure 3, P).

At the cortex of the worm intestine (top plane), RME-1 labels mature BREs, which form an extensive tubulovesicular meshwork underneath the plasma membrane (Figure 3J). Wild- type animals display very little RME-1 labeled cytoplasmic puncta (middle plane) (Figure 3M). Under a higher objective (100x) lens, the size and intensity of RME-1 positive BREs increased (Figure 3, G-I and Supplemental Figure 5D), while the endosome number remained comparable to wild-type (Figure 3P). Interestingly, *sdpn-1* mutants caused striking redistribution of RME-1 positive endosomes to the 'middle' focal plane (Figure 3M-O, P and Supplemental Figure). Consistent with a role in basolateral recycling transport, loss of SDPN-1 function did not alter RAB-11 labeled apical recycling endosomes (Supplementary Figure S6, A-D).

These data illustrate that SDPN-1 is important for the integrity of early endosomes and BREs. Based on the accumulation defect in recycling cargo, we propose a model wherein SDPN-1 facilitates the exit of recycling cargo from the early endosome.

Loss of SDPN-1 traps recycling cargo hTFR in endosomes that are positive for early and recycling markers.

To explore SDPN-1's role in the dispatch of cargo from the early endosome, we next analyzed the localization of recycling cargo that accumulated in *sdpn-1* mutants. In wild-type animals at steady-state we observe few intracellular hTFR::GFP puncta

positive for early endosome marker tagRFP::RAB-5 (Figure 4, A-A'''). Upon depletion of SDPN-1 by RNAi we observed the same abnormal accumulation of hTFR::GFP observed in *sdpn-1(ok1667)* mutants (Figure 4, B-B'''). Importantly, quantification of the degree of colocalization between hTFR::GFP and tagRFP::RAB-5 in *sdpn-1* animals revealed a dramatic increase in colocalization, indicating that loss of SDPN-1 traps recycling cargo in the early endosome (Figure 4, E). A minor overlap between tagRFP::RME-1 and hTFR::GFP was detected in wild-type animals (Figure 4, C-C'''). However in *sdpn-1(RNAi)* animals, we also observed a dramatic increase between RME-1 positively labeled BREs and hTFR recycling cargo (Figure 4, D-D'''& E). Interestingly, the site of hTFR accumulation coincided with the redistribution of RME-1 labeled endosomes that appear in the medial plane of the intestine.

At steady state, hTFR was found in the RAB-7 compartment (Supplemental Figure, S7, A-A'''). Upon RNAi knockdown of SPDN-1 protein, we observed the same abnormal accumulations of RAB-7 labeled endosomes and hTFR recycling cargo (Supplemental Figure, S7, B-B'''). Interestingly, quantification of the degree in overlap for animals depleted of SDPN-1 by RNAi remained comparable to wild-type (Supplemental Figure S7, E). Further, hTFR did not overlap extensively with RAB-10 labeled endosomes in wild-type (Supplemental Figure 7, C-C''') nor *sdpn-1(RNAi)* animals (Supplemental Figure S7, D'D'''). We also report that the degree of colocalization in *spdn-1(RNAi)* animals remained comparable to wild-type (Supplemental Figure S7, D'D'''& E).

Taken together, *sdpn-1* mutants accumulate recycling cargo in structures positive for early and recycling endosome structures. Importantly, loss of SDPN-1 function does not represent a global increase in internalization since the accumulations of hTFR failed to increase in enlarged RAB-7 endosomes.

SDPN-1 predominately resides on early and recycling endosomes

If SDPN-1 functions directly in early endosome to recycling endosome transport we would expect to find SDPN-1 protein enriched on early endosomes, recycling endosomes, or both. To determine this we performed a series of colocalization studies in the intestinal cells of living intact animals. Intestine-specific expression of GFP-tagged SDPN-1 labels abundant cytoplasmic puncta near the basolateral surface. Previous work suggested that SDPN-1 resides on recycling endosomes (Shi *et al.*, 2007; Pant *et al.*, 2009)Shi 2007). To address this question in more depth, we used spinning disk confocal microscopy to compare the localization of SDPN-1::GFP with additional organelle markers. In particular we found that SDPN-1::GFP colocalizes best with a subset of RAB-5 positive endosomes that reside close to the basolateral plasma membrane at the periphery of the adult intestinal cells (Figure 5, A-A’’’) as judged using Pearson’s correlation coefficient (Figure 5, C). We also confirmed colocalization of SDPN-1::GFP with tagRFP::RME-1, although to a lesser degree than with RAB-5 (Figure 5, B-B’’’). This is the first report demonstrating that the F-BAR protein SDPN-1 is a resident component of early endosomes, where it could function in membrane budding reactions to promote early endosome to recycling endosome transport.

We also observed sparse colocalization of SDPN-1::GFP with late endosomal marker RAB-7 (Supplemental Figure S8, A-A''). Additional analysis indicated that SDPN-1::GFP failed to colocalize with the Golgi marker MANS::mCherry (Supplemental Figure S8, B-B'').

RAB-10 controls RAB-5 recruitment to SDPN-1 positive endosomes.

Loss of SDPN-1 causes accumulation of RAB-10 endosomes (Figure 3J-l). To test if this relationship is reciprocal, or instead works in only one direction, we sought to determine if SDPN-1 localization is dependent on RAB-10 function. Upon depletion of RAB-10 protein, SDPN-1::GFP appeared diffuse with a reduction in the number of remaining positively labeled structures (Figure 6, B and C). This is similar to the diffusive GFP::RME-1 labeling in *rab-10* mutants, which results in the concomitant loss of tubulovesicular meshwork found near the basolateral plasma membrane (ref chen 2006 and 2010). As expected wild-type animals displayed extensive colocalization between RAB-5 and SDPN-1 labeled endosomes (Figure 6, A-A'''). Our previous work in *rab-10* mutants, showed that these give rise to grossly enlarged RAB-5 positive endosomes (Chen *et al.*, 2006; Shi *et al.*, 2010; Liu and Grant, 2015) Remarkably, these enlarged RAB-5 positive endosomes failed to colocalize to the periphery of the remaining SDPN-1 positive endosomes in *rab-10(RNAi)* animals (Figure 6, C'C''') as determined by Pearson's correlation coefficient (Figure 6,D).

These results suggest that RAB-10 functions upstream of SDPN-1 to coordinate downstream recycling events. Interestingly, our colocalization analysis further suggests

that the directionality of RAB-10-dependent recycling transport is governed in part through the coupling of RAB-5 to SDPN-1 endosomal membranes.

Filamentous actin localizes to SDPN-1 positive endosomes.

Mammalian studies of syndapin function at the plasma membrane suggest that syndapin promotes actin polymerization (Qualmann *et al.*, 1999; Qualmann and Kelly, 2000). Since actin polymerization on endosomes could function to promote the formation and function of recycling tubules, we sought to determine if SDPN-1-positive endosomes display enrichment of F-actin (Kessels and Qualmann, 2006b; Puthenveedu *et al.*, 2010; Giridharan *et al.*, 2013). To test this we quantified the localization of F-actin, as reported by RFP::LifeAct, an F-actin biosensor, on SDPN-1 positive endosomes in the intestine of living intact animals (Figure 7, A-A'''). Under steady state conditions, confocal micrographs revealed considerable colocalization of LifeAct and SDPN-1, with a Pearson's correlation coefficient of 0.6 (Figure 7, B). These data demonstrate that SDPN-1-positive endosomes structures are enriched with filamentous actin.

***sdpn-1* mutants fail to recruit filamentous actin to early endosomes.**

If SDPN-1 mediated actin polymerization is necessary for efficient transport from the early endosome to the recycling endosome, we might expect to observe reduced F-actin levels on early endosomes upon loss of SDPN-1. To test this we analyzed colocalization of GFP-LifeAct and early endosome marker RFP::RAB-5 in the intestinal epithelium. As with SDPN-1, we found that LifeAct is enriched on early endosomes positive for RAB-5 (Figure 8, A-A'''). After *sdpn-1 RNAi* or in *sdpn-1(ok1667)* mutants, RAB-5 labeled endosomes were visibly enlarged and were largely depleted of LifeAct (Figure 8, B-B'''). The degree of colocalization was determined by Pearson's correlation coefficient (Figure

8, C). We were unable to detect enrichment of LifeAct on RAB-7 labeled (Supplemental Figure 9, A-A'') and RME-1 labeled (Supplemental Figure 9, B-B'') endosomes. As expected, enlarged RAB-5 labeled endosomes were also depleted of F-actin in *rab-10(RNAi)* mutant animals (Supplemental Figure S10 B-B''') when compared to wild-type animals (Supplemetnal Figure S10, A-A'''). The degree of colocalization was determined by Pearson's correlation coefficient (Supplemental Figure S10, C).

These results indicate that SDPN-1 is important for F-actin accumulation at the early endosome and dependent on RAB-10 function. An attractive hypothesis suggests that SDPN-1's role on early endosomes may contribute to productive formation or scission of transport carriers from early endosomes en route to recycling endosomes.

Discussion

In mammalian cell culture the syndapin 2 protein has been implicated in endocytic recycling, primarily because it binds to recycling regulators EHD1/mRme-1 and MICAL-L1 (Braun 2005, Panapakkam 2013). However, analysis of the requirement of syndapin in endocytic recycling in mammalian cells has been hampered by a requirement for syndapin in clathrin-mediated uptake from the plasma membrane, and by potential redundancy among the 3 separate genes encoding syndapins in mammals. To more clearly analyze the requirements for syndapin in recycling we took advantage of an uncharacterized deletion mutant in the single syndapin/pacsin family gene encoded in the *C. elegans* genome. Although the sequence reported to link syndapin 2 to EHD proteins is not evolutionary conserved in worm SDPN-1, and *C. elegans* lacks a MICAL-L1 homolog, our analysis shows that SDPN-1 does indeed function in endocytic cargo recycling.

We defined the requirements for SDPN-1 in recycling by analyzing a variety of recycling cargo proteins in a *sdpn-1* deletion mutant. Loss of SDPN-1 did not appear to trap any of these cargo proteins at the plasma membrane, allowing a clearer analysis of Syndapin function in endocytic recycling than has been possible in mammalian cells. A specific group of cargo proteins that recycle along the early endosome to recycling endosome to plasma membrane route (hTAC, hTFR and DAF-4) accumulated intracellularly in *sdpn-1* mutants, with trapped recycling cargo clearly accumulating organelles positive for early endosome and BREs. These results suggested that SDPN-1 functions in early endosome to recycling endosome transport, an interpretation that is supported by our

finding that tagged forms of SDPN-1 are clearly enriched on endosomes that contain early and BRE makers. Interestingly, the cargo proteins trapped in *sdpn-1* mutants include examples internalized by clathrin-dependent and clathrin-independent mechanisms, supporting the idea that these cargo types converge in their endocytic transport at the level of the early endosome. Importantly, loss of SDPN-1 did not perturb the localization of retrograde recycling cargo or a model degradative cargo, suggesting that SDPN-1 functions in the exit of specific recycling cargo from the early endosome.

We deem it likely that the observed accumulations of recycling cargo are a consequence of the redistribution of recycling endosomes and the enlargement of early endosomes in *sdpn-1* mutants. *sdpn-1* mutants did not perturb the trafficking of model degradative cargo CD4-dileucine, suggesting that SDPN-1 is not required for the degradative function of late endosomes. Rather, we propose that the observed abnormal morphology of late endosomes in *sdpn-1* mutants is a result of morphologically abnormal early endosomes, and suggest that such late endosomes are still capable of membrane protein degradation and retromer-based recycling to the Golgi.

We demonstrated that full length SDPN-1 is capable of tubulating acidic membranes *in vitro.* One might speculate that SDPN-1 participates in endosomal tubulation, a process that has been proposed to mediate the geometric based sorting of recycling cargo leaving the early endosome (Maxfield and McGraw, 2004). It remains unclear whether these tubules represent the precursors of the tubular recycling endosome compartment (Maxfield and McGraw, 2004a). Intriguingly, the subcellular localization of SDPN-1 is

enriched on both early and recycling endosomes. Our *in vivo* analysis also reveals that the endosomal site of hTFR cargo accumulation in *sdpn*-1 mutants was composed of early and recycling markers. Based on these results we propose that SDPN-1 may facilitate the biogenesis of recycling tubules emanating from the early endosomes that are specific for the transport of cargo to the recycling endosome. Additional studies are needed to confirm whether the formation of recycling endosomes is formed in part by SDPN-1 remodeling of early endosome fission products.

To ensure the direction of recycling endosomal maturation, RAB GTPases and their effectors coordinate the molecular machinery on endosomes. RAB-10 acts as a molecular bridge for early and recycling endosomes, as indicative of its defects in both endosomal markers. *rab-10* mutants display grossly enlarged endosomes with the concomitant loss of RME-1 labeled BREs. Here we show that RAB-10 not only regulates the recruitment of SDPN-1 to endosomes but also facilitates the coupling of RAB-5 to the remaining SDPN-1 labeled structures found at the periphery of the intestine. The correct localization of SDPN-1 to RAB-5 endosomes could represent a subdomain on early endosomes that ensures the dispatch recycling cargo to mature BREs.

Local actin polymerization is also closely associated with membrane budding and fission (Merrifield, 2004; Jović *et al.*, 2009; Romer *et al.*, 2010; Temkin *et al.*, 2011). Actin polymerization on vesicles has been proposed to provide mechanical tension needed to drive vesiculation from donor membrane compartments (Merrifield, 2004; Jović *et al.*,

2009; Romer *et al.*, 2010; Temkin *et al.*, 2011). In fact, syndapin dependent actin polymerization has been proposed to promote many actin driven cellular processes including release of clathrin coated vesicles from the plasma membrane and their movement into the cytoplasm (Qualmann and Kelly, 2000; Romer *et al.*, 2010). The SH3 domain of mammalian syndapin has been shown to bind to actin nucleation-promoting factors (NPFs) including N-WASP and Cordon-Bleu (Cobl) that in turn activate ARP2/3 to polymerize actin, although it is not clear if the these known syndapin-interacting NPFs are found on endosomes (Qualmann *et al.*, 1999; Modregger *et al.*, 2000; Qualmann and Kelly, 2000). Another mechanism proposed for membrane-associated actin is in the stabilization of tubular microdomains on endosomes, as demonstrated in the case of the β2-adrenergic receptor, although syndapin is not known to participate in this process (Puthenveedu *et al.*, 2010). Previous studies in Drosophila, report that syndapin localizes to the cleavage furrow and recruits actin regulators to mediate cytoskeletal remodeling during cytokinesis (Takeda *et al.*, 2013; Sherlekar and Rikhy, 2016)

Because of the importance of actin-based mechanisms in various membrane sculpting events and the association of syndapin with actin regulation we considered a model for early endosomal SDPN-1 in which SDPN-1 promotes a localized burst of actin polymerization concomitant with F-BAR-mediated membrane bending. Indeed we observed a clear enrichment of filamentous actin on SDPN-1 positive endosomes and found that loss of SDPN-1 disrupts the normal enrichment of F-actin on early endosomes. Thus, while further analysis will be required to determine the precise function of such syndapin-regulated endosomal actin, it is likely that syndapin-mediated

endosomal cargo recycling depends upon local syndapin-driven endosomal F-actin accumulation.

Materials and Methods

General methods and strains

All *C. elegans* strains used in this study were derived from the wild-type Bristol strain N2. Genetic crosses and other *C. elegans* husbandry were performed according to standard protocols (Brenner, 1974). Strains expressing transgenes were grown at 20°C. A complete list of the strains used in this study can be found in Table S1.

RNA interference studies were performed using the feeding method (Timmons and Fire, 1998). Feeding constructs were obtained from Ahringer library and sequenced verified. For all experiments, L4 stage animals were treated for 30hr and F1 progeny were scored as adults.

Phenotypic Analysis

Wild-type (N2) and *sdpn-1* mutant worms were grown on solid nematode growth medium (NGM) seeded with *E.coli* OP50 plates. Synchronized L4 staged worms grown at 20°C were scored using a Normaski microscope. Brood size: Five L4 worms were transferred every 24 hours for two days. Eggs laid were counted to determine brood size. If the worm was lost during transfer, that data set was discarded.

Plasmid and Transgenic Strains

For intestinal-specific expression GFP or RFP/mCherry fusion transgenes were cloned into the previously described *vha-6* promoter-driven vector modified with a Gateway

cassette inserted at the Asp718I site just upstream of the GFP and RFP coding region (Chen *et al.*, 2006). All PCR products of the genes of interest were first cloned into the Gateway entry vector pDONR211 by BP reaction (Invitrogen). Isolation of pDONR221 plasmids carrying genes of interest were transferred into the intestinal expression vectors by Gateway recombination cloning, in the LR clonase II (Invitrogen) reaction to generate N-terminal/C-terminal fusions. Low-copy integrated transgenic animals expressing all of these plasmids were obtained by microparticle bombardment (Praitis et al 2001).

To construct the GFP-tagged *sdpn-1* transgene driven by its own promoter, *sdpn-1* genomic and promoter sequences were PCR amplified from the *C. elegans* genomic DNA. Amplified PCR products were then cloned into the entry vector pDONR221 and then transferred into the *C. elegans* pPD117.01 vector containing the Gateway cassette (Invitrogen), followed by GFP coding sequences, let-858 3' UTR sequences and the *unc-119* gene of *C. briggsae*. The GFP tagged construct was bombarded into *unc-119(ed3)* mutant animals to establish low copy integrated transgenic lines by particle bombardment (Praitis and Maduro, 2011).

Protein expression

A PreScission site was added to the full length SDPN-1 cDNA by standard PCR and cloned into a pGEX2T expression plasmid (Amersham) to yield a N-terminally GST-PreScission fusion protein.

Control glutathione S-transferase (Zwaagstra *et al.*) and GST-SDPN-1 fusion proteins were expressed in the *Escherichia coli* Artic Express cells (Stratagene). Bacterial cultures grown in LB were induced at an OD600 of 0.8 with 0.1 mM IPTG and grown

overnight at 12C. Bacterial cells were lysed in 50 mM HEPES (pH 7.5), 400 mM NaCl, 1 mM DTT, 1 mM Phenyl-methyl- sulfonyl fluoride (PMSF) (Sigma Aldrich, St. Louis, MO) using the high pressured homgenizer C. Lysed cells were centrifuged at 10,000*g* for 30 min in a Sorvall SS-34 rotor (Sorvall). The soluble supernatant fraction was centrifuged for another 40 min at 4 °C at 100,000*g* in a Beckman Ti-70 ultracentrifuge rotor (Beckman). Equilbrated with lysis buffer, the supernatant was applied to the Glutathione sepharose 4B column (GE Amersham). The column with bound protein was washed thoroughly with wash buffer (20 mM HEPES at pH 7.5, 150 mM NaCl, 1mM MgCl2, 1 mM DTT). The GST moiety was cleaved by using the 225 ug PreScission protease (GE Amersham). To check the purity of tagless protein, cleaved SDPN-1 was analyzed by SDS-PAGE followed by Coomassie staining. Cleaved protein was eluted with several volumes of wash buffer and snap frozen in liquid nitrogen and stored in the -80C. For proteoliposome assays, the frozen aliquots were rapidly thawed, then spun at 20,000*g* at 4°C to remove any aggregated protein. Protein concentration was determined under denaturing conditions by absorbance at 280 nm.

Liposome preparation

Phosphatidylserine (PtdSer) lipids were purchased from Avanti Polar Lipid Inc (Alabaster). For liposome preparation, chloroform was evaporated under continuous stream of argon gas and subjected to vacuum desiccation overnight. PtdSer lipids were then resuspended at 1mg/ml concentration in argo-purged liposome buffer (20 mM HEPES at pH 7.5, 150 mM NaCl, 1 mM $MgCl_2$). 0.4 um average diameter liposomes were formed by using 0.4 um polycoarbonate track-etched membrane filters Whatman Ltd) with a Avanti Mini Extruder as per manufacturer's instructions (Polar Lipids, Inc).

Liposome tubulation assays For proteoliposome tubulation assays, 2.5μM SDPN-1 was incubated with 0.5 mg/ml final concentration of 100% PtdSer liposomes in liposome buffer. All samples were incubated on ice for 4 min and 12 min after the start of protein addition the samples were spotted on 300 mesh carbon-formvar-coated copper grid (Prokopenko *et al.*). Grids were negatively stained with 1% uranyl acetate at 25C for 1.5 minutes. To examine membrane morphologies, electron microscopy was performed using a JEOL 1200 EX or JEOL 100 CX transmission electron microscope at 80 KV. Images were obtained at 50,000x magnification as indicated. Quantification of liposome tubule diameter was performed using Fiji (Image J) Measurement function. Mean values were calculated and plotted on graphs. Standard error of the mean (SEM) was calculated and used as Y-error bars on graphs.

Transmission Electron Microscopy

Young adult wild-type animals were prepared for electron microscopy by a standard immersion fixation protocol (Hall, 1995). Well fed animals were moved from the culture plate into buffered aldehyde fixative, and immediately cut open with a razor blade to allow access to the fixative past the cuticle. After fixing in aldehydes, worms were rinsed in buffer and re-fixed in buffered osmium tetroxide, en bloc stained with uranyl acetate, then dehydrated and embedded into Epon for thin sectioning. Mutant animals (*ok1667*) prepared by high pressure freezing and freeze substitution (HPF/FS) following a standard protocol (Hall et al., 2012). Briefly, animals were moved from the culture plate into an HPF sample carrier in a slurry of *E. Coli*, the sample carrier closed and fast frozen in a Baltec HM 010 high pressure freezer. Frozen samples were freeze

substituted into 2% osmium tetroxide, 2% water in acetone over 5 days, then rinsed in cold acetone and embedded in plastic. For all samples, thin sections were collected on a diamond knife, mounted on Formvar-coated slot grids, post-stained with uranyl acetate and examined in a Philips CM10 electron microscope, fitted with an Olympus Morada digital camera. For best views of the intestinal lumen, we chose animals that had been sectioned lengthwise, and we viewed the anterior lumen at the level of INT 1 and INT2, before the intestine is squeezed by the gonad, and behind the swollen lumen of anterior most portion of INT1.

Microscopy and Image Analysis. Live worms were mounted on 10% agarose pads with 10 mM levamisol as described previously (Sato et al 2005). Multiwavelength fluorescence colocalzation images were obtained using the Axio Imager. Z1 (Carl Zeiss MicroImaging) equipped with YOKOGAWA CSU-X1 spinning disk, Photometrics Evolve 512 EMCCD camera, captured using Metamorph software (Universal Imaging). Out of focus light from captured images was removed with constrained iterative deconvolution algorithm using AutoQuant X5 (AutoQuant Imaging). Images taken in the DAPI channel were used to identify broad-spectrum intestinal autofluorescences caused by lipofuscin-positve lysosome-like organelles (Clokey and Jacobson, 1986, Hermann et al., 2005). Quantification of colocalization images were done using the open source Fiji (Image J) software (Schindelin *et al.*, 2012) Fiji: an open-source plat- form for biological-image analysis. To obtain intestinal images of GFP fluorescence with interference from autofluorescence, we used argon 488-nm excitation and the spectral fingerprinting function of the Zeiss LSM510/710 Meta confocal microscope system (Carl Zeiss Micro

Imaging) as described previously (Chen *et al.*, 2006). Quantification of images were performed with Metamorph Version 6.3r2 (Universial Imaging).

Acknowledgements

We would like to thank David Luo, Tanvi Gopal, and Peter Schweinsberg for technical assistance in making plasmid clones and biolistic transgenic lines. Michael Pierce and Joseph Kramer for help with confocal microscopy. This work was supported by the NIH Grants GM067237 and GM103995 (to B.D.G.), 6R24OD010943 (to D.H.H), and the Anne B. and James B. Leathem Fellowship (to A.M.G).

Figure legends

Figure 1. (A) Genomic structure of *sdpn-1* gene and the location of the *ok1667* mutant deletion. *ok1667* is a 2547 bp deletion from the second exon to the eighth exon. (B) The *ok1667* allele deletes sequences encoding aa90-351, encompasses the majority of the F-BAR domain, and places other sequences out of frame. (C-E) *In vitro* membrane tubulation of Ptd-Ser liposomes by full length SDPN-1. Electron micrographs of acidic liposomes Ptd-Ser liposomes (0.05 mg/ml average 400 μm diameter) incubated with 2.5 μM of (C) GST or (D) full length SDPN-1. (E) Statistical Analysis: Diameters of membrane tubules shown in (D) were quantified on at least 3 independently prepared EM grids. Scale bar, 200 μm.

Figure 1

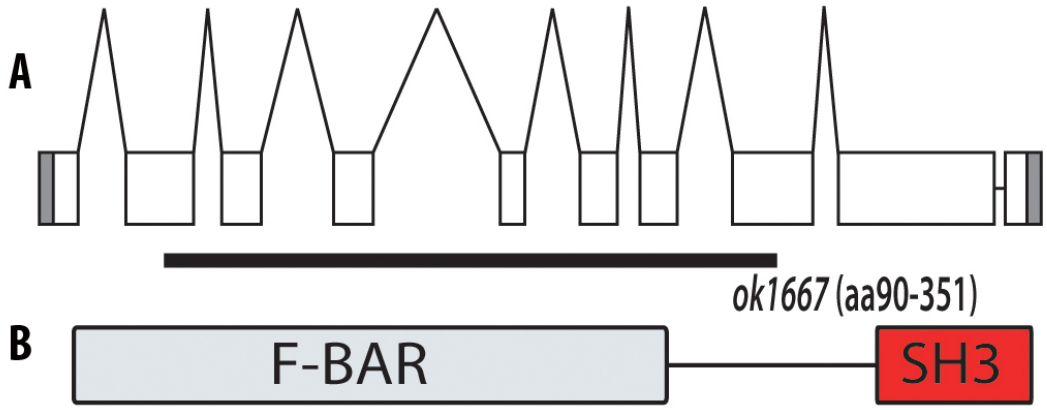
A
ok1667 (aa90-351)
B
F-BAR
SH3

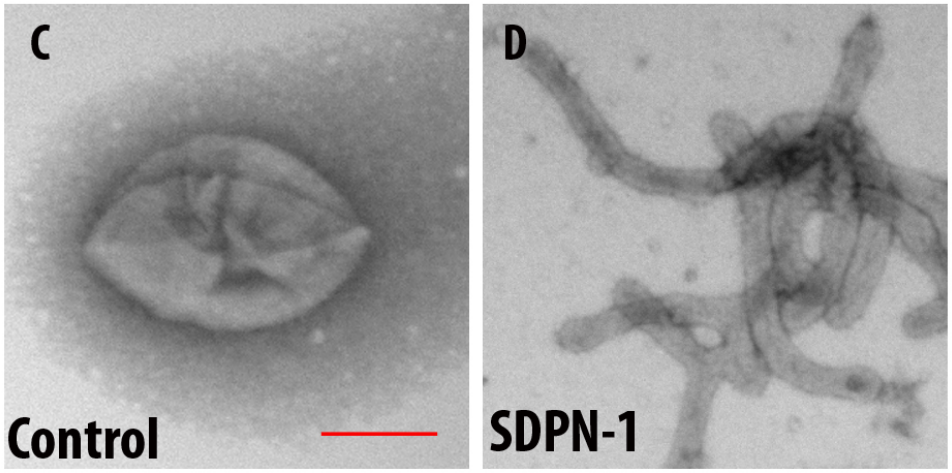
C
Control
D
SDPN-1

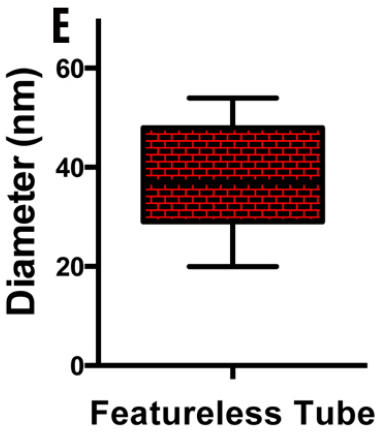
E
Diameter (nm)
60
40
20
0
Featureless Tube

Figure 2. *sdpn-1* mutants disrupt cargo traveling from the early to recycling endosome. All images are laser scanning confocal micrographs of the worm intestine expressing GFP-tagged transmembrane cargo proteins whose post-internalization trafficking routes are well characterized. In wild-type worms, the (A) human transferrin receptor, hTfR::GFP and (D) the IL-2 receptor alpha chain [hTAC::GFP] predominantly label the basolateral plasma membrane. Loss of SDPN-1 function results in intracellular accumulation of recycling cargos (B) hTfR::GFP and (E) hTAC-GFP. Quantification of (D) hTFR::GFP and (F) hTAC::GFP micrographs. Total intensity was measured for 6 animals for each genotype sampled in three different regions of each intestine. Expression remained comparable to wild-type in *sdpn-1(ok1667)* mutants for the WNT ligand chaperone, MIG-14::GFP (G&H), and the degradative transmembrane receptor CD4-dileucine (J&K) Quantification of MIG-14::GFP (I) and CD4-dileucine (L) micrographs. Total intensity was measured for 6 animals for each genotype sampled in three different regions of each intestine. Error bars represent SEM. ****P<0.0001 (student's t-test). Scale bar, 10 μm.

Figure 2

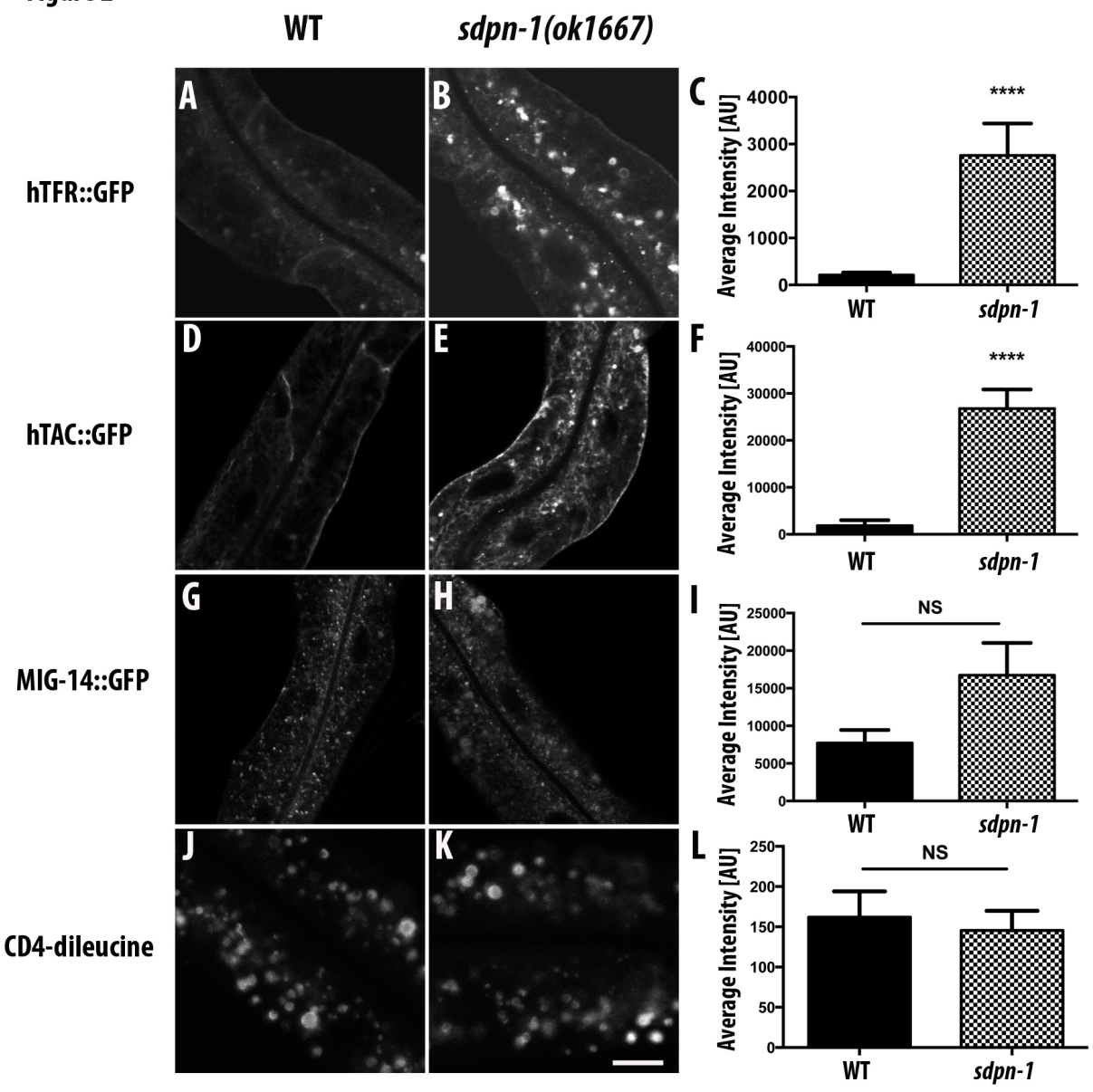
WT
sdpn-1(ok1667)
hTFR::GFP
hTAC::GFP
MIG-14::GFP
CD4-dileucine
A
B
C
D
E
F
G
H
I
J
K
L
Average Intensity [AU]
4000
3000
2000
1000
0
****
WT
sdpn-1
40000
30000
20000
10000
25000
15000
5000
NS
250
200
150
100
50

Figure 3. SDPN-1 differentially affects endosomal morphology**.** All images are laser scanning confocal micrographs of the worm intestine expressing GFP-tagged fusion proteins that are resident markers for distinct endosomal compartments. *sdpn-1* mutants show accumulation of early endosomes labeled with GFP::RAB-5 and late endosomes marked with GFP::RAB-7 and GFP::RAB-10 labeled BREs. Control micrographs in the wild-type background (A) GFP::RAB-5, (D) GFP::RAB-7 and (G) GFP::RAB-10. Confocal images in the *sdpn-1(ok1667)* background are shown for (B) GFP::RAB-5, (E) GFP::RAB-7, and (H) GFP::RAB-10. Quantification of total intensity for (C) GFP::RAB-5, (F) GFP::RAB-7, and (I) GFP::RAB-10 micrographs.

Error bars represent SEM: ***P<0.001, ****P<0.0001 (student's t-test). Scale bar, 10 μm (B, E, H) Confocal micrographs taken at higher magnification (100x) show detailed organization of GFP::RME-1 labeled tubulovesicular meshwork (top plane). Intensity of GFP::RME-1 (K) in *sdpn-1* mutants increase when compared to (J) wild-type. When compared to (M) wild-type, cross sectional views show a redistribution of RME-1 labeled endosomes in (N) *sdpn-1(ok1667)* mutant animals. Quantification of GFP::RME-1 micrographs (L) top[basolateral] and (O) middle [cross section]. Error bars represent SEM: ***P<0.001, ****P<0.0001 (student's t-test). (P) GFP- labeled puncta number of each endosomal compartment. Error bars represent SEM: *P<0.05, **P<0.01, ****P<0.0001 (two-way ANOVA). Scale bar, 10 μm (K, N). 6 animals for each genotype sampled in three different regions of each intestine.

Figure 3

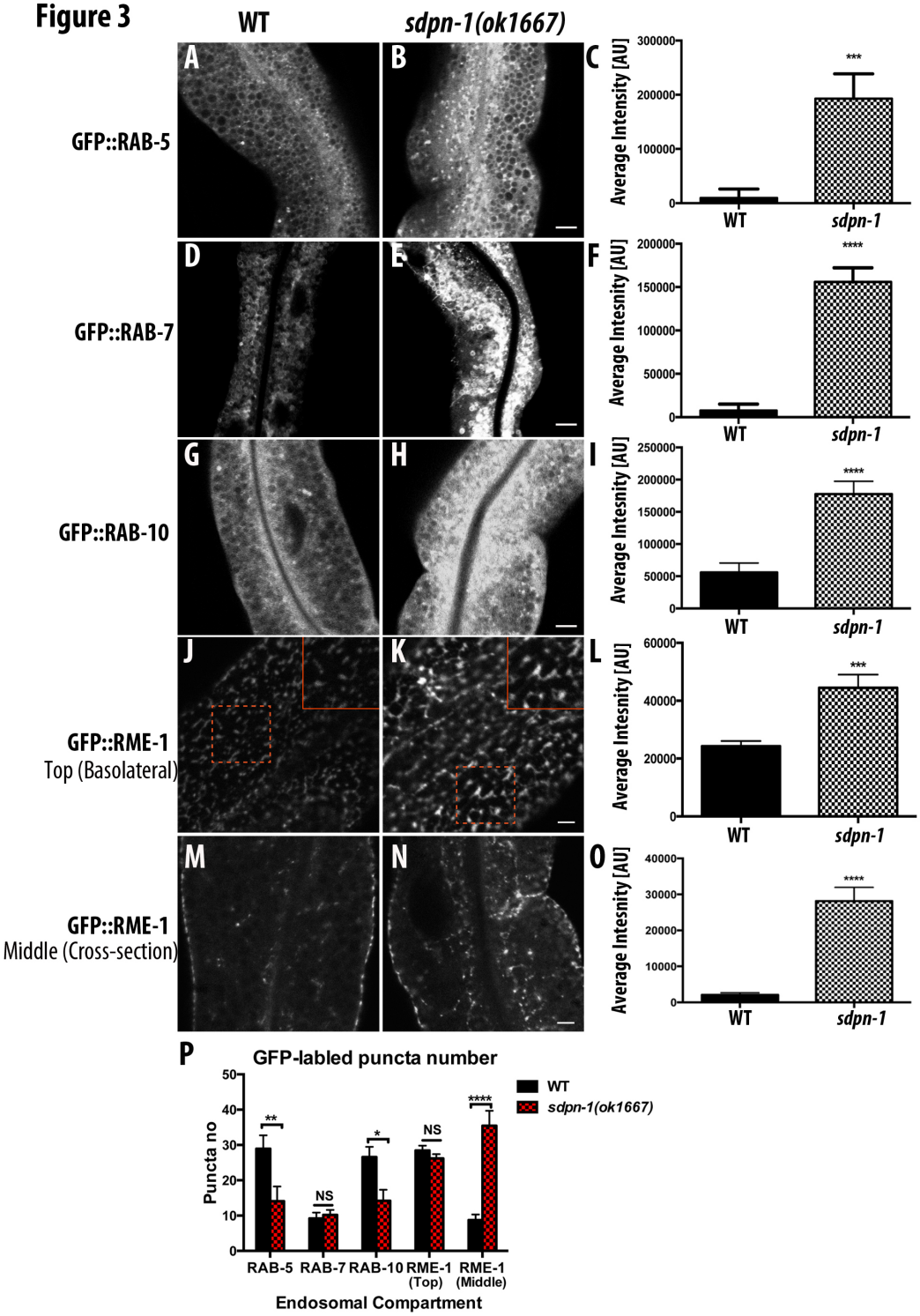
WT
sdpn-1(ok1667)
A
B
C
GFP::RAB-5
Average Intensity [AU]
300000
200000
100000
0
***
WT
sdpn-1
D
E
F
GFP::RAB-7
Average Intesnity [AU]
200000
150000
100000
50000
0
****
WT
sdpn-1
G
H
I
GFP::RAB-10
Average Intesnity [AU]
250000
200000
150000
100000
50000
0
****
WT
sdpn-1
J
K
L
GFP::RME-1
Top (Basolateral)
Average Intesnity [AU]
60000
40000
20000
0
***
WT
sdpn-1
M
N
O
GFP::RME-1
Middle (Cross-section)
Average Intesnity [AU]
40000
30000
20000
10000
0
****
WT
sdpn-1
P
GFP-labled puncta number
Puncta no
50
40
30
20
10
0
**
NS
*
NS
****
WT
sdpn-1(ok1667)
RAB-5
RAB-7
RAB-10
RME-1 (Top)
RME-1 (Middle)
Endosomal Compartment

Figure 4. Loss of SDPN-1 traps recycling cargo hTFR in abnormal compartment positive for early and recycling markers. All micrographs are from deconvolved 3D confocal image stacks acquired in intact living animals expressing intestinal specific GFP and RFP tagged proteins. White arrow heads depict positive colocalization. Under control conditions recycling cargo hTFR::GFP and tagRFP::RAB-5-labeled early endosomes displayed minimal overlap under (A-A'''). A strong increase in localization of hTFR::GFP and tagRFP::RAB-5 was observed in (B-B''') *sdpn-1 RNAi* animals. (D-D''') hTFR::GFP and tagRFP::RME-1 displayed an increase in overlap in *sdpn-1 RNAi* animals when compared to (C-C'") control conditions. In each image autofluorescent lysosome-like organelles appear in blue in all three channels, whereas GFP appears only in the green channel and RFP appears only in the red channel. Green and red signal that does not overlap with the blue channel represent pure GFP and RFP signals respectively. (C) Pearson's correlation coefficient for each endosomal compartment. n =6 animals. Error bars represent SEM: **P<0.01. Scale bar, 10 μm.

Figure 4

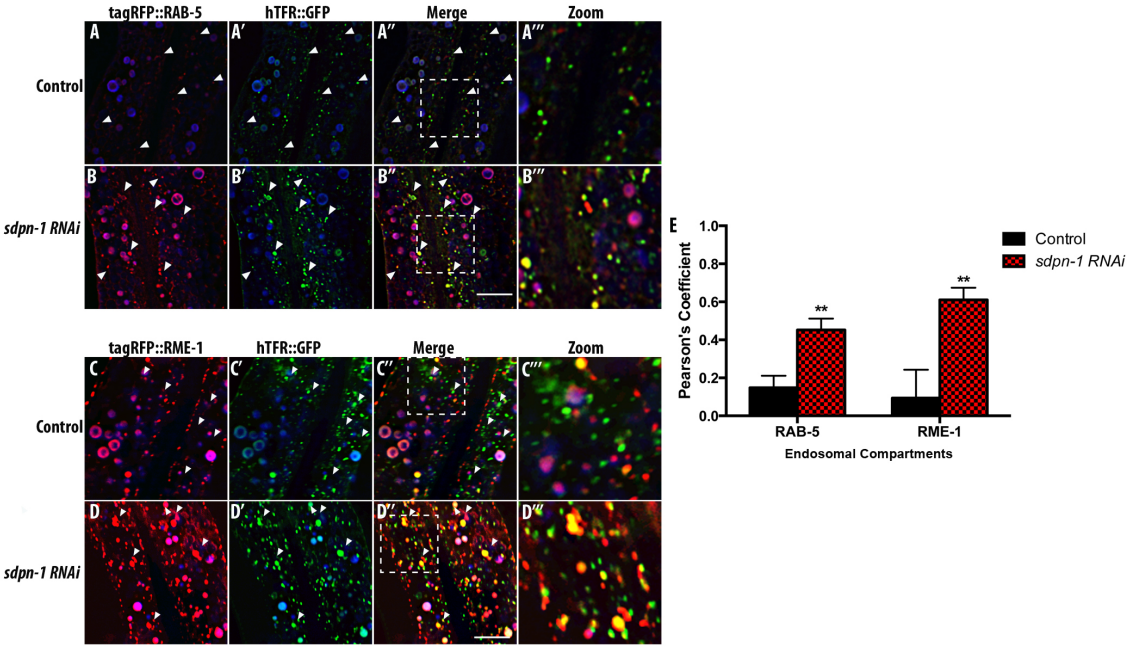
tagRFP::RAB-5
hTFR::GFP
Merge
Zoom
Control
sdpn-1 RNAi
tagRFP::RME-1
hTFR::GFP
Merge
Zoom
Control
sdpn-1 RNAi
E
Pearson's Coefficient
1.0
0.8
0.6
0.4
0.2
0.0
**
**
RAB-5
RME-1
Endosomal Compartments
Control
sdpn-1 RNAi

Figure 5. SDPN-1 predominately resides on early and recycling endosomes All micrographs are from deconvolved 3D confocal image stacks acquired in intact living animals expressing intestinal specific GFP- and RFP- tagged proteins. (A-A''') SDPN-1::GFP resides on RAB-5 labeled early endosomes. White Arrowheads indicate endosomes labeled by both SDPN-1::GFP and tagRFP-RAB-5. (A''') Magnified image of (A'') is designated by the rectangular outline. (B-B''') SDPN-1::GFP is also enriched on tagRFP-RME-1 endosomes. White arrowheads indicate positive colocalization between SDPN-1::GFP and tagRFP::RME-1. (B''') Magnified image of (B'') is designated by the rectangular outline. (C) Pearson's correlation coefficient for colocalization of SDPN-1::GFPGFP with tagRFP-RAB-5 and tagRFP-RME-1. n =6 animals. Error bars represent SEM: $P<0.01$. Scale bar, 10 μm.

Figure 5

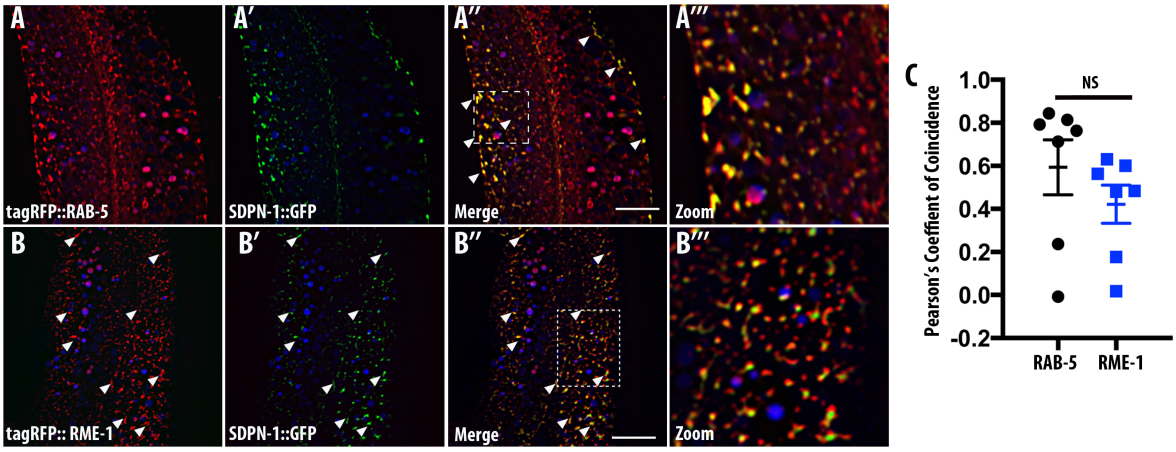
A
A′
A″
A‴
tagRFP::RAB-5
SDPN-1::GFP
Merge
Zoom
B
B′
B″
B‴
tagRFP:: RME-1
SDPN-1::GFP
Merge
Zoom
C
Pearson's Coeffient of Coincidence
1.0
0.8
0.6
0.4
0.2
0.0
-0.2
NS
RAB-5
RME-1

Figure 6. *rab-10(RNAi)* animals fail to recruit SDPN-1 to endosomes and segregates RAB-5 from the remaining SDPN-1 labeled structures. All micrographs are from deconvolved 3D confocal image stacks acquired in intact living animals expressing intestinal specific GFP and RFP tagged proteins. Under (A-A''') control conditions SDPN-1::GFP and tagRFP::RAB-5 colocalize extensively on endosomes. White arrow heads indicate positive overlap. (C-C''') *rab-10(RNAi)* mutants displayed a decrease in overlap between SDPN-1::GFP AND RAB-5:: GFP. Grey arrows indicate SDPN-1::GFP labeled structures devoid of RAB-5. In each image autofluorescent lysosome-like organelles appear in blue in all three channels, whereas GFP appears only in the green channel and RFP appears only in the red channel. Green and red signal that does not overlap with the blue channel represent pure GFP and RFP signals respectively. (B) Quantification of SDPN-1::GFP puncta number. (D) Pearson's correlation coefficient for SDPN-1::GFP and tagRFP::RAB-5. n =6 animals. Error bars represent SEM: **P<0.01. Scale bar, 10 μm.

Figure 6

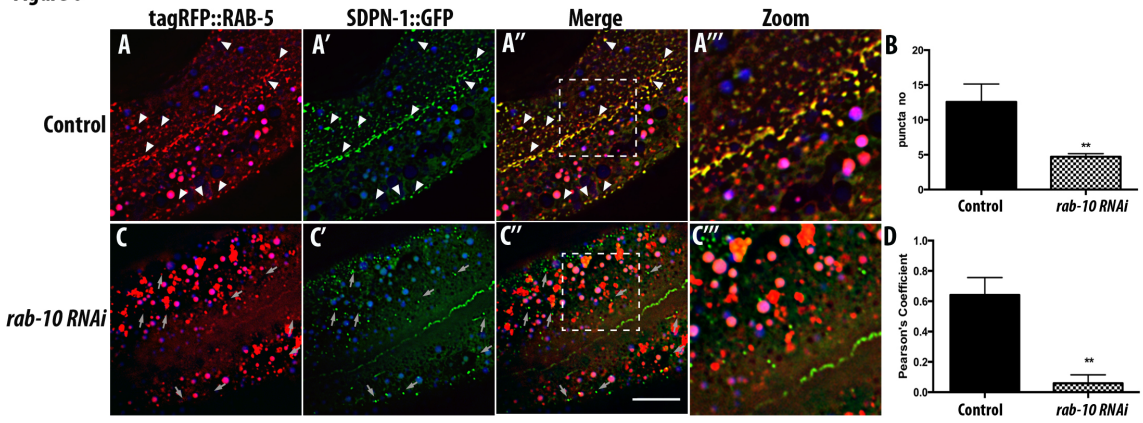
tagRFP::RAB-5
SDPN-1::GFP
Merge
Zoom
A
A′
A″
A‴
Control
C
C′
C″
C‴
rab-10 RNAi
B
puncta no
20
15
10
5
0
**
Control
rab-10 RNAi
D
Pearson's Coefficient
1.0
0.8
0.6
0.4
0.2
0.0
**
Control
rab-10 RNAi

Figure 7. Filamentous actin localizes to SDPN-1 positive endosomes**.** All micrographs are from deconvolved 3D confocal image stacks acquired in intact living animals expressing intestinal specific GFP- and RFP- tagged proteins. LifeAct-tagRFP, an F-actin biosensor containing 17 amino acids of the yeast actin binding protein ABP-140, was used to report filamentous actin in intestinal cells. White arrow heads depict positive overlap. (A-A''') SDPN-1::GFP- positive labeled endosomes are enriched in filamentous actin. Arrowheads correspond to positive colocalization between SDPN-1::GFP and LIFE ACT::tagRFP. (A''') Magnified image of (A'') is designated by the rectangular outline. In each image autofluorescent lysosomse-like organelles appear in blue in all three channels, whereas GFP appears only in the green channel and RFP appears only in the red channel. Green and red signal that does not overlap with the blue channel represent pure GFP and RFP signals respectively. (C) Pearson's correlation coefficient for colocalization of SDPN-1::GFPGFP with LifeAct-tagRFP was 0.6 on average. n =6 animals. Error bars represent SEM. Scale bar, 10 μm.

Figure 7

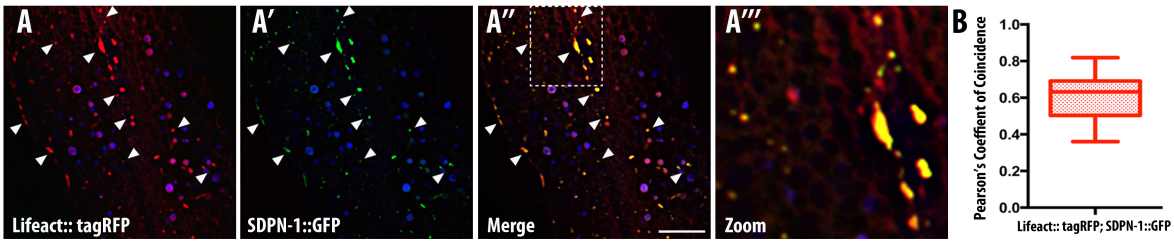
A
A′
A″
A‴
B
Lifeact:: tagRFP
SDPN-1::GFP
Merge
Zoom
Pearson's Coeffient of Coincidence
1.0
0.8
0.6
0.4
0.2
0.0
Lifeact:: tagRFP; SDPN-1::GFP

Figure 8. SDPN-1 recruits filamentous actin to early endosomes

All micrographs are from deconvolved 3D confocal image stacks acquired in intact living animals expressing intestinal specific GFP-tagged recycling cargo Life act-GFP and tagRFP-RAB-5 in Control RNAi (A-A''') and *sdpn-1(RNAi)* (B-B'''). In control animals, LifeAct::GFP positive puncta is enriched on tagRFP::RAB-5 labeled early endosomes White arrowheads indicate positive colocalization. (B-B''') A striking decrease in localization of LifeAct::GFP and tagRFP::RAB-5 was seen in *sdpn-1 RNAi* animals. Grey arrows indicate early endosomes depleted of filamentous actin. In each image autofluorescent lysosomse-like organelles appear in blue in all three channels, whereas GFP appears only in the green channel and RFP appears only in the red channel. Green and red signal that does not overlap with the blue channel represent pure GFP and RFP signals respectively. (C) Pearson's correlation coefficient for colocalization of LifeAct::GFP with tagRFP::RAB-5. n =6 animals. Error bars represent SEM.***P<0.001 (student's t-test) Scale bar, 10 μm.

Figure 8

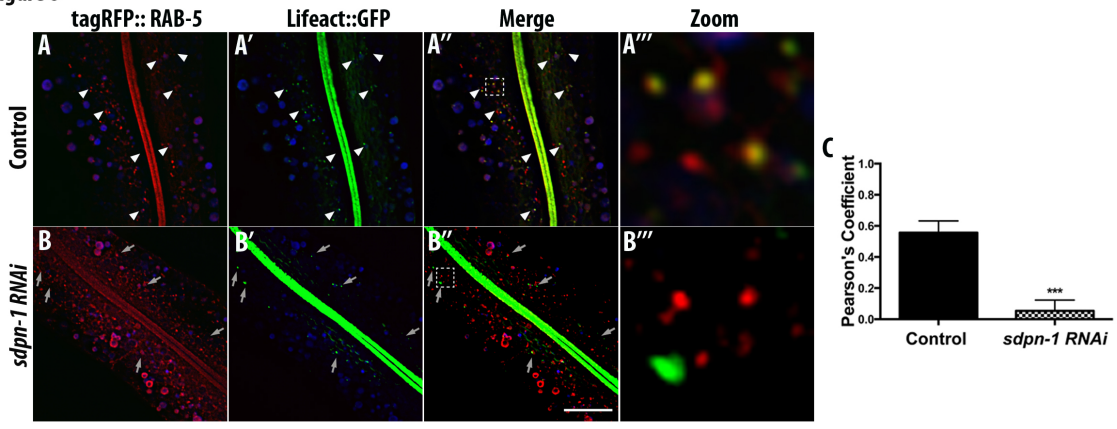
tagRFP:: RAB-5
Lifeact::GFP
Merge
Zoom
Control
sdpn-1 RNAi
A
A′
A″
A‴
B
B′
B″
B‴
C
Pearson's Coefficient
1.0
0.8
0.6
0.4
0.2
0.0
***
Control
sdpn-1 RNAi

Supplemental Figure S1. Expression profile of SDPN-1 in *C. elegans.* Confocal images of the (A) pharynx (arrowhead), and neuron (arrow), (B) intestine (Middle); arrow heads indicate the basolateral intestinal puncta and membranes, and (C) arrows indicate the apical intestinal membrane and basolateral intracellular puncta. Scale bar 10 μm.

Supplementary Figure S1

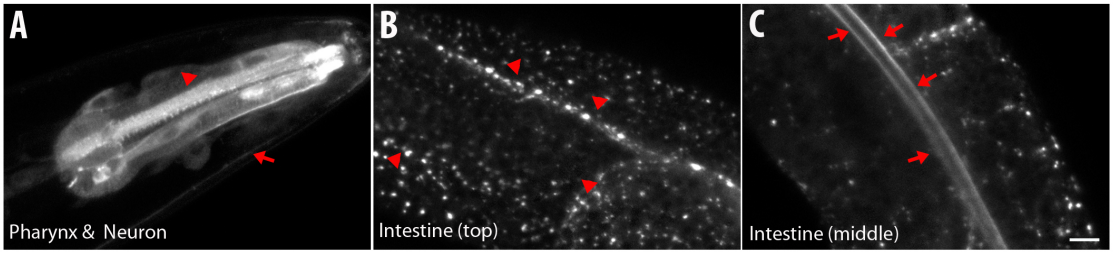

Supplemental Figure S2. *sdpn-1* mutants display differential trafficking phenotypes of TGF-beta receptors DAF-4 (type II) and SMA-6 (type I). Loss of SPDN-1 function resulted in aberrant accumulations of recycling-dependent cargo DAF-4::GFP. In contrast, for SMA-6::GFP, a retromer dependent cargo, levels in *sdpn-1* mutants were comparable to wild-type. n =6 animals. Error bars represent SEM:***P<0.001. Scale bar, 10 μm.

Supplementary Figure S2

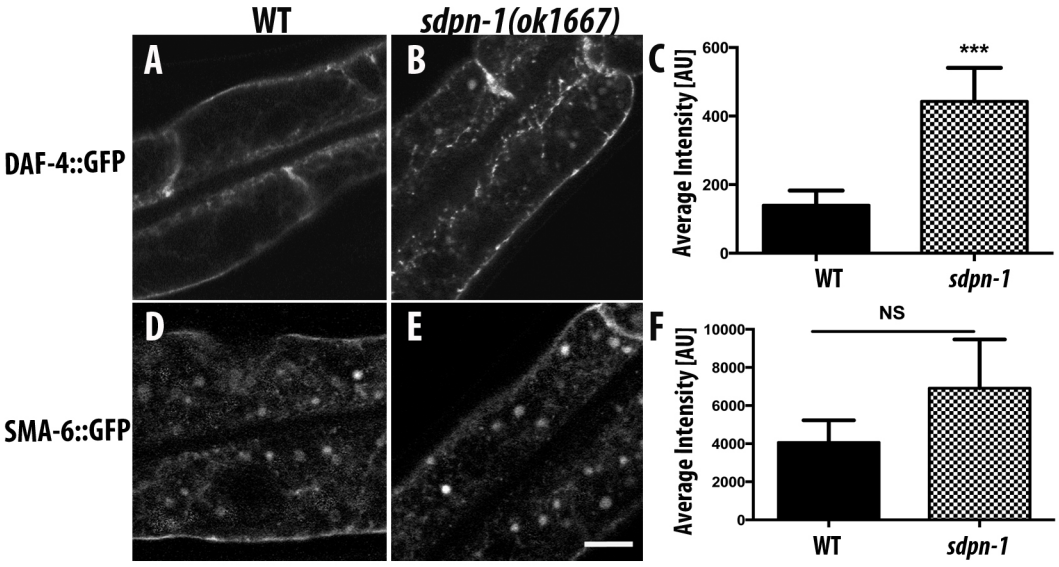

Supplemental Figure S3. SDPN-1::tagRFP can rescue the intestinal phenotype of *sdpn-1(ok1667)* null mutants. Confocal images of the intestine: (A) Control hTFR::GFP, (B) *ok1667;*hTFR::GFP, (C) and *ok1667,* hTFR::GFP, SDPN-1::tagRFP. Red Arrow indicate abnormal accumulations of hTFR::GFP. (D). Quantification of total intensity for micrographs. 6 animals for each genotype sampled in three different regions of each intestine. Error bars represent SEM. *P< 0.05, **P< 0.01 by analysis of variance (Beramendi *et al.*). Scale bar, 10 μm

Supplemental Figure S3

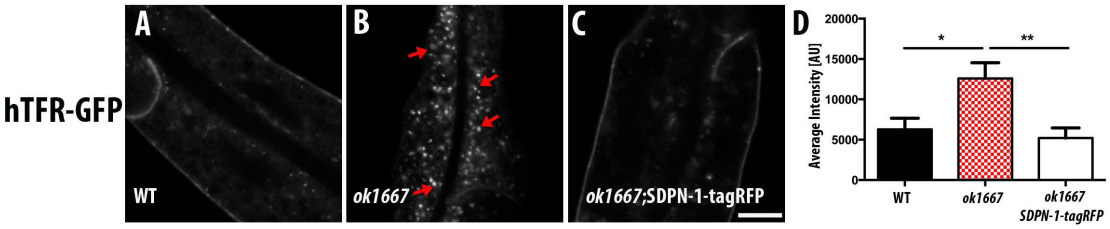

Supplemental Figure S4. Loss of function mutation in *sdpn-1* displays a convoluted lumen but normal microvilli. (A). 3D max projection of confocal micrographs representing (A) wild-type and (B) *sdpn-1* mutant intestinal cells revealed perturbations in the apical lumen (n =6 animals). TEM images: (C) wild-type shows normal distribution of organelles and a single lumen. (D) *sdpn-1* animals displayed a grossly expanded lumen. In comparison to (E) wild-type animals, (F) loss of SDPN-1 function did not disrupt the integrity of the associated microvilli and terminal web. Scale bar 10 μm (B), 5 μm (D), 1μm (F).

Supplemental Figure S4

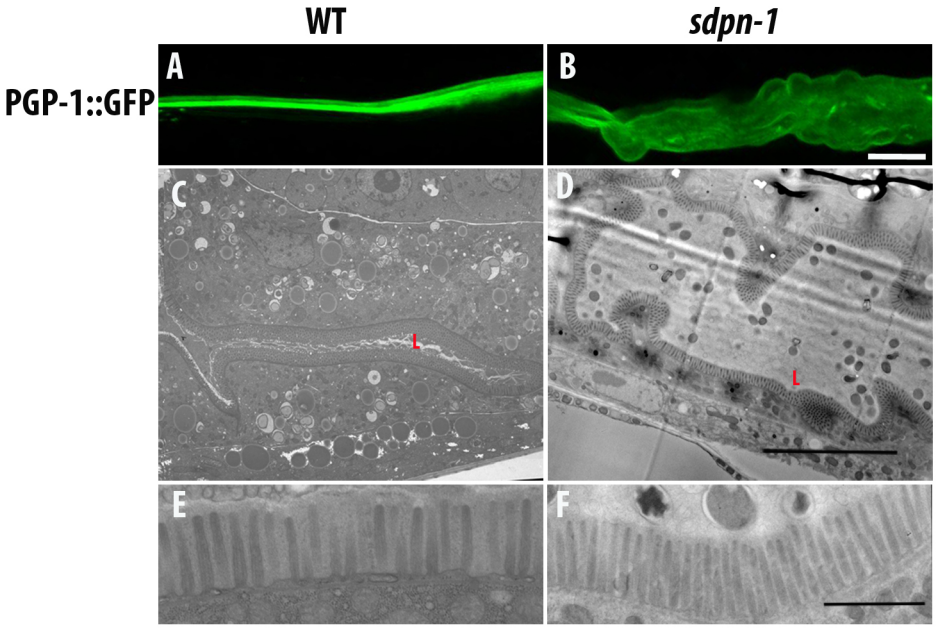

Supplemental Figure S5. Average area for GFP-labeled endosomal compartments. Quantification of the average area (per unit region) for GFP-labeled endosomal compartment. (A) GFP::RAB-5, (B) GFP::RAB-7, (C) GFP::RAB-10, (D) GFP::RME-1. Error bars are SEM: Asterisks indicate significant differences in the one-tailed Student's t-test (*P<0.05, *** P< 0.001),**** P< 0.0001). 6 animals of each genotype sampled in three different regions of each intestine positioned at random.

Supplemental Figure 5

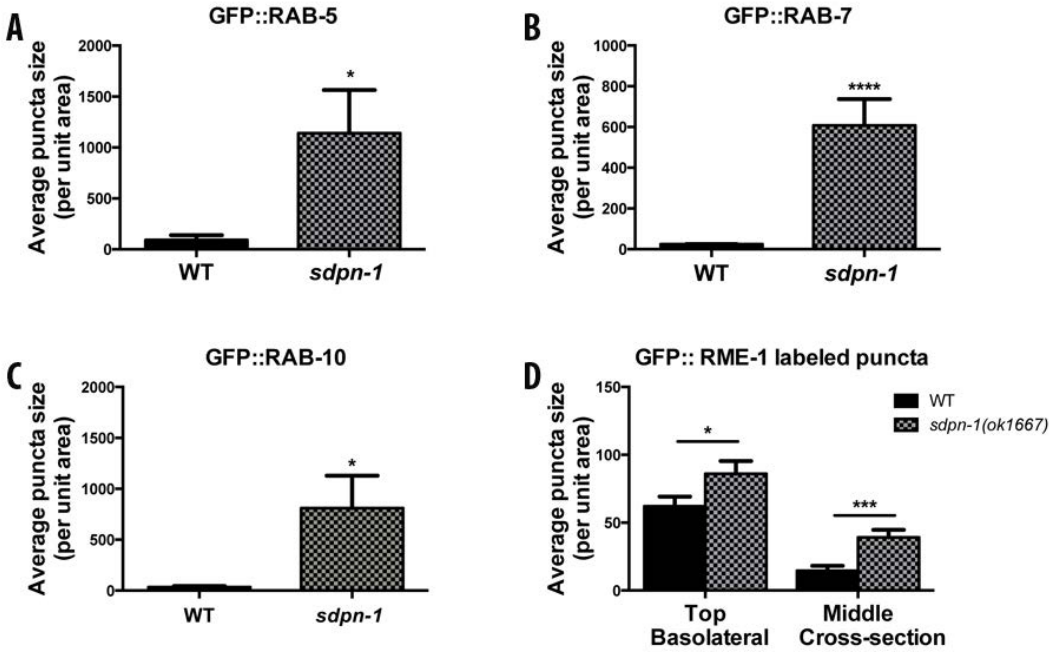

Supplemental Figure S6. *sdpn-1* mutants did not disrupt GFP::RAB-11 apical recycling endosomes. Apical recycling endosomes remained normal in *sdpn-1 (RNAi)* mutants. All images are laser scanning confocal micrographs of the worm intestine expressing GFP::RAB_11. (A&B) Expression and morphology in *sdpn-1(RNAi*) remained comparable to wild-type. Statistical analysis: (D) Average area (per unit area) and (E) Average Intensity. Error bars are SEM. 6 animals of each genotype sampled in three different regions of each intestine positioned at random. Scale bar, 10 μm.

Supplemental Figure 6

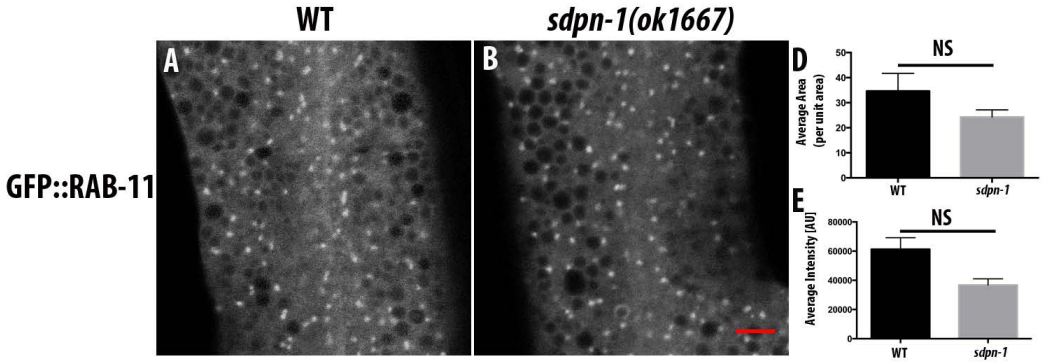

Supplemental Figure S7. Accumulations of recycling cargo are not trapped in RAB-7 labeled late endosomes and RAB-10 labeled BREs. Representative images of (A-A’’’) control animals (B-B’’’) *sdpn-1(RNAi)* animals expressing, recycling cargo hTFR::GFP and tagRFP::RAB-7-labeled late endosomes. White arrow heads depict positive overlap. Representative images of (C-C’’’) control animals (D-D’’’) *sdpn-1(RNAi)* animals expressing, recycling cargo hTFR::GFP and tagRFP::RAB-10-labeled BREs. Grey arrows indicate recycling cargo hTFR devoid of RAB-10. In each image autofluorescent lysosome-like organelles appear in blue in all three channels, whereas GFP appears only in the green channel and RFP appears only in the red channel. Green and red signal that does not overlap with the blue channel represent pure GFP and RFP signals respectively. (C) Pearson’s correlation coefficient for each endosomal compartment. n =6 animals. Error bars represent SEM. Scale bar, 10 μm

Supplemental Figure 7

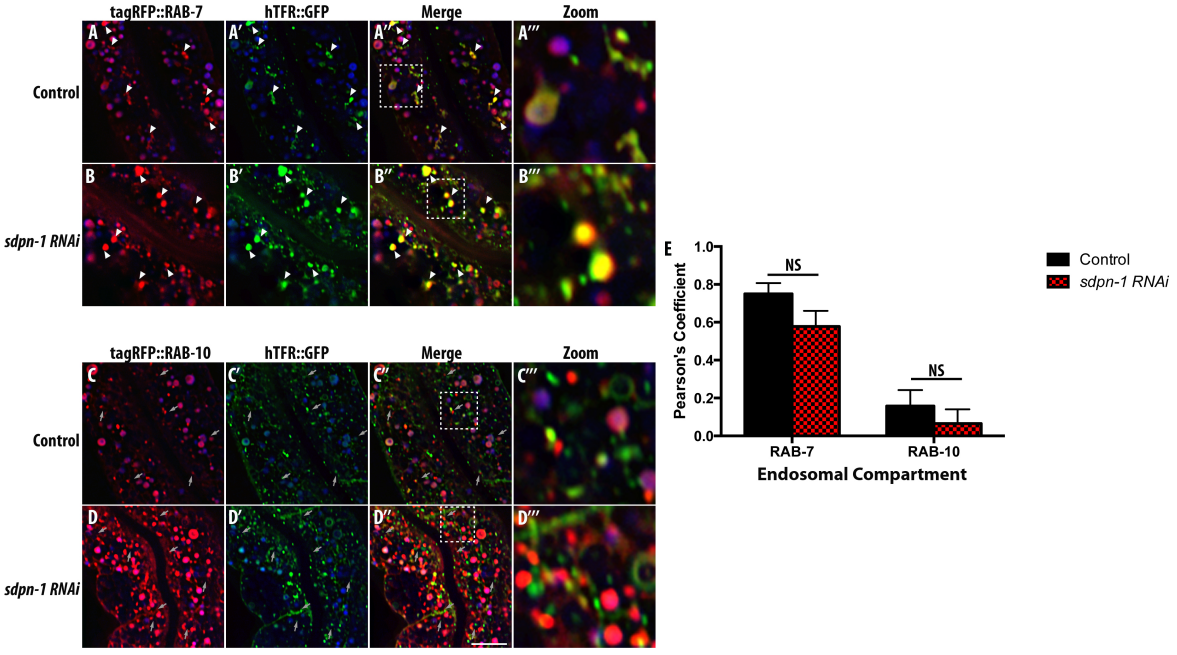

Supplemental Figure S8. SDPN-1 is occasionally found on late endosomes and is not enriched on Golgi. (A-A'') SDPN-1::GFP partially colocalizes with RAB-7 labeled late endosomes. (B-B'') SDPN-1::GFP is not found on Golgi structures (n =6 animals). All micrographs are from deconvolved 3D confocal image stacks acquired in intact living animals expressing intestinal specific GFP- and RFP- tagged proteins. Scale bar, 10 μm.

Supplemental Figure 8

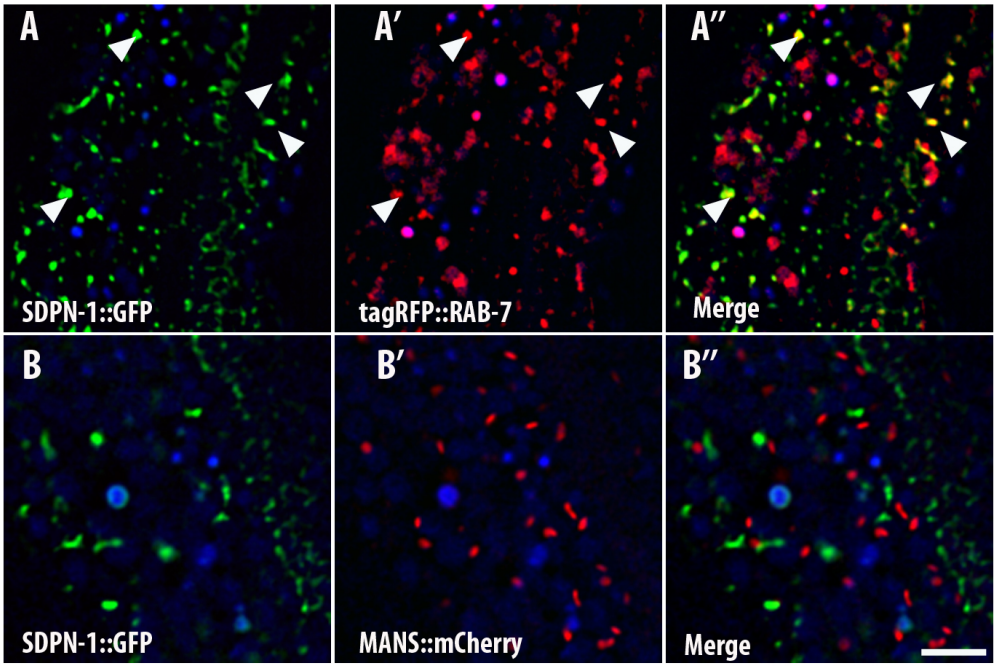

Supplemental Figure S9. LifeAct is not enriched on late or recycling endosomes. All micrographs are from deconvolved 3D confocal image stacks acquired in intact living animals expressing intestinal specific GFP- and RFP- tagged proteins. (A-A'') LifeACT::GFP is not found on (A-A'') tagRFP::RAB-7 labeled late endosomes nor (B-B'') tagRFP::RME-1 labeled BRE. (n =6 animals). Scale bar, 10 μm.

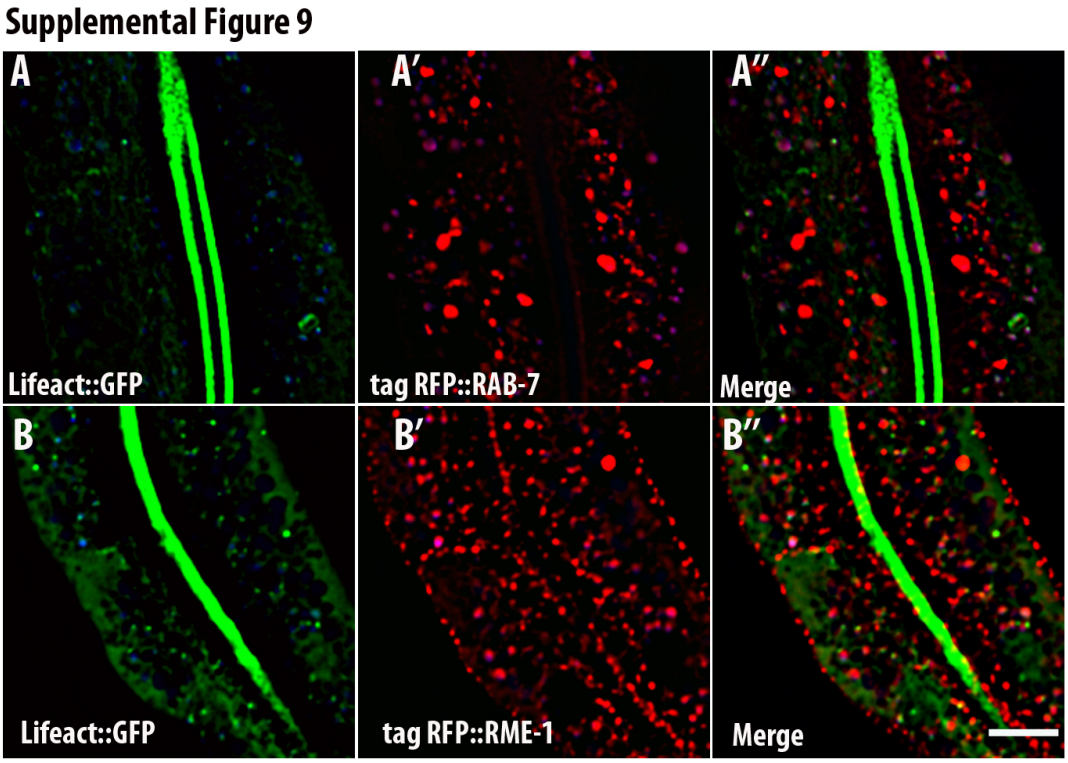

Supplemental Figure S10. RAB-10 recruits filamentous actin to early endosomes.

All micrographs are from deconvolved 3D confocal image stacks acquired in intact living animals expressing intestinal specific GFP-tagged recycling cargo Life act-GFP and tagRFP-RAB-5 in (A-A’’’) In control animals, LifeAct::GFP positive puncta is enriched on tagRFP::RAB-5 labeled early endosomes. White arrowheads indicate positive colocalization. (B-B’’’) A striking decrease in localization of LifeAct::GFP and tagRFP::RAB-5 was seen in *rab-10(RNAi)* animals. Grey arrows indicate early endosomes depleted of filamentous actin. In each image autofluorescent lysosomse-like organelles appear in blue in all three channels, whereas GFP appears only in the green channel and RFP appears only in the red channel. Green and red signal that does not overlap with the blue channel represent pure GFP and RFP signals respectively. (C) Pearson’s correlation coefficient for colocalization of LifeAct::GFP with tagRFP::RAB-5. n =6 animals. Error bars represent SEM.****P<0.001 (student’s t-test) Scale bar, 10 μm

Supplemental Figure 10

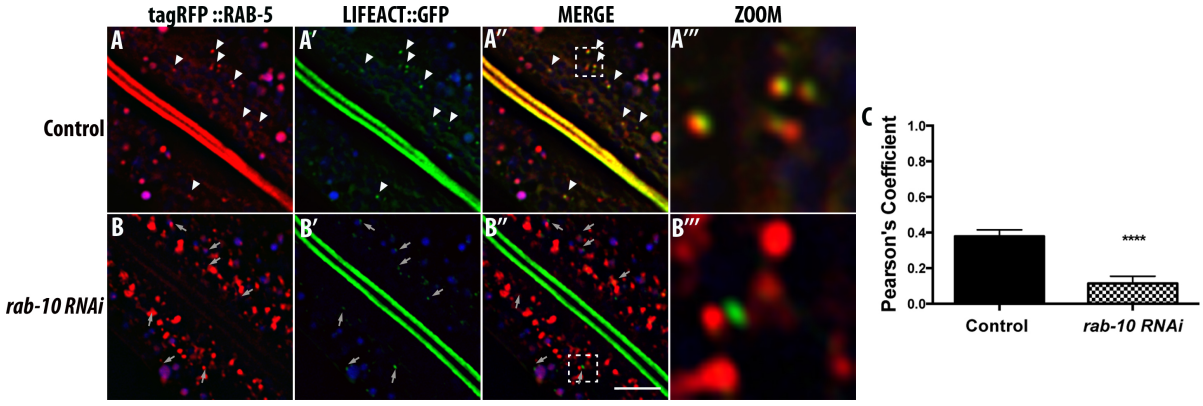

Chapter III

BMP signaling requires retromer-dependent recycling of the type I receptor

This work is published under the same title by Ryan J. Gleason* Adenrele M. Akintobi*, Barth D. Grant and Richard W. Padgett in Proc. Natl, Acad. Sci 111 2578-2583 (2014).
*Both authors contributed equally to this work

For this work I designed experiments, generated constructs, transgenic animals, carried out genetic crosses, analyzed data, and optimized biochemical protocols geared towards the characterization of endosomal protein complexes.

Introduction

Bone morphogenetic proteins (BMPs) are members of the transforming growth factor β (TGFβ) superfamily of ligands that regulate an array of early developmental processes across metazoan phylogenies. Aberrant BMP signaling results in tumorigenesis in multiple tissues and also contributes to a variety of other important disorders (Wakefield and Hill, 2013). BMP ligands signal through a heteromeric complex of two transmembrane serine–threonine kinase receptors, referred to as the type I and type II receptors. On binding of the ligand to the receptors, a series of signaling events culminate in regulating gene expression.

The output of conserved signal transduction pathways, including those mediated by epidermal growth factor receptor, Notch, and G protein-coupled receptors, depend not only on the activation of these receptors by extracellular stimuli but also on the endocytic internalization and postendocytic trafficking of the receptors, which regulates the availability and compartmentalization of the signal transduction machinery (Miaczynska *et al.*, 2004) (Scita and Di Fiore, 2010) (Hanyaloglu and von Zastrow, 2008). Once endocytosed into early endosomes, signal transduction receptors are either sorted into a recycling pathway that will return the molecule to the cell surface for another round of signaling or are sorted into a degradative pathway via multivesicular bodies and late endosomes to be degraded in the lysosome. Although initial studies to identify the molecular complexes that regulate TGFβ receptor recycling have focused on the type II receptor and are limited, reports have shown that recycling of the type II receptor is mediated by recycling endosomes (Mitchell *et al.*, 2004) (Penheiter *et al.*, 2010).

In *Caenorhabditis elegans*, a conserved BMP signaling pathway, the Sma/Mab pathway, regulates diverse developmental processes including cell/body size, male-tail morphogenesis, dorso-ventral cell patterning, immune regulation, and olfactory learning, among others (Zhang and Zhang, 2012, Foehr, 2008 #141, Savage, 1996 #142, Nicholas, 2004 #143). In the *C. elegans* Sma/Mab pathway, the secreted ligand DBL-1 (decapentaplegic/bone morphogenetic protein-like-1) binds the type II, DAF-4 (dauer formation-defective-4), and type I, SMA-6 (small-6), receptor complex, and DAF-4 phosphorylates SMA-6, which in turn phosphorylates key residues on SMAD (small and mothers against decapentaplegic) proteins, allowing them to accumulate in the nucleus and acti- vate or repress target gene transcription. The DBL-1 signal is received by SMA-6/DAF-4 complexes expressed in the hypodermis, intestine, and other peripheral tissues.

Some studies of TGFβ trafficking and signaling in mammalian Mv1Lu cells have indicated that TGFβ signaling requires clathrin-mediated internalization of activated receptors to transduce signals to the nucleus via SMADs, presumably because receptor–SMAD interaction requires early endosome adapters (Di Guglielmo *et al.*, 2003). However, other studies in the same cell line report the opposite, that blocking clathrin-dependent endocytosis of TGFβ-receptors enhances signal transduction (Chen *et al.*, 2009). Thus, it remained important to test the requirements for receptor endocytosis in transducing TGFβ signals in an intact animal model such as *C. elegans*. We also set out both to identify molecular sorting complexes that regulate BMP receptor

type I and II recycling and to determine how receptor recycling affects signaling. Our in vivo results provide strong evidence that clathrin-dependent endocytosis is necessary for BMP signaling in *C. elegans.* Furthermore, we find that after internalization, two distinct recycling pathways regulate the transport of the type I and type II receptors back to the cell surface. Recycling of the type I receptor is regulated by the retromer complex, whereas the type II receptor is recycled via a distinct recycling pathway regulated by ARF-6 (ADP-ribosylation factor-6). In addition, we found that the type I receptor cytoplasmic tail binds directly to the retromer complex. Our work establishes a direct link between retromer-dependent recycling and BMP signaling in vivo, identifies distinct recycling pathways for the type I and type II receptors, and provides a genetically tractable system to study the regulation of vesicle trafficking on the BMP signaling pathway.

Results

Clathrin-Dependent Endocytosis Is Necessary for BMP Receptor Internalization and Signaling. To test the requirements for receptor internalization on signal transduction within intact animals in vivo, we determined the effects of loss of clathrin-adapter protein (AP)-2 subunits on Sma/Mab pathway signaling in *C. elegans*. We found that mutants lacking *C. elegans* μ2-adaptin (DPY-23) or α2-adaptin (APA-2) displayed body size defects as severe as those in animals completely lacking the type I receptor SMA-6 (Fig. 1F). Furthermore, molecular analysis confirmed this interpretation, indicating a severe block in Sma/Mab signaling in the hypodermis and intestine of *dpy-23* and *apa-2* mutants. This included analysis of a hypodermal expression of a concatamer of smad-binding elements driving GFP [the reporter acting downstream of SMAD (RAD-SMAD) reporter] and quantitative RT-PCR (qRT-PCR) analysis of

transcript levels of two intestine-specific genes whose expression levels are regulated by the Sma/Mab pathway (Fig. 1 G and H) (Mochii *et al.*, 1999; Roberts *et al.*, 2010; Tian *et al.*, 2010)

If these effects are mediated through the receptors, we would expect to find BMP receptors trapped at the cell surface under these conditions. We determined the subcellular localization of SMA-6 and DAF-4 in the large, well-characterized epithelial cells of the *C. elegans* intestine, using low-copy number transgenes driven by an intestine-specific promoter (Fig. 1A). GFP-tagged SMA-6 and DAF-4 are functional, as shown in this and previous work (Fig. 1F) (Patterson *et al.*, 1997). We found that both SMA-6::GFP and DAF- 4::GFP, visualized in otherwise wild-type intact living animals, localized to the basolateral plasma membrane, where they are in position to receive signaling molecules secreted by neurons (Fig. 1 B and I). SMA-6::GFP and DAF-4::GFP also labeled intracellular puncta, at least some of which we identified as endosomes.

We determined that SMA-6::GFP accumulated to much higher levels on the intestinal basolateral plasma membrane in animals depleted of AP-2 subunits by RNAi, indicating that SMA-6 requires AP-2 for endocytosis (Fig. 1 B–E). However, DAF-4 surface levels did not change in response to depletion of AP-2, suggesting that DAF-4 is AP-2-independent (Fig. 1 I–L). Previous studies of BMP receptor internalization in mammalian cell culture indicated that the type II receptor was internalized via clathrin-dependent and clathrin-independent mechanisms, whereas the type I receptor was strictly clathrin-dependent (Yao *et al.*, 2002; Di Guglielmo *et al.*, 2003; Hartung *et al.*, 2006). Thus, type II receptor DAF-4 may be internalized by clathrin-independent mechanisms or may use

alternative clathrin adapters. Further analysis demonstrated that surface levels of SMA-6 and DAF-4 did not increase in animals devoid of the ligand DBL-1, suggesting that receptor internalization does not require ligand binding (Fig. S1). We conclude that AP-2-dependent endocytosis of the type I receptor SMA-6 is necessary for signal transduction in the Sma/Mab pathway.

Postendocytic Trafficking and Signaling of the BMP Type I and Type II Receptors Are Regulated by Distinct Recycling Pathways. Once internalized by endocytosis, receptors are trafficked to early endosomes, from which they may be recycled to the plasma membrane or delivered to the lysosome. Several recycling pathways exist, including routes through the endocytic recycling compartment (ERC) and/or the trans-Golgi network (Grant and Donaldson, 2009). RME- 1 is a founding member of the conserved EHD/RME-1 (Eps15 homology-domain containing/receptor-mediated endocytosis-1) protein family and is required for a variety of recycling events, including ERC to plasma membrane transport and endosome to Golgi transport (Lin *et al.*, 2001b, Grant, 2008 #115). Importantly, we found that loss of RME-1 resulted in dramatically different defects in the subcellular localization of SMA-6 and DAF-4; DAF-4::GFP accumulated in intracellular vesicles, whereas overall levels of SMA-6:: GFP were severely reduced, suggesting that SMA-6 was being inappropriately degraded (Fig. 2 A, B, L, and M). Previous work indicated that a block in recycling to the plasma membrane via the ERC often results in intracellular trapping of receptors, whereas blocks in retromer-dependent recycling often results in missorting of receptors to the lysosome, where they are degraded (Lin *et al.*, 2001b; Gokool *et al.*, 2007; Temkin *et al.*, 2011; Zhang and Zhang, 2012).

Consistent with this idea, the accumulation of intracellular DAF-4 in the intestine of *rme-1* mutants strongly resembled the accumulation of well-characterized ERC cargo hTAC::GFP (human IL-2 receptor α-chain) in *rme-1* mutants (Fig. S2 A–C). The loss of SMA-6::GFP in the intestine of *rme-1* mutant animals resembled the loss of retromer-dependent cargo MIG-14::GFP (abnormal cell migration-14) in *rme-1* mutant animals (Fig. S2 D–F).

To test directly whether type I receptor SMA-6 recycling is dependent on the retromer pathway, we analyzed receptor localization in mutants lacking the core retromer subunit VPS-35 (vacuolar protein sorting factor-35) and several sorting nexins (SNX-1, SNX-3, and SNX-27) that may be specific for particular subsets of retromer-dependent cargo (Temkin *et al.*, 2011, Pfeffer, 2013 #156, Cullen, 2012 #157, Harterink, 2011 #158). *vps-35* mutants and *snx-3* mutants were severely defective in SMA-6 trafficking, whereas *snx-1* mutants were mildly defective and *snx-27* did not appear to affect SMA-6 (Fig. 2 A and C–F). Thus, SMA-6 is retromer-dependent and depends heavily on SNX-3, similar to known retromer cargo MIG-14/Wls (Wntless), a conserved membrane protein dedicated to the secretion of Wnt proteins. A key regulator specific to the ERC to plasma membrane recycling pathway is the small GTPase ARF-6. SMA-6 localization was unchanged in arf-6 deletion mutants, indicating the specificity of the requirement for retromer (Fig. 2 A and G).

Consistent with the idea that type II receptor DAF-4 recycles by a distinct mechanism, DAF-4 was not affected by loss of retromer core subunit VPS-35 (Fig. 2 L and O). Instead, we found that DAF-4::GFP accumulated in endosomes in arf-6 mutants (Fig. 2 L

and N). Thus, DAF-4 is retromer-independent and ARF-6-dependent, the opposite of SMA-6.

If the receptor recycling pathways we identified for SMA-6 and DAF-4 are physiologically important for Sma/Mab signaling, we would expect that such signaling would be defective in recycling pathway mutants. To determine whether recycling of the type I and type II receptors is important for Sma/Mab signaling, we again assayed 3 outputs of Sma/Mab signaling in two epithelial tissue types, the hypodermis and intestine. We found that body size was strongly reduced in *rme-1*, *vps-35*, and *arf-6* mutants, although not as severely as in mutants completely lacking the type I receptor SMA-6 (Fig. 2K). Furthermore, we found that in *vps- 35* and *rme-1* mutants, hypodermal expression of the RAD- SMAD reporter and qRT-PCR analysis intestine-specific Sma/ Mab target gene expression were reduced to levels similar to those found in mutants lacking the SMA-6 receptor, indicating the importance of receptor recycling to the ability of the cells to signal (Fig. 2 I and J). In addition, we found that in *arf-6 (tm1447),* hypodermal expression of the RAD-SMAD reporter was reduced to levels similar to *rme-1* and *vps-35* mutants (Fig. 2Q). Taken together, our genetic and cell biological data demonstrate that distinct recycling pathways control the postendocytic itinerary of the type I and type II BMP receptors and that such recycling is critical to maintain cellular signaling capacity.

SMA-6 Is Mislocalized to the Lysosome in Retromer Mutants After Clathrin-Dependent Endocytosis. To investigate our model further, we characterized the fate of SMA-6 in retromer mutants. We expected that SMA-6 levels were strongly reduced in retromer mutants because instead of recycling SMA-6, retromer mutants missort retromer-dependent cargo to the late endosome and lysosome (Arighi *et al.*, 2004; Yang *et al.*, 2008; Temkin *et al.*, 2011). Indeed, we found that in wild-type cells, only 20% of

SMA-6::GFP colocalized to the late endosome/lysosome marker tagRFP::RAB-7 (tag-red fluorescent protein::Rab GTPase-7), whereas 56% of SMA-6::GFP colocalized with tagRFP::RAB-7 in *vps-35* mutants (Fig. 3). Furthermore, much of the remaining SMA-6::GFP signal remaining in *vps-35* mutants appeared to be in the lumen of RAB-7-positive endosomes/lysosomes, whereas RAB-7 is restricted to the limiting membrane of these organelles. Thus, the 56% colocalization of SMA-6 with RAB-7 in *vps-35* mutants likely represents an underestimate of SMA-6 missorting. As a further test of this model, we also used a genetic epistasis approach, blocking plasma membrane endocytosis or lysosome-mediated degradation, in a retromer-deficient *vps-35* mutant. In a *vps-35* mutant depleted of μ2-adaptin (DPY-23) by RNAi, SMA- 6::GFP is not degraded and is trapped at the basolateral plasma membrane (Fig. 4 A–F). This indicates that retromer is not required for sorting SMA-6 until after its endocytosis from the plasma membrane. Furthermore, we found that in a *vps-35* mutant depleted of CUP-5/mucolipin1 (celomocyte uptake-defective-5), a protein required for lysosome function, the loss of SMA-6:: GFP was blocked and, instead, SMA-6::GFP accumulated in the degradation-deficient late endosome/lysosome hybrid organelles characteristic of *cup-5* mutants, and mildly at the plasma membrane (Treusch *et al.*, 2004) (Fig. 4 G–L). Thus, we also conclude that in a retromer mutant, postendocytic missorting sends SMA-6 to lysosomes, where it is inappropriately degraded.

SMA-6 Binds Directly to the Retromer Complex.

Our results suggested that SMA-6 might be a direct target of the retromer sorting complex during its transit through endosomes after endocytosis. If this is true, we expected to find a physical interaction between the intracellular domain of SMA-6 and retromer. As a first test of this, we incubated lysates from *C. elegans* expressing GFP-

tagged VPS-35 with beads containing immobilized SMA-6 intracellular domain purified from *Escherichia coli* as a GST fusion. GFP::VPS-35 protein was retained on the SMA-6-containing beads, but not by control beads containing GST alone (Fig. 5A). We next sought to determine whether such interaction was direct. We performed a similar assay using purified recombinant retromer cargo-selective complex (Vps35/Vps26/ Vps29) and immobilized SMA-6 intracellular domain. VPS-35, VPS-26, and VPS-29 form a heterotrimer subcomplex of the retromer that mediates cargo recognition. The intracellular domain of the well-known retromer-dependent cargo protein, the cation-independent mannose-6-phosphate receptor (CI-MPR), was used as a positive control. SMA-6 pulled down the recombinant retromer cargo-selective complex in a similar manner to the CI-MPR positive control (Fig. 5B) (Tabuchi *et al.*, 2010). These results indicate that SMA-6 binds directly to retromer to mediate its intracellular sorting.

Discussion

Members of the TGFβ superfamily of signal transduction pathways are conserved from early multicellular animals, such as trichoplax, to humans (Huminiecki *et al.*, 2009). Thus, our findings regarding the interplay of BMP receptor trafficking and signaling outputs have important implications for related receptors throughout metazoan phylogenies. Recently, two close vertebrate homologs of SMA-6, BMPRIA(ALK3) (bone morphogenetic protein type IA receptor/activin-like kinase 3) and ACVRIB(ALK4) (activin re- ceptor type IB/activin-like kinase 4), were identified to be down- regulated in a proteomic study for cell-surface receptors altered by SNX27- and VPS35-depleted human HeLa cells (Steinberg *et al.*, 2013). Although not investigated in individual detail, high-throughput proteomics suggested that ACVRIB was down-regulated in both SNX27- and VPS35-depleted cells, whereas BMPRIA was only down-regulated in

SNX27-depleted cells. The cell surface proteome analysis identified only type I TGFβ superfamily receptors to be down-regulated. In contrast, no type II receptors were found to be down-regulated. A more distant homolog of SMA-6, TGFβR1 (ALK5) (transforming growth factor-β receptor type I/activin-like kinase 5), was also suggested to be down-regulated in VPS35- and SNX27-depleted HeLa cells (Steinberg *et al.*, 2013). Although a recent study failed to show a VPS35 RNAi effect in Madin–Darby canine kidney cells on TGFβR1(ALK5) (Yin *et al.*, 2013), they did demonstrate that TGFβRII was mislocalized to both the basolateral and apical membrane, as opposed to its normal localization to the basolateral membrane. Examination of the role of the retromer complex on BMP signaling in *Drosophila* has been incongruent (Harterink *et al.*, 2011) (Korolchuk *et al.*, 2007) (Zhang *et al.*, 2011). On the basis of our genetic and cell biological data, as well as the preliminary data from the mammalian proteomic analysis, it is very likely that retromer-dependent regulation of type I BMP and Activin receptors is a conserved mechanism of TGFβ-receptor regulation. Here we demonstrate that blocking receptor internalization, or receptor recycling, results in down-regulation of BMP signal transduction. This provides insight into how specific internalization and recycling pathways influence the molecular compartmentalization of the BMP receptors and provides insight into how altering this compartmentalization affects the signaling strength of the pathway. The identification of two distinct transport pathways for SMA-6 and DAF-4 during recycling of the receptors back to the plasma membrane suggests a mechanism by which aberrant signaling of these receptors can be avoided through physical disassociation of the active heteromeric complexes. Previously discovered differences in the rate of biosynthesis of the type I and II receptors were observed (Wells *et al.*, 1997). Both the difference in rate of biosynthesis and the difference in trafficking, we report, may contribute to the difference in the half-life of the type I receptor, which

has been identified to be longer than that of the type II receptor (Koli and Arteaga, 1997; Wells *et al.*, 1997)

In summary, our data demonstrate a novel function of the retromer in regulating BMP signaling through the regulation of a BMP type I receptors' intracellular recycling. In addition, this regulation is unique to the type I receptor and did not affect the type II receptor in *C. elegans*, which we found traffics through an ARF-6-dependent recycling pathway. Taken together, our work shows the physiological importance of endocytosis and recycling to TGFβ signaling in the context of an intact developing organism and identifies a surprising mechanism to keep the type I and type II receptors apart as they depart the signaling endosome. We propose that this disparate recycling of the two receptors allows termination of signal transduction within the endosomal system while preserving both receptors for further rounds of signaling. Delineating the endocytic compartmentalization and pathways that regulate BMP signaling provides novel opportunities to characterize the effect of tumor-associated BMP receptor mutations on the compartmentalization of the receptors and in developing pharmacological inhibitors of BMP signaling in various diseases.

Materials and Methods

General Methods and Strains. All *Caenorhabditis elegans* strains were derived originally from wild-type Bristol strain N2, and all strains were grown at 20°C on standard nematode growth media plates seeded with OP50 Escherichia coli. Worm cultures, genetic crosses, and other *C. elegans* husbandry were performed according to standard protocols (Brenner, 1974). A complete list of strains used in this study can be found in

Table S1. RNAi was performed using the feeding method (Timmons and Fire, 1998). Feeding constructs were from the Ahringer library (Kamath and Ahringer, 2003), and empty vector, L4440, was used as a control. For experiments, larval stage L4 animals were treated for 24 h and imaged as young adults.

Plasmids and Transgenic Strains. To construct GFP fusion transgenes for expression in the worm intestine or hypodermis, previously described tissue-specific promoters of *pvha-6* (intestine) and *pelt-3* (hypodermis) were used (Wang *et al.*, 2002). *C. elegans* genomic DNA of SMA-6 (small-6) and DAF-4 (dauer formation-defective-4), lacking the terminal stop codon, were cloned into entry vector pDONR221 (Invitrogen) by PCR and BP reaction and then transferred into expression vectors by Gateway recombination cloning (Invitrogen) to generate C-terminal fusions. Complete plasmid sequences are available on request. Low-copy integrated transgenic lines for these plasmids were obtained by the microparticle bombardment method (Praitis *et al.*, 2001). Transgenic strain wkEx101 was generated through microinjection of rescue plasmid pRG62 (pelt-3:: SMA-6::GFP) (10 ng/μL), and pCFJ90 (*pmyo-2*::mCherry) as a coinjection marker, extrachromosomal arrays were maintained (Mello and Fire, 1995).

Microscopy and Image Analysis. Live worms were mounted on 2% (wt/vol) agarose pads with tetramisole. To obtain images of GFP fluorescence without interference from *C. elegans* gut autofluorescence, we used the spectral profile function of the Leica SP5 confocal microscope system to establish a spectral profile of the autofluorescence to separate the autofluorescence from the experimentally determined GFP spectrum, using argon 488-nm excitation. The worm intestine consists of 20 individual epithelial cells with

distinct apical, lateral, and basal regions, positioned as bilaterally symmetric pairs to form a long tube around the lumen. The focal planes captured in this study are designated as the Top plane, which captures the top of the intestinal tube, demonstrating the basolateral surface of the intestine, and the Middle plane, which captures the midsagittal cross section of the intestine presenting both the apical and basolateral surfaces. Quantification of images were performed using the open-source Fiji software (Schindelin *et al.*, 2012). Within any set of comparable images, the image capture and scaling conditions are identical. The same threshold values were used for all images within a given experiment. For each marker comparison, at least six animals were analyzed. Three randomly selected regions per animal were analyzed, using circular regions of defined area. Quantification of fluorescence intensities was performed. The average total intensity was calculated. Colocalization images were performed on L4 staged samples, using a confocal microscope equipped with the confocal imager (CARV II; BD Biosciences). For quantitative colocalization analysis, all image manipulations were performed with Fiji open-source software, using the colocalization threshold plugin. Colocalization analysis was conducted using the Costes method to establish a threshold, fluorescent intensities for both SMA-6:: GFP and TagRFP::RAB-7 (Tag-red fluorescent protein::Rab GTPase-7) were then scatterplotted for each pixel, and pixels with similar intensity values for both channels were counted as colocalized. Both Pearson's coefficient and Mander's split coefficients were calculated using Fiji software.

Body Size Measurements. Animals were picked at the L4 stage, incubated at 20°C for 24 h, and photographed. Images from individual animals were captured from a dissecting microscope, using a Qimaging Retiga 1300 cooled color digital camera

system and QCapture2 software (Quantitative Corporation). Lengths of animals were determined using the open-source Fiji software (Schindelin *et al.*, 2012).

qRT-PCR Gene Expression Analysis of Intestine-Specific Sma/Mab Target Gene Expression for F35C5.9 and R09H10.5. cDNA libraries were constructed from whole-animal RNA lysates of L3 staged, N2, *sma-6(wk7), apa-2(ox422), rme-1(b1045)*, and *vps-35*(hu68), using Qiagen RNeasy Plus mini kit and the iScript cDNA synthesis kit (BioRad). SYBR Green PCR reactions were carried out using the Applied Biosystems Prism 7000 Real-time PCR system and the iQ SYBR Green supermix (BioRad). Each experimental transcript was tested in triplicates and compared with an internal control gene, tubulin α-2 chain (TBA-1), and a no template control. Data were analyzed using Applied Biosystems SDS software, allowing the software to set the baseline. The cycle threshold (CT) was set manually, making sure it was within the exponential phase of amplification. The comparative CT method (ΔΔCT) was used for quantitation.

Protein Expression and Purification. For the purification of GST fusion proteins, a negative control GST plasmid was expressed in New England BioLabs Express Iq-competent *Escherichia coli cells.* GST-SMA-6 (intracellular domain, aa 237–663) and GSTcation-independent mannose-6-phosphate receptor (CI-MPR) (positive control) were expressed in the ArcticExpress strain of *E. coli* (Stratagene). Bacterial pellets of GST bacterial pellet were lysed in 20 mL B-PER Bacterial Protein Extraction Reagent (Pierce) with Complete Protease Inhibitor Mixture Tablets (Sun *et al.*). Bacterial pellets of the GST-SMA-6 intracellular domain and GST-CI-MPR were lysed using a EmulsiFlex-C3 homogenizer (Avestin) at 15,000 psi in 25 mL bacterial lysis buffer [50 mM Tris·HCL (pH 8.0), 20% (wt/vol) sucrose, 10% (wt/vol) glycerol, 2 mM DTT] with Complete Protease Inhibitor Mixture tablets (Sun *et al.*). Extracts were cleared by centrifugation,

and supernatants were incubated with glutathione-Sepharose 4B beads (Amersham Pharmacia) at 4 °C for 2 h

GST Pull-Down Assays. GST fusions were incubated with recombinant (3xFLAG)VPS26-(3xFLAG)VPS29-(3xFLAG)VPS35-His6 complex, and the pull-down was performed as described (Tabuchi *et al.*, 2010). For *in vivo* GST pull-down experiments, transgenic animals expressing *pvha-6*::GFP::VPS-35 were used as input and grown on nematode growth media plates seeded with OP50 bacteria. Worms were washed off gently and suspended in ice-cold M9 buffer. Wholeworm lysate was extracted using the yeast bead beater with 5-mm Zirconia Silicon beads. The lysate was precleared by incubation, using glutathione Sepharose 4B beads coated with GST protein for 30 min. The precleared lysate was allowed to incubate for 1 h with control GST or GST-SMA-6 (aa 237–663) fusion protein containing the intracellular domain. After five sequential washes in wash buffer (Hepes at pH 7.4, 150 mM KCl, 1 mM MgCl2, 2 mM DTT, and 0.6 mg/mL BSA), the proteins were eluted by boiling in 70 μL of 2× SDS/PAGE sample buffers. Eluted proteins were separated on SDS/PAGE [12% (wt/vol) polyacrylamide], blotted to nitrocellulose, and stained with Ponceau S to detect GST fusion proteins. After blocking, the blot was probed with anti-GFP antibody

Acknowledgements

We thank C. Rongo, N. Kane, and P. Schweinsberg for helpful discussions and technical assistance, and Y. Kohara (National Institute of Genetics, Japan) and the *C. elegans* Genetics Center for cDNA and strains. This work was supported by grants from the National Institutes of Health (R01GM103995 to R.W.P. and B.D.G.; R01GM67237 to B.D.G.), a Busch Biomedical Grant (to R.W.P. and B.D.G.), a Charles and Johanna Busch Predoctoral Fellowship (to R.J.G.), and a National Science Foundation-Integrated

Graduate Education and Research Traineeship (Stem Cell Science and Engineering; 0801620 to R.J.G.).

Figure legends

Fig. 1. AP-2 adaptor complex mutants, *dpy-23(e480)* and *apa-2(ox422),* display reduced body size phenotypes, inhibit Sma/Mab signaling, and block receptor internalization of SMA-6::GFP. (A) Schematic depiction of the *C. elegans* intestine to demonstrate focal planes captured to study SMA-6 and DAF-4 localization. White arrowheads indicate lateral membrane, and yellow arrowheads indicate apical lumen of the intestine. (B–D) Micrographs of SMA-6::GFP expressed in the intestine to compare localization in control L4440(RNAi), a*pa-2 (RNAi),* and *dpy-23(RNAi)*. On the top (basolateral) focal plane, arrowheads indicate lateral membrane. (E) Quantification of SMA-6::GFP micrographs (n = 6). (F) Body length of N2 wild-type, *sma-6(wk7), dpy-23(e480), apa-2(ox422),* and transgenic rescue strain *pelt-3*::SMA- 6::GFP; *sma-6(wk7).* (G) Expression of the RAD-SMAD GFP reporter in wild-type, *sma-6(wk7), dpy-23(e480),* and *apa-2(ox422).* Staged at larval stage L3. (n = 6). (H) qRT-PCR of intestinally expressed genes F35C5.9 and R09H10.5 in wild-type, *sma-6(wk7), dpy-23(e480),* and *apa-2(ox422).* (I–K) Micrographs of DAF-4::GFP expressed in the intestine to compare localization in control L4440 RNAi, *apa-2(RNAi),* and *dpy-23(RNAi).* On the top (basolateral) focal plane, arrowheads indicate lateral membrane. (L) Quantification of DAF-4:: GFP micrographs (n = 6). Error bars, SEM. ***P < 0.001. See also Fig. S1.

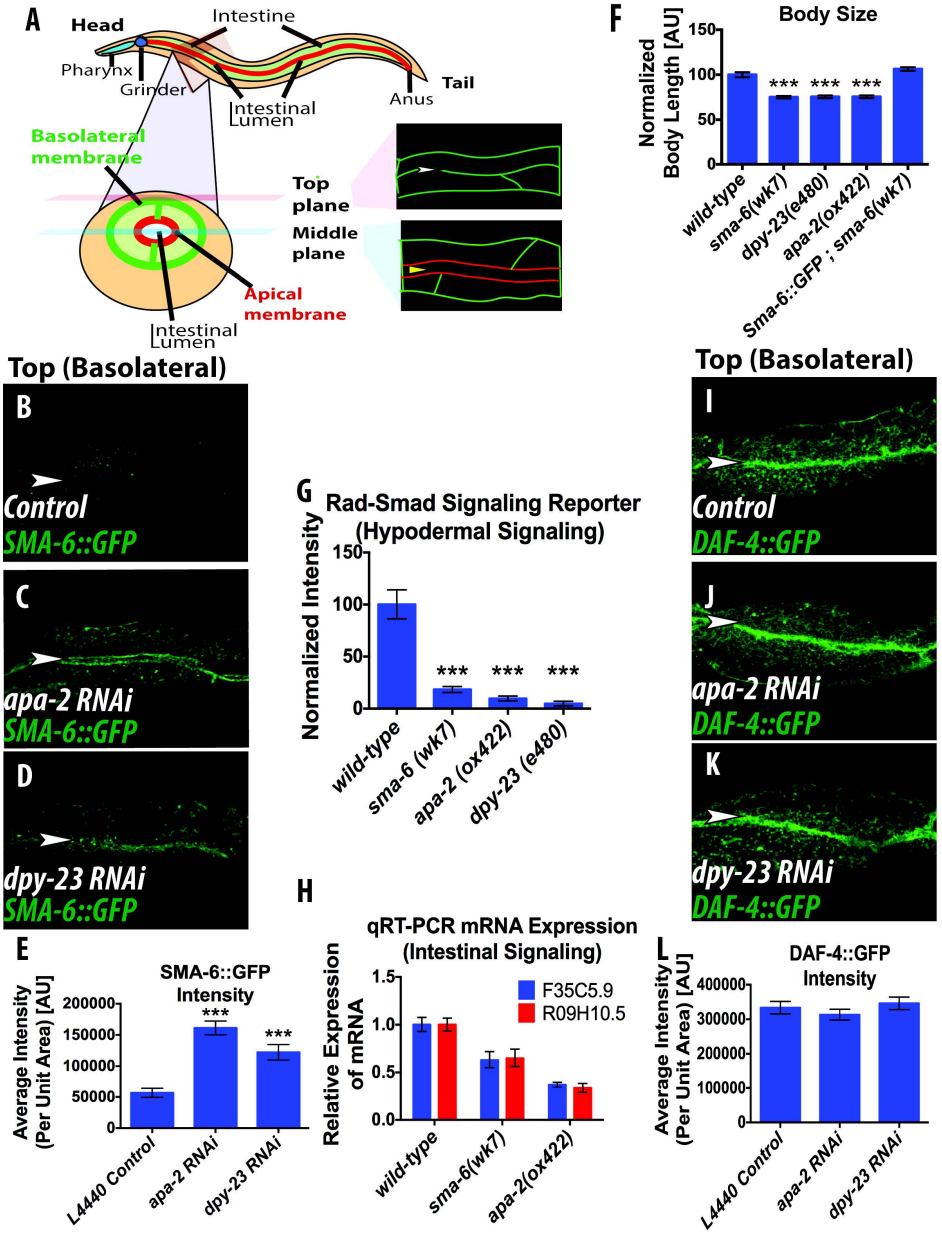
A
Head
Intestine
Pharynx
Grinder
Intestinal Lumen
Anus
Tail
Basolateral membrane
Top plane
Middle plane
Apical membrane
Intestinal Lumen
F
Body Size
Normalized Body Length [AU]
150
100
50
0
***
***
***
wild-type
sma-6(wk7)
dpy-23(e480)
apa-2(ox422)
Sma-6::GFP ; sma-6(wk7)
Top (Basolateral)
B
Control
SMA-6::GFP
C
apa-2 RNAi
SMA-6::GFP
D
dpy-23 RNAi
SMA-6::GFP
G
Rad-Smad Signaling Reporter
(Hypodermal Signaling)
Normalized Intensity
150
100
50
0
***
***
***
wild-type
sma-6 (wk7)
apa-2 (ox422)
dpy-23 (e480)
Top (Basolateral)
I
Control
DAF-4::GFP
J
apa-2 RNAi
DAF-4::GFP
K
dpy-23 RNAi
DAF-4::GFP
H
qRT-PCR mRNA Expression
(Intestinal Signaling)
Relative Expression of mRNA
1.5
1.0
0.5
0.0
F35C5.9
R09H10.5
wild-type
sma-6(wk7)
apa-2(ox422)
E
SMA-6::GFP Intensity
Average Intensity (Per Unit Area) [AU]
200000
150000
100000
50000
0
***
***
L4440 Control
apa-2 RNAi
dpy-23 RNAi
L
DAF-4::GFP Intensity
Average Intensity (Per Unit Area) [AU]
400000
300000
200000
100000
0
L4440 Control
apa-2 RNAi
dpy-23 RNAi

Fig. 2. Disparate phenotypes of DAF-4::GFP and SMA-6::GFP in the absence of endocytic recycling protein RME-1, retromer complex mutants *vps-35* (hu68) and *snx-3*(tm1595), and recycling endosome mutant *arf-6(tm1447).* (A–G) Micrographs of SMA-6:: GFP expressed in the intestine to compare localization in wild-type, *rme-1*(b1045), *vps-35(hu68), snx-3(tm1595), snx-1(tm847), snx-27(tm5356),* and *arf-6 (tm1447).* On the top (basolateral) focal plane, white arrowheads indicate lateral membrane. (H) Quantification of SMA-6::GFP micrographs (n = 6). (I) Expression of the RAD-SMAD GFP reporter in wild-type, *sma-6(wk7), vps-35(hu68),* and *rme-1(b1045)* staged at L3 (n = 6). (J) qRT-PCR of intestinally expressed genes F35C5.9 and R09H10.5 in wild-type, *sma-6 (wk7), rme-1(b1045),* and *vps-35(hu68).* (K) Body length of N2 wild-type, sma-6(wk7), *rme-1(b1045), vps-35(hu68),* and *arf-6(tm1447).* (L–O) Micrographs of DAF-4::GFP expressed in the intestine to compare localization in wild-type, *rme-1(b1045), arf-6(tm1447),* and *vps-35(hu68)* in the middle (midsagittal cross-section) focal plane. Yellow arrowheads indicate apical lumen of the intestine. (L′–O′) Magnified regions annotated by dotted squares in L–O. Arrows indicate aberrant accumulation in mutant backgrounds. (P) Quantification of DAF-4::GFP micrographs (n = 6). (Q) Expression of the RAD-SMAD GFP reporter in wildtype*, sma-6(wk7),* and *arf-6(tm1447)* staged at L3 (n = 6). Error bars, SEM. ***P < 0.001; *P ≤ 0.05. See also Fig. S2.

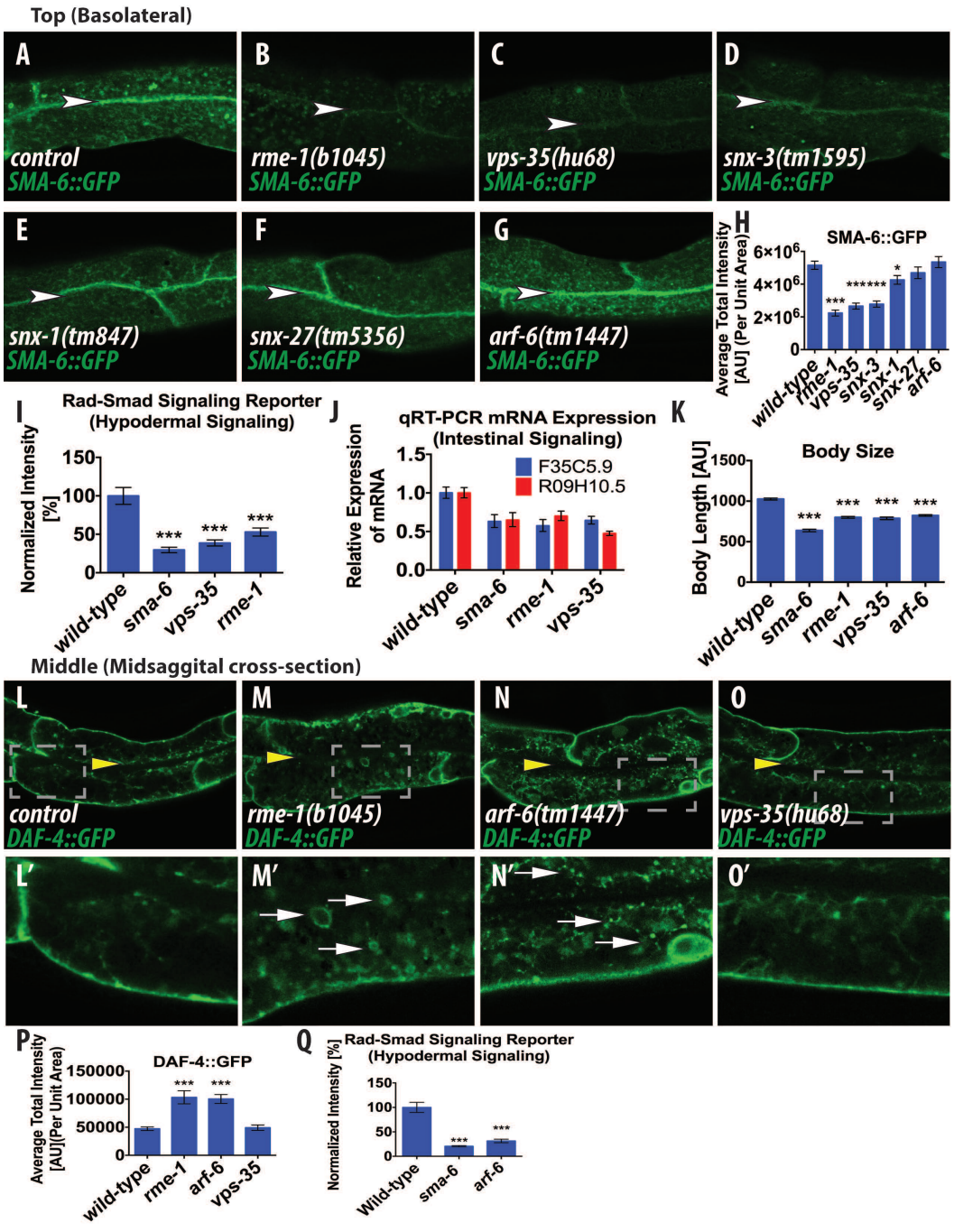
Top (Basolateral)
A
control
SMA-6::GFP
B
rme-1(b1045)
SMA-6::GFP
C
vps-35(hu68)
SMA-6::GFP
D
snx-3(tm1595)
SMA-6::GFP
E
snx-1(tm847)
SMA-6::GFP
F
snx-27(tm5356)
SMA-6::GFP
G
arf-6(tm1447)
SMA-6::GFP
H
SMA-6::GFP
Average Total Intensity [AU] (Per Unit Area)
6×10^6
4×10^6
2×10^6
0
wild-type
rme-1
vps-35
snx-3
snx-1
snx-27
arf-6
I
Rad-Smad Signaling Reporter (Hypodermal Signaling)
Normalized Intensity [%]
150
100
50
0
wild-type
sma-6
vps-35
rme-1
J
qRT-PCR mRNA Expression (Intestinal Signaling)
Relative Expression of mRNA
F35C5.9
R09H10.5
1.5
1.0
0.5
0.0
wild-type
sma-6
rme-1
vps-35
K
Body Size
Body Length [AU]
1500
1000
500
0
wild-type
sma-6
rme-1
vps-35
arf-6
Middle (Midsaggital cross-section)
L
control
DAF-4::GFP
M
rme-1(b1045)
DAF-4::GFP
N
arf-6(tm1447)
DAF-4::GFP
O
vps-35(hu68)
DAF-4::GFP
L′
M′
N′
O′
P
DAF-4::GFP
Average Total Intensity [AU](Per Unit Area)
150000
100000
50000
0
wild-type
rme-1
arf-6
vps-35
Q
Rad-Smad Signaling Reporter (Hypodermal Signaling)
Normalized Intensity [%]
150
100
50
0
Wild-type
sma-6
arf-6

Fig. 3. SMA-6 is mislocalized to the lysosome when retromer-dependent recycling is impaired. (A-A″) Colocalization of SMA-6::GFP with TagRFP::RAB- 7 expressed in the intestine to compare localization in wild-type in the middle (midsagittal cross-section) focal plane. Yellow arrowheads indicate apical lumen of the intestine. (A″′) Magnified image of A″ is designated by dashed rectangular outline. (B–B″) Colocalization of SMA-6::GFP with TagRFP::RAB-7 in *vps-35(hu68)* in the middle (midsagittal cross-section) focal plane. Yellow arrowheads indicate apical lumen of the intestine. (B″′) Magnified image of B″ designated by dashed rectangular outline. (C) Quantification of SMA-6::GFP colocalization with TagRFP::RAB-7. (D) Pearson and Mander's coefficients for colocalization of SMA-6::GFP with TagRFP:: RAB-7. n = 6. Error bars, SEM. ***P < 0.001.

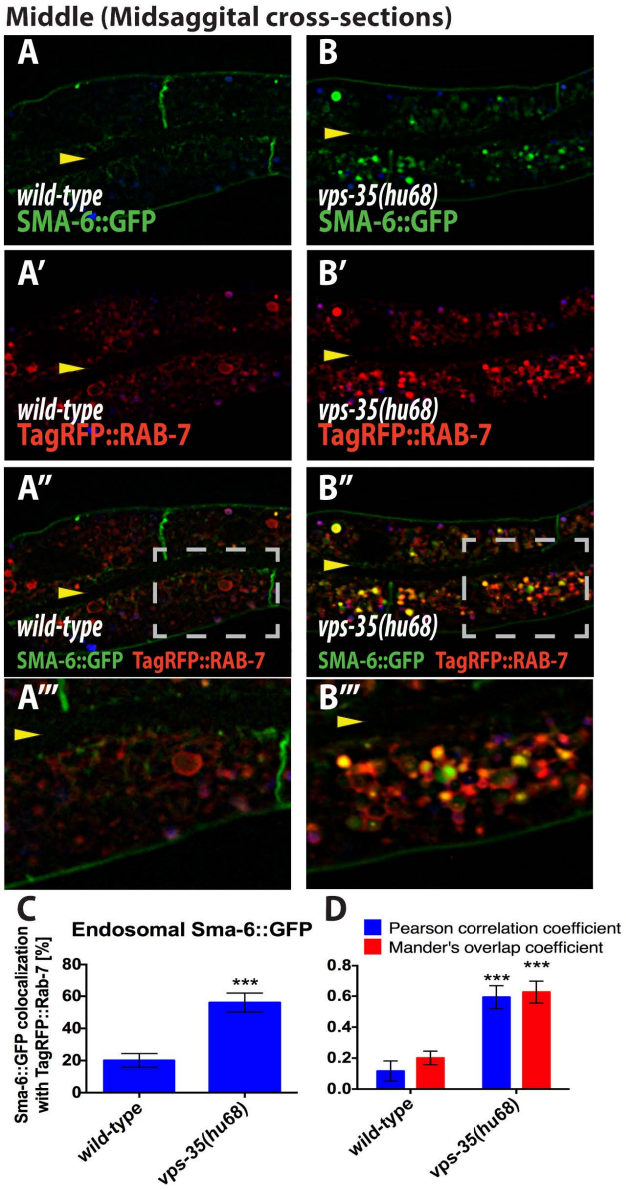
Middle (Midsaggital cross-sections)
A
wild-type
SMA-6::GFP
B
vps-35(hu68)
SMA-6::GFP
A′
wild-type
TagRFP::RAB-7
B′
vps-35(hu68)
TagRFP::RAB-7
A″
wild-type
SMA-6::GFP TagRFP::RAB-7
B″
vps-35(hu68)
SMA-6::GFP TagRFP::RAB-7
A‴
B‴
C
Endosomal Sma-6::GFP
Sma-6::GFP colocalization with TagRFP::Rab-7 [%]
80
60
40
20
0
***
wild-type
vps-35(hu68)
D
Pearson correlation coefficient
Mander's overlap coefficient
0.8
0.6
0.4
0.2
0.0
***
***
wild-type
vps-35(hu68)

Fig. 4. Retromer-dependent recycling occurs after biosynthesis and internalization. (A and B) Micrographs of SMA-6::GFP to compare localization on the top (basolateral) focal plane in control L4440(RNAi), *dpy-23(RNAi).* White arrowheads indicate lateral membrane. (C) Quantification of SMA-6::GFP micrographs from A and B (n = 6). (D and E) Micrographs of *vps-35(hu68);*SMA-6::GFP to compare localization on the top (basolateral) focal plane in control L4440 (RNAi), *dpy-23(RNAi).* White arrowheads indicate lateral membrane. (F) Quantification of *vps-35(hu68)*; SMA-6::GFP micrographs from D and E (n = 6). (G and H) Micrographs of SMA-6::GFP to compare localization in control L4440(RNAi), *cup-5(RNAi)* in the middle (midsagittal cross-section) focal plane. Yellow arrowheads indicate apical lumen of the intestine. (I) Quantification of SMA-6::GFP micrographs from G and H (n = 6). (J and K) Micrographs of *vps-35(hu68);* SMA-6:: GFP to compare localization in control L4440(RNAi), *cup-5(RNAi)* in the middle (midsagittal cross-section) focal plane. Yellow arrowheads indicate apical lumen of the intestine. (L) Quantification of *vps-35(hu68);* SMA-6::GFP micrographs from J and K (n = 6). Error bars, SEM. ***P < 0.001; **P ≤ 0.01.

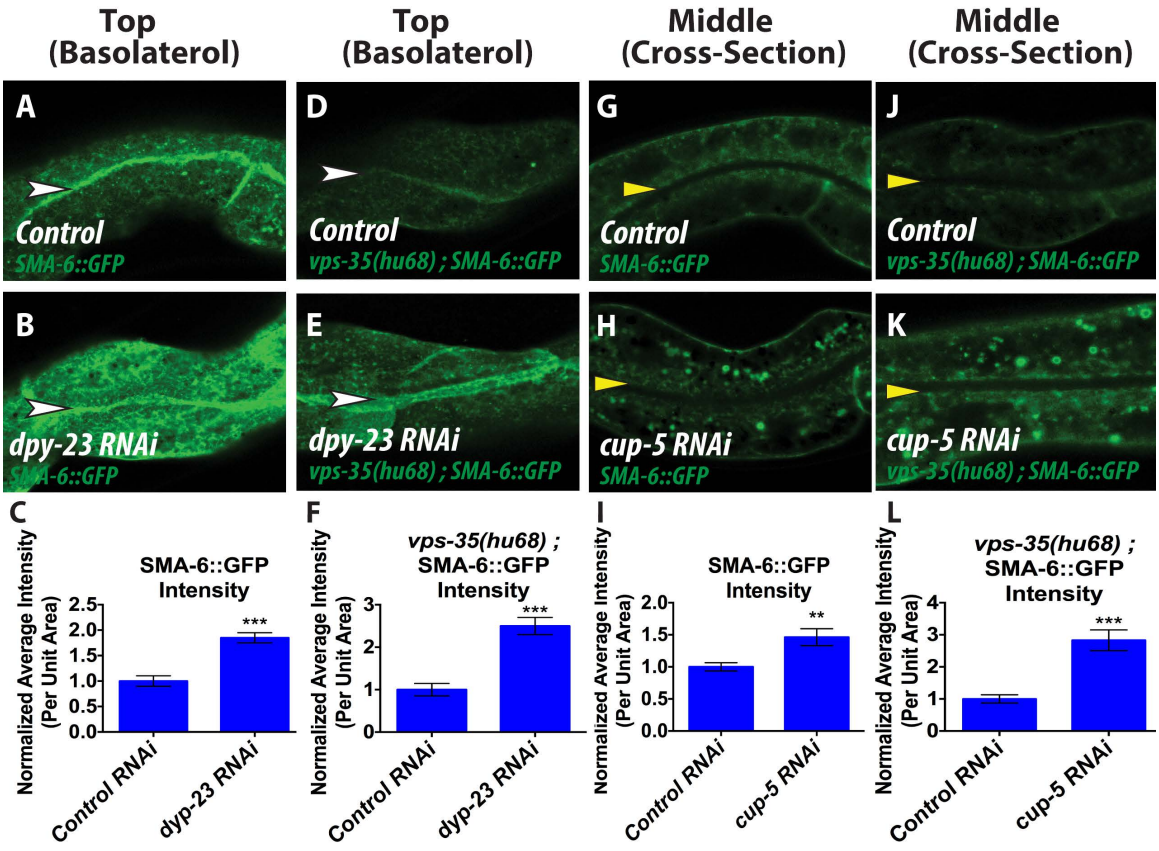
Top (Basolaterol)
Top (Basolaterol)
Middle (Cross-Section)
Middle (Cross-Section)
A
Control
SMA-6::GFP
D
Control
vps-35(hu68) ; SMA-6::GFP
G
Control
SMA-6::GFP
J
Control
vps-35(hu68) ; SMA-6::GFP
B
dpy-23 RNAi
SMA-6::GFP
E
dpy-23 RNAi
vps-35(hu68) ; SMA-6::GFP
H
cup-5 RNAi
SMA-6::GFP
K
cup-5 RNAi
vps-35(hu68) ; SMA-6::GFP
C
SMA-6::GFP Intensity
Normalized Average Intensity (Per Unit Area)
***
Control RNAi
dyp-23 RNAi
F
vps-35(hu68) ; SMA-6::GFP Intensity
***
Control RNAi
dyp-23 RNAi
I
SMA-6::GFP Intensity
**
Control RNAi
cup-5 RNAi
L
vps-35(hu68) ; SMA-6::GFP Intensity
***
Control RNAi
cup-5 RNAi

Fig. 5. The retromer complex binds the intracellular domain of SMA-6. (A) Glutathione beads loaded with recombinant GST or GST-SMA-6 intracellular domain were incubated with a lysate prepared from transgenic worms expressing GFP::VPS-35. Unbound proteins were washed away, and bound proteins were eluted with Laemmli sample buffer, separated by SDS/PAGE, and analyzed by Western blot with anti-GFP antibody. The GFP::VPS-35 band observed in worms at 120 kDa was bound by the GST-SMA-6 intracellular domain, but not by GST alone. Input lanes contain 10% (vol/vol) worm lysate used in the binding assays. Loading of bait GST (26 kDa) or GST-SMA-6 (100 kDa) was visualized by Ponceau S. (B) Purified recombinant FLAG(FLAG epitope tag)-tagged retromer complex [consisting of the proteins (3xFLAG)Vps26- (3xFLAG)Vps29-(3xFLAG)Vps35-His6) incubated with purified GST or GST fusion proteins bearing the wild-type intracellular domains of SMA-6 and CI-MPR as control. Proteins were pulled down with glutathione-Sepharose beads, bound FLAG-tagged retromer components were detected with an antibody to the FLAG-tag, and proteins were visualized with Ponceau S.

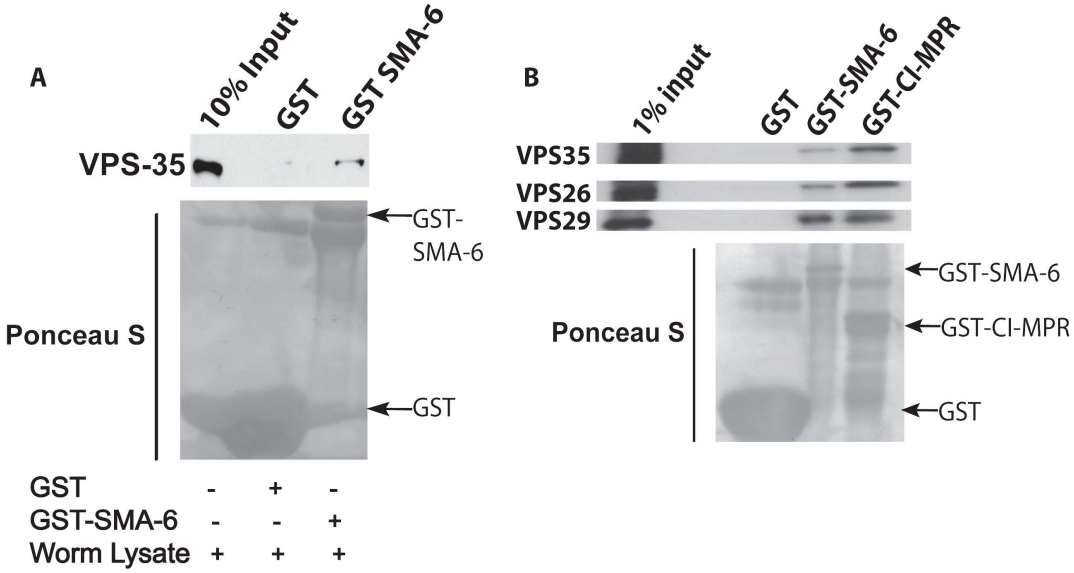
A
10% Input
GST
GST SMA-6
VPS-35
GST-
SMA-6
Ponceau S
GST
GST - + -
GST-SMA-6 - - +
Worm Lysate + + +
B
1% input
GST
GST-SMA-6
GST-CI-MPR
VPS35
VPS26
VPS29
GST-SMA-6
GST-CI-MPR
Ponceau S
GST

Fig. S1. DAF-4::GFP and SMA-6::GFP in *dbl-1(wk70),* the Sma/Mab pathway ligand. (A and B) Micrographs of DAF-4::GFP in wild-type and *dbl-1(wk70)* on the top (basolateral) focal plane. White arrowheads indicate lateral membrane. (C) Quantification of DAF-4::GFP micrographs from A and B (n = 6). (D and E) Micrographs of SMA-6::GFP in wild-type and dbl-1(wk70) on the top (basolateral) focal plane. White arrowheads indicate lateral membrane. (F) Quantification of SMA-6::GFP micrographs from D and E (n = 6) Error bars, SEM. Changes in levels were not significant, as P = 0.056 for DAF-4::GFP and P = 0.36 for SMA-6::GFP.

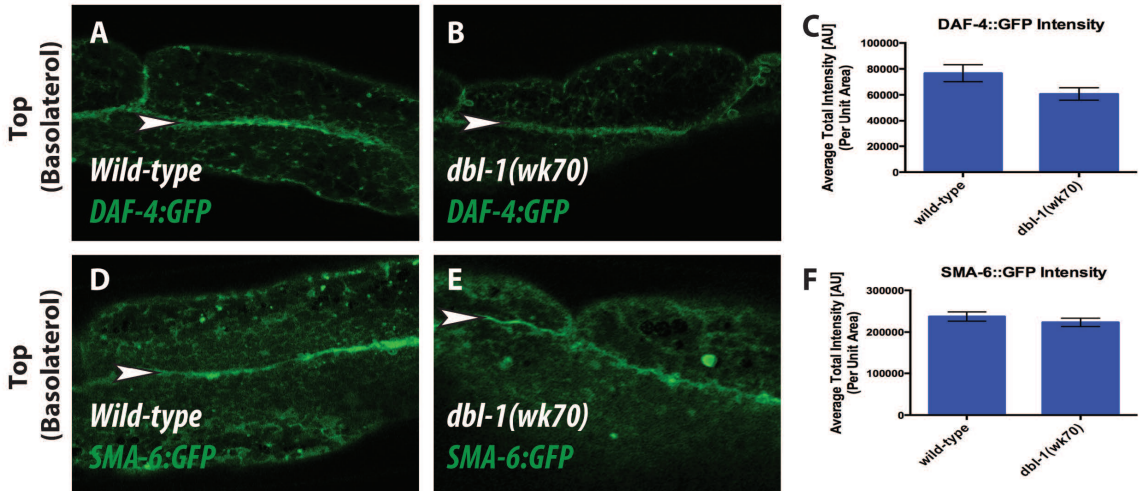
Top
(Basolaterol)
A
Wild-type
DAF-4:GFP
B
dbl-1(wk70)
DAF-4:GFP
C
DAF-4::GFP Intensity
Average Total Intensity [AU]
(Per Unit Area)
100000
80000
60000
40000
20000
0
wild-type
dbl-1(wk70)
Top
(Basolaterol)
D
Wild-type
SMA-6:GFP
E
dbl-1(wk70)
SMA-6:GFP
F
SMA-6::GFP Intensity
Average Total Intensity [AU]
(Per Unit Area)
300000
200000
100000
0
wild-type
dbl-1(wk70)

Fig. S2. Trafficking of known receptor-mediated endocytosis cargo receptors, hTAC::GFP (human IL-2 receptor α-chain) and MIG-14::GFP (abnormal cell migration-14), expressed in *rme-1(b1045).* (A and B) Micrographs of hTAC:GFP in *rme-1(b1045)* in the middle (midsagittal cross-section) focal plane. Yellow arrowheads indicate apical lumen of the intestine. (C) Quantification of hTAC::GFP micrographs from A and B (n = 6). (D and E) Micrographs of MIG-14::GFP in *rme-1(b1045)* on the top (basolateral) focal plane. White arrowheads indicate lateral membrane. (F) Quantification of MIG-14::GFP micrographs from D and E (n = 6). Error bars, SEM. ***P < 0.001

.

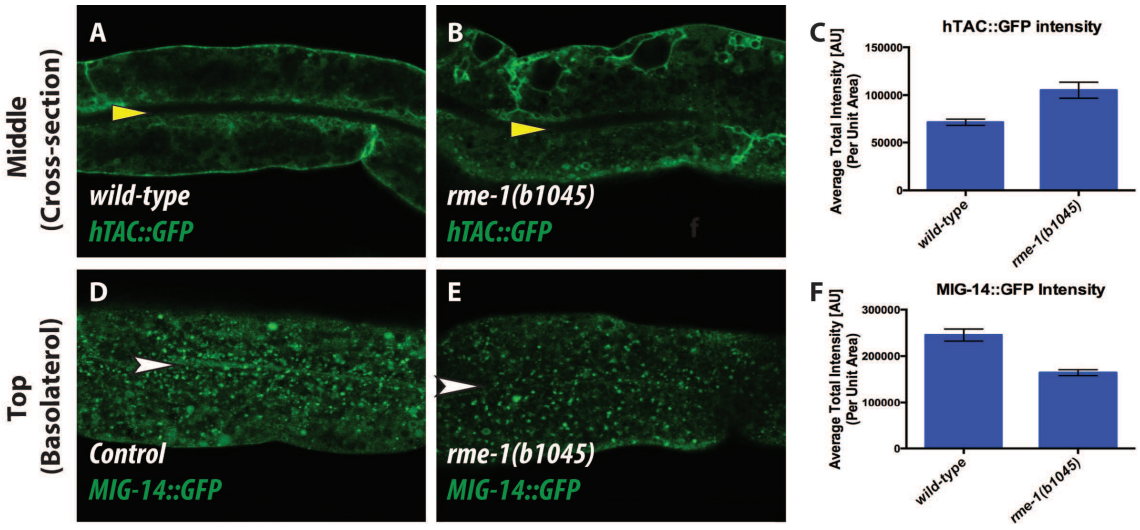
Middle
(Cross-section)
A
wild-type
hTAC::GFP
B
rme-1(b1045)
hTAC::GFP
C
hTAC::GFP intensity
Average Total Intensity [AU]
(Per Unit Area)
150000
100000
50000
0
wild-type
rme-1(b1045)
Top
(Basolaterol)
D
Control
MIG-14::GFP
E
rme-1(b1045)
MIG-14::GFP
F
MIG-14::GFP Intensity
Average Total Intensity [AU]
(Per Unit Area)
300000
200000
100000
0
wild-type
rme-1(b1045)

Chapter IX

Conclusions

From the same endosome, cells have engineered mechanisms to specialize distinct vesicular cargo carriers intended for various transport routes. The molecular details, which specify each route, remain unclear and under rigorous investigation. The studies preformed have addressed two fundamental questions in endosomal transport. The first aim of these studies illustrates the F-BAR protein coordinates the transport recycling cargos that leave the early endosome. Through our efforts we are the first to identify two distinct endosomal trafficking pathways that modulate TGFβ signaling. The novelty of this work suggests that the differential sorting of the Type I and II receptor is an effective way to terminate TGFβ signaling.

Disparate endosomal recycling of the Type I and Type II receptors regulate TGFβ signaling

C. elegans has served as a powerful model system to elucidate the molecular components that regulate TGFβ signaling. The Sma/Mab pathway is a conserved TGFβ signaling pathway that regulates body size, male tail development, olfactory learning, reproductive aging, and immunity (Patterson and Padgett 2000, Kurz and Tan 2004, Nicholas and Hodgkin 2004). A forward genetic screen, which screened for body size, led to the discovery of mutations in *dbl-1, sma-2, sma-3, sma-4, daf-4, sma-6, sma-9, sma-10.*

With an initial interest in TGFβ receptor-mediated trafficking, we used the *C. elegans* intestine to examine the endosomal pathways that modulate their intracellular sorting. RNAi studies showed that the depletion of the clathrin adaptors, *apa-2(alpha)* or *dpy-*

23(mu), not only blocked internalization of the SMA-6 receptor but also perturb Sma/Mad signaling**.** Animals deficient in either AP-2 subunit gave rise to small worms.

Another exciting aspect of these studies illustrate for the first time that post-internalization of DAF-4 (type II) and SMA-6 (type I) sort the receptors into two distinct endosomal sorting complexes. Specifically, SMA-6 (type I) receptor directly interacts with the retromer complex to recycle back to the plasma membrane. Mutants deficient in the VPS-trimer, *vps-35,* ultimately mis-traffic SMA-6 to the lysosomal compartment (Chapter III). Two color colocalization studies showed that in *vps-35* mutants SMA-6 receptor (SMA-6::GFP) was enriched in the late endosomal compartment (tagRFP::RAB-7). In contrast DAF-4 (type II) is not only independent of retromer, but traffics to the recycling endosome through the ARF-6-dependent pathway. Ultimately, the consequences of these endocytic defects impair Sma/Mab signaling. *arf-6, vps-35* and *rme-1* displayed a 25% reduction in body size. qRT-PCR also showed a decrease in intestinal specific transcript levels and a reduction in RAD/SMAD-reporter. We propose that the spatiotemporal regulation of signaling is orchestrated in part by distinct endocytic sorting complexes

Future directions

II. Identifying the retromer binding motif on the cytoplasmic tail of type 1.

Collectively these experiments (Chapter 3) suggest that there is a cytoplasmic motif on the Type I receptor that directs retromer-dependent sorting. One method that could successfully identify the retromer-specific protein motif on the cytoplasmic tail is the yeast 2-hybrid system (Fields and Song, 1989)**.** To identify the DNA sequence that

codes for the retromer binding motif, successive truncations of the intracellular domain of SMA-6 (type I) can provide the unique opportunity to narrow down the domain that is sufficient to bind the retromer complex.

Alternatively, one can introduce point mutations into cytoplasmic tail of SMA-6 using low fidelity PCR. The truncations and point mutations generated by PCR can be expressed in yeast as fusions to the B42 transcriptional activation domain (prey). VPS-35-26-29 can be expressed individually into the yeast reporter strain as a fusion with the DNA-binding domain of LexA (bait). Interaction between the bait (retromer) and prey can be assayed by complementation of leucine auxotroph [LEU2 Growth Assay]. Taken together, the individual characterization of the VPS trimer can further delineate which member of the complex binds preferentially to the intracellular domain of SMA-6.

Upon isolation of the cytoplasmic retromer-binding motif, co-immunoprecipitation experiments can be preformed to validate the physical interaction with the bacterially expressed VPS-35,-26,-29 trimer (similar to experiments performed in Chapter 3). As proof of principle, one can abolish the interaction by introducing a series of alanine mutations into the cytoplasmic tail the type I receptor and look for loss of binding. I anticipate that these mutations remove the 3D surface features within the cytoplasmic tail that are specific to bind retromer.

Using the power of the CRISPR technology, structure-function analysis can be executed in the worm intestine seamlessly (Paix *et al.*, 2014; Paix *et al.*, 2015; Paix *et al.*, 2016). We can engineer the same point mutations in the binding motif of the endogenous Ce-

SMA-6 (type I) locus. To examine intracellular trafficking defects in vivo we can also introduce a c-terminal GFP at the end of each SMA-6 mutant allele. Two-color colocolization studies with markers specific for different endsomal compartments can help us identify the subcellular localization of these mutant alleles. Confocal microscopy can be used to visualize the intracellular sorting defects that these mutations cause in vivo. I anticipate that perturbations disrupting the retromer binding motif will ultimately miss-sort the SMA-6 (type I) receptor to the lysosome compartment. We can also examine the ability of these mutant receptors to signal by measuring their body size.

Together, these studies have a significant impact on defining the recognition sequences that modulate retromer dependent sorting. Thus far the field has not identified a 'strong' consensus motif that is sufficient for retromer binding (Tabuchi *et al.*, 2010). Mutational analysis of DMT-1-II receptor have identified Øx(Leu/Met)x, which is sufficient to bind retromer [Ø designates any hydrophobic residue and the x represents any amino acid]. As expected disruption of this motif mis-trafficks DMT-1-II to the lysosome. The binding motif WLM of the cation-indpendent mannose-6-phosphate receptor (CI-MPR) (Tabuchi *et al.*, 2010) fits the requirements and sufficient to traffic DMT-1-II. Other established retromer-dependent cargo, sortilin (Tabuchi *et al.*, 2010) and in yeast DPAP-A (Nothwehr *et al.*, 2000), contain motifs that are similar but do not fulfill the binding requirement. One possible explanation for an "elusive' recognitions sequence may lie in the fact that different receptors bind preferentially to the VPS-trimer. The answer may lie in the 3D surface that is displayed on each cytoplasmic tail of each receptor.

Unfortunately, the structural characterization of these known binding motifs remain unclear (Bonifacino and Hurley, 2008; Collins, 2008; Collins *et al.*, 2008). It will be interesting to get a working crystal structure of each receptor motif bound to the VPS-trimer. Careful characterization of the structural features displayed on each structure may help identify a common scaffold, which is sufficient for retromer-dependent recycling

Examining impaired BMP receptor trafficking in mammalian cells.

Our initial findings in the nematode show that endocytic recycling regulators modulate BMP signaling. Primary mouse tumors devoid of BMPR1 impair mammary tumor formation and metastasis (Owens *et al.*, 2012; Owens *et al.*, 2013; Owens *et al.*, 2015). One interesting question is whether impaired recycling on BMP receptors prevent mammary carcinomas and invasion. We hypothesize that impaired recycling of BMPR receptors in the absence of endocytic regulators will inhibit the formation of mammary tumors and metastasis. In addition, direct regulation of BMPR1 trafficking can be tested by engineering mutations that disrupt the retromer-binding motif. I anticipate that mutations in this motif would impair retromer-dependent recycling and misstraffic BMPR1 to late endosomes. Immunoblotting of pSMAD-1,-5 can be used to confirm signaling. Physiologically, primary mammary tumors that harbor the mutant BMPR1 should have delayed growth and wound closure in comparison to wild-type. Taken together, these experiments address conservation and suggest regulators in endocytic trafficking can be used as a potential therapy for breast cancer.

SDPN-1-dependent actin recruitment on early endosomal tubules coordinates exit of cargo destined to the ERC.

Remarkably, the cell has devised effective mechanisms to specialize each transportation route. After internalization, the early endosome is a major focal point for various trafficking decisions that occur throughout the cell (Thompson *et al.*, 2007). The field is only beginning to elucidate the elaborate trafficking network that coordinates the molecular sorting stations on early endosomes. Re-examination *in vivo* reveals that SDPN-1 is part of the early endosomal trafficking machinery that coordinates the exit of cargo destined for the recycling endosome.

In the *C. elegans* intestine, SDPN-1 is not required for the internalization of basolateral cargo. Consequently our mutant analysis enabled us to closely examine SDPN-1's role on various post-internalization trafficking pathways. Upon examination of *sdpn-1* mutants, our results are in agreement with a conserved role in recycling. Specifically, the loss of SDPN-1 fails to display differential requirements for any of the recycling cargos destined for the recycling endosome. Interestingly, the loss of SDPN-1 protein solely affected recycling cargo (hTAC, hTFR and DAF-4) destined to return to the plasma membrane through the recycling endosome. Interestingly, the localization of the degradative, apical, and retromer dependent cargos remained comparable to wild-type animals.

Further, to support a defect in recycling transport, CDE recycling cargo hTFR was found in hybrid organelles positive for early and recycling makers in *sdpn-1* mutant animals.

This observation suggests that loss of SDPN-1 protein results in the retention of recycling cargo in a hybrid compartment composed of early and recycling markers.

If SDPN-1 is indeed responsible for this exit step from the early endosome, one may anticipate an enlargement of RAB-5 positive structures. In agreement with our hypothesis, *sdpn-1* mutants displayed enlarged RAB-5 positive endosomes. This is in line with a role in the biogenesis of membrane tubules from the early endosome compartment. We also observed a redistribution of RME-1 positive recycling endosomes to the medial plane. The accumulation of early endosomes and redistribution of recycling endosomes found in *sdpn-1* animals suggest a role in specializing the early and recycling compartments.

This work further suggest that SDPN-1 mediated recruitment of actin is required for biogenesis of cargo carries on early endosomes. We have recorded an enrichment of filamentous actin on SDPN-1 positive structures. Taken together, our genetic analysis refines SDPN-1's role in endocytic recycling. We report that SDPN-1's residence on early endosomes coordinates the transport of cargo to the recycling endosome. These results support a model wherein membrane deformation requires localized cytoskeletal rearrangements to ensure the biogenesis of cargo carriers. One exciting possibility is that SDPN-1 is coordinating recycling cargo to the same endosomal network that is destined for the recycling endosome. Our results are in agreement with previous reports found in mammalian cell culture systems that suggest diverse recycling cargo meet in

the endosomal system (Naslavsky 2004). Further studies are needed to identify the downstream molecular players that orchestrate SDPN-1 mediated actin polymerization.

Time lapsed regulation of Syndapin/SDPN-1 dependent actin polymerization on early endosomes.

Our studies show that gross accumulations of early endosomes are associated with the loss of actin in *sdpn-1* mutant animals (Chapter II). Actin polymerization helps to pull apart tubules containing recycling endosomes (Chibalina *et al.*, 2007), which is involved in efficient sorting in the early endosome. Lessons from mammalian cell culture report that loss of actin motor, Myosin IV motor trapped hTFR in 'swollen' early endosomes and reduced tubules (Chibalina *et al.*, 2007). Little is known about the intermediates that mature along the recycling pathway. By examining the dynamics of endosomal transport in an intact organism, we can shed light on the molecular underpinnings that coordinate the exit of recycling cargo from the early endosome. Our work suggest that while deforming membranes, SDPN-1 is employing localized burst of actin polymerization on early endosomes to ensure proper exit of tubules carrying material destined for the recycling endosome. Through time-lapsed imaging of animals expressing Lifeact::tagRFP and GFP::RAB-5, we can record SDPN-1 mediated actin dynamics on early endosomal membranes over time. I anticipate that *sdpn-1* mutant animals will delay the release of actin-positive tubules from the early endosome. Such analysis will allow us to record the short-range movement of early endosomes carrying recycling cargo.

SDPN-1 ensures recycling endosome maturation by compartmentalizing early endosomes from mature BREs.

As previously discussed in Chapter I, coincidence detection requires a number of effectors to specialize a local microenvironment on endosomes. On one endosome, distinct subdomains serve as another layer of control to ensure the segregation of cargo into distinct transport routes. Here we show that depletion of SDPN-1 function causes recycling cargo to accumulate in structures of early and recycling endosome markers. We propose that SDPN-1 specializes a distinct subdomain on early endosomes that supports the maturation of RME-1 positive BRE. This is an attractive hypothesis, which requires investigation. An exciting study would be to examine the subcellular localization of RAB-5 and RME-1 positive endosomes in *sdpn-1* mutant animals. Extensive colocalization between RME-1 and RAB-5 is not apparent in wild-type animals. I anticipate that the absence of SDPN-1 will give rise to enlarged endosomal compartment positive for RAB5 and RME-1.

The mosaic distribution and fluidity of each membrane compartment is carried out in part by the activation state of RAB-GTPases. RAB-GTPases are evolutionary conserved monomeric proteins, whose activation state helps to define each compartment along the heterogeneous endosomal network. To ensure the integrity of each endosomal compartment a RAB cascade model helps to explain the unidirectional transport between compartments. Specifically a GTP-bound RAB recruits a guanine exchange factor, GEF, to activate the succeeding RAB GTPase along the transport route. Sequentially the downstream GTP bound RAB recruits a GAP to inactive the earlier acting RAB-GTPase. The mechanistic cues that switch the RAB activation along

recycling network remain elusive. It is speculated that a combinatorial assembly of effectors help to switch an active RAB off and vise versa.

Here we show that loss of RAB-10 function disrupts SDPN-1 recruitment to endosomes. Interestingly, enlarged RAB-5 positive endosomes failed to colocalize to the periphery of the remaining SDPN-1 positive endosomes in *rab-10(RNAi)* animals The correct localization of SDPN-1 to RAB-5 endosomes could represent a subdomain on early endosomes that ensures the dispatch recycling cargo to mature BREs. In agreement with our model, we should witness formation of SDPN-1 positive tubules leaving the early endosome through time-lapsed imaging in wild-type animals expressing tagRFP::RAB-5 and SDPN-1::GFP. As illustrated in steady state conditions, *rab-10* mutants should be devoid of tubules positive for SDPN-1.

Another fundamental requirement that defines each transportation route is the deformation of lipid membranes. The efficacy of the endosomal transportation system is mediated by the dynamic arrangement of membrane domains on endosomes (Sonnichesen 2000). Specifically F-BAR domain proteins are essential players for membrane bending, budding, tubulation, fission, and fusion. Remodeling the lipid membrane is a crucial step that drives synchronized sorting on the early endosome. The global affect on basolateral transmebrane recycling cargo suggests that SDPN-1 may mediate the geometric based sorting of recycling cargo leaving the early endosome. It will be interesting to see if SDPN-1 is capable of tubulating PI(Krystal *et al.*) P liposomes

that are reminiscent of the early endosome *in vitro*. Such experiments will shed light on the molecular underpinnings that define the recycling subdomain on early endosomes.

Acknowledgement of Previous Publications

Ryan J. Gleason, Adenrele M. Akintobi, Barth D. Grant, and Richard W. Padgett, 2014. BMP signaling requires retromer-depdendent recycling of the type I receptor. *Proc. Natl, Acad. Sci* 11, 2578-2583

Bibliography

Ahmed, S., Bu, W., Lee, R.T., Maurer-Stroh, S., and Goh, W.I. (2010). F-BAR domain proteins: Families and function. Commun Integr Biol *3*, 116-121.

Anggono, V., Smillie, K.J., Graham, M.E., Valova, V.A., Cousin, M.A., and Robinson, P.J. (2006). Syndapin I is the phosphorylation-regulated dynamin I partner in synaptic vesicle endocytosis. Nat Neurosci *9*, 752-760.

Arighi, C.N., Hartnell, L.M., Aguilar, R.C., Haft, C.R., and Bonifacino, J.S. (2004). Role of the mammalian retromer in sorting of the cation-independent mannose 6-phosphate receptor. J Cell Biol *165*, 123-133.

Bashkirov, P.V., Akimov, S.A., Evseev, A.I., Schmid, S.L., Zimmerberg, J., and Frolov, V.A. (2008). GTPase cycle of dynamin is coupled to membrane squeeze and release, leading to spontaneous fission. Cell *135*, 1276-1286.

Bauer, F., Urdaci, M., Aigle, M., and Crouzet, M. (1993). Alteration of a yeast SH3 protein leads to conditional viability with defects in cytoskeletal and budding patterns. Mol Cell Biol *13*, 5070-5084.

Beramendi, A., Peron, S., Casanova, G., Reggiani, C., and Cantera, R. (2007). Neuromuscular junction in abdominal muscles of Drosophila melanogaster during adulthood and aging. J Comp Neurol *501*, 498-508.

Bonifacino, J.S., and Hurley, J.H. (2008). Retromer. Curr Opin Cell Biol *20*, 427-436.

Braun, A., Pinyol, R., Dahlhaus, R., Koch, D., Fonarev, P., Grant, B.D., Kessels, M.M., and Qualmann, B. (2005). EHD proteins associate with syndapin I and II and such interactions play a crucial role in endosomal recycling. Mol Biol Cell *16*, 3642-3658.

Brenner, S. (1974). The genetics of Caenorhabditis elegans. Genetics *77*, 71-94.

Burke, P., Schooler, K., and Wiley, H.S. (2001). Regulation of epidermal growth factor receptor signaling by endocytosis and intracellular trafficking. Mol Biol Cell *12*, 1897-1910.

Caplan, S., Naslavsky, N., Hartnell, L.M., Lodge, R., Polishchuk, R.S., Donaldson, J.G., and Bonifacino, J.S. (2002). A tubular EHD1-containing compartment involved in the recycling of major histocompatibility complex class I molecules to the plasma membrane. EMBO J *21*, 2557-2567.

Cereijido, M., Robbins, E.S., Dolan, W.J., Rotunno, C.A., and Sabatini, D.D. (1978). Polarized monolayers formed by epithelial cells on a permeable and translucent support. J Cell Biol *77*, 853-880.

Chen, C.C., Schweinsberg, P.J., Vashist, S., Mareiniss, D.P., Lambie, E.J., and Grant, B.D. (2006). RAB-10 is required for endocytic recycling in the Caenorhabditis elegans intestine. Mol Biol Cell *17*, 1286-1297.

Chen, C.L., Hou, W.H., Liu, I.H., Hsiao, G., Huang, S.S., and Huang, J.S. (2009). Inhibitors of clathrin-dependent endocytosis enhance TGFbeta signaling and responses. J Cell Sci *122*, 1863-1871.

Chen, M.S., Burgess, C.C., Vallee, R.B., and Wadsworth, S.C. (1992). Developmental stage- and tissue-specific expression of shibire, a Drosophila gene involved in endocytosis. J Cell Sci *103 (Pt 3)*, 619-628.

Chen, M.S., Obar, R.A., Schroeder, C.C., Austin, T.W., Poodry, C.A., Wadsworth, S.C., and Vallee, R.B. (1991). Multiple forms of dynamin are encoded by shibire, a Drosophila gene involved in endocytosis. Nature *351*, 583-586.

Chibalina, M.V., Seaman, M.N., Miller, C.C., Kendrick-Jones, J., and Buss, F. (2007). Myosin VI and its interacting protein LMTK2 regulate tubule formation and transport to the endocytic recycling compartment. J Cell Sci *120*, 4278-4288.
Collins, B.M. (2008). The structure and function of the retromer protein complex. Traffic *9*, 1811-1822.
Collins, B.M., Norwood, S.J., Kerr, M.C., Mahony, D., Seaman, M.N., Teasdale, R.D., and Owen, D.J. (2008). Structure of Vps26B and mapping of its interaction with the retromer protein complex. Traffic *9*, 366-379.
Cullen, P.J. (2008). Endosomal sorting and signalling: an emerging role for sorting nexins. Nat Rev Mol Cell Biol *9*, 574-582.
Da Costa, S.R., Sou, E., Xie, J., Yarber, F.A., Okamoto, C.T., Pidgeon, M., Kessels, M.M., Mircheff, A.K., Schechter, J.E., Qualmann, B., and Hamm-Alvarez, S.F. (2003). Impairing actin filament or syndapin functions promotes accumulation of clathrin-coated vesicles at the apical plasma membrane of acinar epithelial cells. Mol Biol Cell *14*, 4397-4413.
Danino, D., and Hinshaw, J.E. (2001). Dynamin family of mechanoenzymes. Curr Opin Cell Biol *13*, 454-460.
Danino, D., Moon, K.H., and Hinshaw, J.E. (2004). Rapid constriction of lipid bilayers by the mechanochemical enzyme dynamin. J Struct Biol *147*, 259-267.
Daumke, O., Lundmark, R., Vallis, Y., Martens, S., Butler, P.J., and McMahon, H.T. (2007). Architectural and mechanistic insights into an EHD ATPase involved in membrane remodelling. Nature *449*, 923-927.
Dawson, J.C., Legg, J.A., and Machesky, L.M. (2006). Bar domain proteins: a role in tubulation, scission and actin assembly in clathrin-mediated endocytosis. Trends Cell Biol *16*, 493-498.
Dharmalingam, E., Haeckel, A., Pinyol, R., Schwintzer, L., Koch, D., Kessels, M.M., and Qualmann, B. (2009). F-BAR proteins of the syndapin family shape the plasma membrane and are crucial for neuromorphogenesis. J Neurosci *29*, 13315-13327.
Di Guglielmo, G.M., Le Roy, C., Goodfellow, A.F., and Wrana, J.L. (2003). Distinct endocytic pathways regulate TGF-beta receptor signalling and turnover. Nat Cell Biol *5*, 410-421.
Doherty, G., and McMahon, H. (2009). Mechanisms of endocytosis. Annual review of biochemistry.
Ferguson, S.M., Raimondi, A., Paradise, S., Shen, H., Mesaki, K., Ferguson, A., Destaing, O., Ko, G., Takasaki, J., Cremona, O., E, O.T., and De Camilli, P. (2009). Coordinated actions of actin and BAR proteins upstream of dynamin at endocytic clathrin-coated pits. Dev Cell *17*, 811-822.
Fields, S., and Song, O. (1989). A novel genetic system to detect protein-protein interactions. Nature *340*, 245-246.
Frost, A., De Camilli, P., and Unger, V.M. (2007). F-BAR proteins join the BAR family fold. Structure *15*, 751-753.
Gallop, J.L., and McMahon, H.T. (2005). BAR domains and membrane curvature: bringing your curves to the BAR. Biochem Soc Symp, 223-231.
Gedamu, E.L., Collins, D.L., and Arnold, D.L. (2008). Automated quality control of brain MR images. J Magn Reson Imaging *28*, 308-319.
Gesbert, F., Sauvonnet, N., and Dautry-Varsat, A. (2004). Clathrin-Independent endocytosis and signalling of interleukin 2 receptors IL-2R endocytosis and signalling. Curr Top Microbiol Immunol *286*, 119-148.

Giridharan, S.S., Cai, B., Vitale, N., Naslavsky, N., and Caplan, S. (2013). Cooperation of MICAL-L1, syndapin2, and phosphatidic acid in tubular recycling endosome biogenesis. Mol Biol Cell *24*, 1776-1790, S1771-1715.

Gleason, R.J., Akintobi, A.M., Grant, B.D., and Padgett, R.W. (2014). BMP signaling requires retromer-dependent recycling of the type I receptor. Proc Natl Acad Sci U S A *111*, 2578-2583.

Gokool, S., Tattersall, D., and Seaman, M.N. (2007). EHD1 interacts with retromer to stabilize SNX1 tubules and facilitate endosome-to-Golgi retrieval. Traffic *8*, 1873-1886.

Grant, B., Zhang, Y., Paupard, M.C., Lin, S.X., Hall, D.H., and Hirsh, D. (2001). Evidence that RME-1, a conserved C. elegans EH-domain protein, functions in endocytic recycling. Nat Cell Biol *3*, 573-579.

Grant, B.D., and Caplan, S. (2008). Mechanisms of EHD/RME-1 protein function in endocytic transport. Traffic *9*, 2043-2052.

Grant, B.D., and Donaldson, J.G. (2009). Pathways and mechanisms of endocytic recycling. Nat Rev Mol Cell Biol *10*, 597-608.

Gu, M., Liu, Q., Watanabe, S., Sun, L., Hollopeter, G., Grant, B.D., and Jorgensen, E.M. (2013). AP2 hemicomplexes contribute independently to synaptic vesicle endocytosis. Elife *2*, e00190.

Hanyaloglu, A.C., and von Zastrow, M. (2008). Regulation of GPCRs by endocytic membrane trafficking and its potential implications. Annu Rev Pharmacol Toxicol *48*, 537-568.

Harterink, M., Port, F., Lorenowicz, M.J., McGough, I.J., Silhankova, M., Betist, M.C., van Weering, J.R., van Heesbeen, R.G., Middelkoop, T.C., Basler, K., Cullen, P.J., and Korswagen, H.C. (2011). A SNX3-dependent retromer pathway mediates retrograde transport of the Wnt sorting receptor Wntless and is required for Wnt secretion. Nat Cell Biol *13*, 914-923.

Hartung, A., Bitton-Worms, K., Rechtman, M.M., Wenzel, V., Boergermann, J.H., Hassel, S., Henis, Y.I., and Knaus, P. (2006). Different routes of bone morphogenic protein (BMP) receptor endocytosis influence BMP signaling. Mol Cell Biol *26*, 7791-7805.

Huminiecki, L., Goldovsky, L., Freilich, S., Moustakas, A., Ouzounis, C., and Heldin, C.H. (2009). Emergence, development and diversification of the TGF-beta signalling pathway within the animal kingdom. BMC Evol Biol *9*, 28.

Itoh, T., Erdmann, K.S., Roux, A., Habermann, B., Werner, H., and De Camilli, P. (2005). Dynamin and the actin cytoskeleton cooperatively regulate plasma membrane invagination by BAR and F-BAR proteins. Dev Cell *9*, 791-804.

Jović, M., Kieken, F., Naslavsky, N., Sorgen, P.L., and Caplan, S. (2009). Eps15 homology domain 1-associated tubules contain phosphatidylinositol-4-phosphate and phosphatidylinositol-(4,5)-bisphosphate and are required for efficient recycling. Mol Biol Cell *20*, 2731-2743.

Kaksonen, M., Sun, Y., and Drubin, D.G. (2003). A pathway for association of receptors, adaptors, and actin during endocytic internalization. Cell *115*, 475-487.

Kamath, R.S., and Ahringer, J. (2003). Genome-wide RNAi screening in Caenorhabditis elegans. Methods *30*, 313-321.

Kessels, M., and Qualmann, B. (2002a). Syndapins integrate N-WASP in receptor-mediated endocytosis. The EMBO Journal.

Kessels, M., and Qualmann, B. (2004a). The syndapin protein family: linking membrane trafficking with the cytoskeleton. Journal of cell science.

Kessels, M., and Qualmann, B. (2006a). Syndapin oligomers interconnect the machineries for endocytic vesicle formation and actin polymerization. Journal of Biological Chemistry.
Kessels, M.M., and Qualmann, B. (2002b). Syndapins integrate N-WASP in receptor-mediated endocytosis. EMBO J *21*, 6083-6094.
Kessels, M.M., and Qualmann, B. (2004b). The syndapin protein family: linking membrane trafficking with the cytoskeleton. J Cell Sci *117*, 3077-3086.
Kessels, M.M., and Qualmann, B. (2006b). Syndapin oligomers interconnect the machineries for endocytic vesicle formation and actin polymerization. J Biol Chem *281*, 13285-13299.
Koli, K.M., and Arteaga, C.L. (1997). Processing of the transforming growth factor beta type I and II receptors. Biosynthesis and ligand-induced regulation. J Biol Chem *272*, 6423-6427.
Korolchuk, V.I., Schutz, M.M., Gomez-Llorente, C., Rocha, J., Lansu, N.R., Collins, S.M., Wairkar, Y.P., Robinson, I.M., and O'Kane, C.J. (2007). Drosophila Vps35 function is necessary for normal endocytic trafficking and actin cytoskeleton organisation. J Cell Sci *120*, 4367-4376.
Krystal, J.H., Gueorguieva, R., Cramer, J., Collins, J., Rosenheck, R., and Team, V.C.N.S. (2008). Naltrexone is associated with reduced drinking by alcohol dependent patients receiving antidepressants for mood and anxiety symptoms: results from VA Cooperative Study No. 425, "Naltrexone in the treatment of alcoholism". Alcohol Clin Exp Res *32*, 85-91.
Kurz, C.L., and Tan, M.W. (2004). Regulation of aging and innate immunity in C. elegans. Aging Cell *3*, 185-193.
Leung, B., Hermann, G., and Priess, J. (1999a). Organogenesis of the Caenorhabditis elegans intestine. Dev Biol.
Leung, B., Hermann, G.J., and Priess, J.R. (1999b). Organogenesis of the Caenorhabditis elegans intestine. Dev Biol *216*, 114-134.
Lin, S., Grant, B., Hirsh, D., and Maxfield, F. (2001a). Rme-1 regulates the distribution and function of the endocytic recycling …. Nature cell biology.
Lin, S.X., Grant, B., Hirsh, D., and Maxfield, F.R. (2001b). Rme-1 regulates the distribution and function of the endocytic recycling compartment in mammalian cells. Nat Cell Biol *3*, 567-572.
Liu, O., and Grant, B.D. (2015). Basolateral Endocytic Recycling Requires RAB-10 and AMPH-1 Mediated Recruitment of RAB-5 GAP TBC-2 to Endosomes. PLoS Genet *11*, e1005514.
Marks, B., Stowell, M.H., Vallis, Y., Mills, I.G., Gibson, A., Hopkins, C.R., and McMahon, H.T. (2001). GTPase activity of dynamin and resulting conformation change are essential for endocytosis. Nature *410*, 231-235.
Massague, J. (2000). How cells read TGF-beta signals. Nat Rev Mol Cell Biol *1*, 169-178.
Massague, J., and Chen, Y.G. (2000). Controlling TGF-beta signaling. Genes Dev *14*, 627-644.
Maxfield, F., and McGraw, T. (2004a). Endocytic recycling. Nat Rev Mol Cell Biol.
Maxfield, F.R., and McGraw, T.E. (2004b). Endocytic recycling. Nat Rev Mol Cell Biol *5*, 121-132.
McGhee, J.D. (2007). The C. elegans intestine. WormBook, 1-36.
McMahon, H.T., and Gallop, J.L. (2005). Membrane curvature and mechanisms of dynamic cell membrane remodelling. Nature *438*, 590-596.

Mello, C., and Fire, A. (1995). DNA transformation. Methods Cell Biol *48*, 451-482.
Meng, H., Tian, L., Zhou, J., Li, Z., Jiao, X., Li, W.W., Plomann, M., Xu, Z., Lisanti, M.P., Wang, C., and Pestell, R.G. (2011). PACSIN 2 represses cellular migration through direct association with cyclin D1 but not its alternate splice form cyclin D1b. Cell Cycle *10*, 73-81.
Merrifield, C.J. (2004). Seeing is believing: imaging actin dynamics at single sites of endocytosis. Trends Cell Biol *14*, 352-358.
Merrifield, C.J., Feldman, M.E., Wan, L., and Almers, W. (2002). Imaging actin and dynamin recruitment during invagination of single clathrin-coated pits. Nat Cell Biol *4*, 691-698.
Merrifield, C.J., Perrais, D., and Zenisek, D. (2005). Coupling between clathrin-coated-pit invagination, cortactin recruitment, and membrane scission observed in live cells. Cell *121*, 593-606.
Miaczynska, M., Pelkmans, L., and Zerial, M. (2004). Not just a sink: endosomes in control of signal transduction. Curr Opin Cell Biol *16*, 400-406.
Misfeldt, D.S., Hamamoto, S.T., and Pitelka, D.R. (1976). Transepithelial transport in cell culture. Proc Natl Acad Sci U S A *73*, 1212-1216.
Mitchell, H., Choudhury, A., Pagano, R.E., and Leof, E.B. (2004). Ligand-dependent and -independent transforming growth factor-beta receptor recycling regulated by clathrin-mediated endocytosis and Rab11. Mol Biol Cell *15*, 4166-4178.
Mochii, M., Yoshida, S., Morita, K., Kohara, Y., and Ueno, N. (1999). Identification of transforming growth factor-beta- regulated genes in caenorhabditis elegans by differential hybridization of arrayed cDNAs. Proc Natl Acad Sci U S A *96*, 15020-15025.
Modregger, J., Ritter, B., Witter, B., Paulsson, M., and Plomann, M. (2000). All three PACSIN isoforms bind to endocytic proteins and inhibit endocytosis. J Cell Sci *113 Pt 24*, 4511-4521.
Naslavsky, N., Boehm, M., Backlund, P.S., Jr., and Caplan, S. (2004). Rabenosyn-5 and EHD1 interact and sequentially regulate protein recycling to the plasma membrane. Mol Biol Cell *15*, 2410-2422.
Naslavsky, N., McKenzie, J., Altan-Bonnet, N., Sheff, D., and Caplan, S. (2009). EHD3 regulates early-endosome-to-Golgi transport and preserves Golgi morphology. J Cell Sci *122*, 389-400.
Nicholas, H.R., and Hodgkin, J. (2004). Responses to infection and possible recognition strategies in the innate immune system of Caenorhabditis elegans. Mol Immunol *41*, 479-493.
Nothwehr, S.F., Ha, S.A., and Bruinsma, P. (2000). Sorting of yeast membrane proteins into an endosome-to-Golgi pathway involves direct interaction of their cytosolic domains with Vps35p. J Cell Biol *151*, 297-310.
Owens, P., Pickup, M.W., Novitskiy, S.V., Chytil, A., Gorska, A.E., Aakre, M.E., West, J., and Moses, H.L. (2012). Disruption of bone morphogenetic protein receptor 2 (BMPR2) in mammary tumors promotes metastases through cell autonomous and paracrine mediators. Proc Natl Acad Sci U S A *109*, 2814-2819.
Owens, P., Pickup, M.W., Novitskiy, S.V., Giltnane, J.M., Gorska, A.E., Hopkins, C.R., Hong, C.C., and Moses, H.L. (2015). Inhibition of BMP signaling suppresses metastasis in mammary cancer. Oncogene *34*, 2437-2449.
Owens, P., Polikowsky, H., Pickup, M.W., Gorska, A.E., Jovanovic, B., Shaw, A.K., Novitskiy, S.V., Hong, C.C., and Moses, H.L. (2013). Bone Morphogenetic

Proteins stimulate mammary fibroblasts to promote mammary carcinoma cell invasion. PLoS One *8*, e67533.

Paix, A., Folkmann, A., Rasoloson, D., and Seydoux, G. (2015). High Efficiency, Homology-Directed Genome Editing in Caenorhabditis elegans Using CRISPR-Cas9 Ribonucleoprotein Complexes. Genetics *201*, 47-54.

Paix, A., Schmidt, H., and Seydoux, G. (2016). Cas9-assisted recombineering in C. elegans: genome editing using in vivo assembly of linear DNAs. Nucleic Acids Res.

Paix, A., Wang, Y., Smith, H.E., Lee, C.Y., Calidas, D., Lu, T., Smith, J., Schmidt, H., Krause, M.W., and Seydoux, G. (2014). Scalable and versatile genome editing using linear DNAs with microhomology to Cas9 Sites in Caenorhabditis elegans. Genetics *198*, 1347-1356.

Pant, S., Sharma, M., Patel, K., Caplan, S., Carr, C.M., and Grant, B.D. (2009). AMPH-1/Amphiphysin/Bin1 functions with RME-1/Ehd1 in endocytic recycling. Nat Cell Biol *11*, 1399-1410.

Patterson, G.I., Koweek, A., Wong, A., Liu, Y., and Ruvkun, G. (1997). The DAF-3 Smad protein antagonizes TGF-beta-related receptor signaling in the Caenorhabditis elegans dauer pathway. Genes Dev *11*, 2679-2690.

Patterson, G.I., and Padgett, R.W. (2000). TGF beta-related pathways. Roles in Caenorhabditis elegans development. Trends Genet *16*, 27-33.

Penheiter, S.G., Singh, R.D., Repellin, C.E., Wilkes, M.C., Edens, M., Howe, P.H., Pagano, R.E., and Leof, E.B. (2010). Type II transforming growth factor-beta receptor recycling is dependent upon the clathrin adaptor protein Dab2. Mol Biol Cell *21*, 4009-4019.

Peter, B.J., Kent, H.M., Mills, I.G., Vallis, Y., Butler, P.J., Evans, P.R., and McMahon, H.T. (2004). BAR domains as sensors of membrane curvature: the amphiphysin BAR structure. Science *303*, 495-499.

Praitis, V., Casey, E., Collar, D., and Austin, J. (2001). Creation of low-copy integrated transgenic lines in Caenorhabditis elegans. Genetics *157*, 1217-1226.

Praitis, V., and Maduro, M.F. (2011). Transgenesis in C. elegans. Methods Cell Biol *106*, 161-185.

Prokopenko, I., Langenberg, C., Florez, J.C., Saxena, R., Soranzo, N., Thorleifsson, G., Loos, R.J., Manning, A.K., Jackson, A.U., Aulchenko, Y., Potter, S.C., Erdos, M.R., Sanna, S., Hottenga, J.J., Wheeler, E., Kaakinen, M., Lyssenko, V., Chen, W.M., Ahmadi, K., Beckmann, J.S., Bergman, R.N., Bochud, M., Bonnycastle, L.L., Buchanan, T.A., Cao, A., Cervino, A., Coin, L., Collins, F.S., Crisponi, L., de Geus, E.J., Dehghan, A., Deloukas, P., Doney, A.S., Elliott, P., Freimer, N., Gateva, V., Herder, C., Hofman, A., Hughes, T.E., Hunt, S., Illig, T., Inouye, M., Isomaa, B., Johnson, T., Kong, A., Krestyaninova, M., Kuusisto, J., Laakso, M., Lim, N., Lindblad, U., Lindgren, C.M., McCann, O.T., Mohlke, K.L., Morris, A.D., Naitza, S., Orru, M., Palmer, C.N., Pouta, A., Randall, J., Rathmann, W., Saramies, J., Scheet, P., Scott, L.J., Scuteri, A., Sharp, S., Sijbrands, E., Smit, J.H., Song, K., Steinthorsdottir, V., Stringham, H.M., Tuomi, T., Tuomilehto, J., Uitterlinden, A.G., Voight, B.F., Waterworth, D., Wichmann, H.E., Willemsen, G., Witteman, J.C., Yuan, X., Zhao, J.H., Zeggini, E., Schlessinger, D., Sandhu, M., Boomsma, D.I., Uda, M., Spector, T.D., Penninx, B.W., Altshuler, D., Vollenweider, P., Jarvelin, M.R., Lakatta, E., Waeber, G., Fox, C.S., Peltonen, L., Groop, L.C., Mooser, V., Cupples, L.A., Thorsteinsdottir, U., Boehnke, M., Barroso, I., Van Duijn, C., Dupuis, J., Watanabe, R.M., Stefansson, K.,

McCarthy, M.I., Wareham, N.J., Meigs, J.B., and Abecasis, G.R. (2009). Variants in MTNR1B influence fasting glucose levels. Nat Genet *41*, 77-81.

Pucadyil, T.J., and Schmid, S.L. (2008). Real-time visualization of dynamin-catalyzed membrane fission and vesicle release. Cell *135*, 1263-1275.

Pucadyil, T.J., and Schmid, S.L. (2009). Conserved functions of membrane active GTPases in coated vesicle formation. Science *325*, 1217-1220.

Puthenveedu, M.A., Lauffer, B., Temkin, P., Vistein, R., Carlton, P., Thorn, K., Taunton, J., Weiner, O.D., Parton, R.G., and von Zastrow, M. (2010). Sequence-dependent sorting of recycling proteins by actin-stabilized endosomal microdomains. Cell *143*, 761-773.

Qualmann, B., and Kelly, R.B. (2000). Syndapin isoforms participate in receptor-mediated endocytosis and actin organization. J Cell Biol *148*, 1047-1062.

Qualmann, B., Roos, J., DiGregorio, P.J., and Kelly, R.B. (1999). Syndapin I, a synaptic dynamin-binding protein that associates with the neural Wiskott-Aldrich syndrome protein. Mol Biol Cell *10*, 501-513.

Radhakrishna, H., and Donaldson, J.G. (1997). ADP-ribosylation factor 6 regulates a novel plasma membrane recycling pathway. J Cell Biol *139*, 49-61.

Rao, Y., Ma, Q., Vahedi-Faridi, A., Sundborger, A., Pechstein, A., Puchkov, D., Luo, L., Shupliakov, O., Saenger, W., and Haucke, V. (2010). Molecular basis for SH3 domain regulation of F-BAR-mediated membrane deformation. Proc Natl Acad Sci U S A *107*, 8213-8218.

Ritter, B., Modregger, J., Paulsson, M., and Plomann, M. (1999). PACSIN 2, a novel member of the PACSIN family of cytoplasmic adapter proteins. FEBS Lett *454*, 356-362.

Roach, W., and Plomann, M. (2007). PACSIN3 overexpression increases adipocyte glucose transport through GLUT1. Biochem Biophys Res Commun *355*, 745-750.

Roberts, A.F., Gumienny, T.L., Gleason, R.J., Wang, H., and Padgett, R.W. (2010). Regulation of genes affecting body size and innate immunity by the DBL-1/BMP-like pathway in Caenorhabditis elegans. BMC Dev Biol *10*, 61.

Rodriguez Boulan, E., and Sabatini, D.D. (1978). Asymmetric budding of viruses in epithelial monlayers: a model system for study of epithelial polarity. Proc Natl Acad Sci U S A *75*, 5071-5075.

Rodriguez-Boulan, E., and Powell, S.K. (1992). Polarity of epithelial and neuronal cells. Annu Rev Cell Biol *8*, 395-427.

Romer, W., Pontani, L.L., Sorre, B., Rentero, C., Berland, L., Chambon, V., Lamaze, C., Bassereau, P., Sykes, C., Gaus, K., and Johannes, L. (2010). Actin dynamics drive membrane reorganization and scission in clathrin-independent endocytosis. Cell *140*, 540-553.

Sato, K., Norris, A., Sato, M., and Grant, B.D. (2014). C. elegans as a model for membrane traffic. WormBook, 1-47.

Savage, C., Das, P., Finelli, A.L., Townsend, S.R., Sun, C.Y., Baird, S.E., and Padgett, R.W. (1996). Caenorhabditis elegans genes sma-2, sma-3, and sma-4 define a conserved family of transforming growth factor beta pathway components. Proc Natl Acad Sci U S A *93*, 790-794.

Savage-Dunn, C., Maduzia, L.L., Zimmerman, C.M., Roberts, A.F., Cohen, S., Tokarz, R., and Padgett, R.W. (2003). Genetic screen for small body size mutants in C. elegans reveals many TGFbeta pathway components. Genesis *35*, 239-247.

Schindelin, J., Arganda-Carreras, I., Frise, E., Kaynig, V., Longair, M., Pietzsch, T., Preibisch, S., Rueden, C., Saalfeld, S., Schmid, B., Tinevez, J.Y., White, D.J.,

Hartenstein, V., Eliceiri, K., Tomancak, P., and Cardona, A. (2012). Fiji: an open-source platform for biological-image analysis. Nat Methods *9*, 676-682.

Scita, G., and Di Fiore, P.P. (2010). The endocytic matrix. Nature *463*, 464-473.

Sever, S., Damke, H., and Schmid, S.L. (2000). Dynamin:GTP controls the formation of constricted coated pits, the rate limiting step in clathrin-mediated endocytosis. J Cell Biol *150*, 1137-1148.

Sherlekar, A., and Rikhy, R. (2016). Syndapin promotes pseudocleavage furrow formation by actin organization in the syncytial Drosophila embryo. Mol Biol Cell *27*, 2064-2079.

Shi, A., Chen, C.C., Banerjee, R., Glodowski, D., Audhya, A., Rongo, C., and Grant, B.D. (2010). EHBP-1 functions with RAB-10 during endocytic recycling in Caenorhabditis elegans. Mol Biol Cell *21*, 2930-2943.

Shi, A., Liu, O., Koenig, S., Banerjee, R., Chen, C.C., Eimer, S., and Grant, B.D. (2012). RAB-10-GTPase-mediated regulation of endosomal phosphatidylinositol-4,5-bisphosphate. Proc Natl Acad Sci U S A *109*, E2306-2315.

Shi, A., Pant, S., Balklava, Z., Chen, C.C., Figueroa, V., and Grant, B.D. (2007). A novel requirement for C. elegans Alix/ALX-1 in RME-1-mediated membrane transport. Curr Biol *17*, 1913-1924.

Shi, A., Sun, L., Banerjee, R., Tobin, M., Zhang, Y., and Grant, B.D. (2009). Regulation of endosomal clathrin and retromer-mediated endosome to Golgi retrograde transport by the J-domain protein RME-8. EMBO J *28*, 3290-3302.

Shimada, A., Niwa, H., Tsujita, K., Suetsugu, S., Nitta, K., Hanawa-Suetsugu, K., Akasaka, R., Nishino, Y., Toyama, M., Chen, L., Liu, Z.J., Wang, B.C., Yamamoto, M., Terada, T., Miyazawa, A., Tanaka, A., Sugano, S., Shirouzu, M., Nagayama, K., Takenawa, T., and Yokoyama, S. (2007). Curved EFC/F-BAR-domain dimers are joined end to end into a filament for membrane invagination in endocytosis. Cell *129*, 761-772.

Steinberg, F., Gallon, M., Winfield, M., Thomas, E.C., Bell, A.J., Heesom, K.J., Tavare, J.M., and Cullen, P.J. (2013). A global analysis of SNX27-retromer assembly and cargo specificity reveals a function in glucose and metal ion transport. Nat Cell Biol *15*, 461-471.

Stowell, M.H., Marks, B., Wigge, P., and McMahon, H.T. (1999). Nucleotide-dependent conformational changes in dynamin: evidence for a mechanochemical molecular spring. Nat Cell Biol *1*, 27-32.

Sun, L., Liu, O., Desai, J., Karbassi, F., Sylvain, M.A., Shi, A., Zhou, Z., Rocheleau, C.E., and Grant, B.D. (2012). CED-10/Rac1 regulates endocytic recycling through the RAB-5 GAP TBC-2. PLoS Genet *8*, e1002785.

Sweitzer, S.M., and Hinshaw, J.E. (1998). Dynamin undergoes a GTP-dependent conformational change causing vesiculation. Cell *93*, 1021-1029.

Tabuchi, M., Yanatori, I., Kawai, Y., and Kishi, F. (2010). Retromer-mediated direct sorting is required for proper endosomal recycling of the mammalian iron transporter DMT1. J Cell Sci *123*, 756-766.

Takeda, T., Robinson, I.M., Savoian, M.M., Griffiths, J.R., Whetton, A.D., McMahon, H.T., and Glover, D.M. (2013). Drosophila F-BAR protein Syndapin contributes to coupling the plasma membrane and contractile ring in cytokinesis. Open Biol *3*, 130081.

Takei, K., McPherson, P.S., Schmid, S.L., and De Camilli, P. (1995). Tubular membrane invaginations coated by dynamin rings are induced by GTP-gamma S in nerve terminals. Nature *374*, 186-190.

Takei, K., Slepnev, V.I., Haucke, V., and De Camilli, P. (1999). Functional partnership between amphiphysin and dynamin in clathrin-mediated endocytosis. Nat Cell Biol *1*, 33-39.

Temkin, P., Lauffer, B., Jager, S., Cimermancic, P., Krogan, N.J., and von Zastrow, M. (2011). SNX27 mediates retromer tubule entry and endosome-to-plasma membrane trafficking of signalling receptors. Nat Cell Biol *13*, 715-721.

Thompson, A., Nessler, R., Wisco, D., Anderson, E., Winckler, B., and Sheff, D. (2007). Recycling endosomes of polarized epithelial cells actively sort apical and basolateral cargos into separate subdomains. Mol Biol Cell *18*, 2687-2697.

Tian, C., Sen, D., Shi, H., Foehr, M.L., Plavskin, Y., Vatamaniuk, O.K., and Liu, J. (2010). The RGM protein DRAG-1 positively regulates a BMP-like signaling pathway in Caenorhabditis elegans. Development *137*, 2375-2384.

Timmons, L., and Fire, A. (1998). Specific interference by ingested dsRNA. Nature *395*, 854.

Treusch, S., Knuth, S., Slaugenhaupt, S.A., Goldin, E., Grant, B.D., and Fares, H. (2004). Caenorhabditis elegans functional orthologue of human protein h-mucolipin-1 is required for lysosome biogenesis. Proc Natl Acad Sci U S A *101*, 4483-4488.

Wakefield, L.M., and Hill, C.S. (2013). Beyond TGFbeta: roles of other TGFbeta superfamily members in cancer. Nat Rev Cancer *13*, 328-341.

Wang, J., Tokarz, R., and Savage-Dunn, C. (2002). The expression of TGFbeta signal transducers in the hypodermis regulates body size in C. elegans. Development *129*, 4989-4998.

Wang, Q., Navarro, M.V., Peng, G., Molinelli, E., Goh, S.L., Judson, B.L., Rajashankar, K.R., and Sondermann, H. (2009). Molecular mechanism of membrane constriction and tubulation mediated by the F-BAR protein Pacsin/Syndapin. Proc Natl Acad Sci U S A *106*, 12700-12705.

Wells, R.G., Yankelev, H., Lin, H.Y., and Lodish, H.F. (1997). Biosynthesis of the type I and type II TGF-beta receptors. Implications for complex formation. J Biol Chem *272*, 11444-11451.

Wu, M., Huang, B., Graham, M., Raimondi, A., Heuser, J.E., Zhuang, X., and De Camilli, P. (2010). Coupling between clathrin-dependent endocytic budding and F-BAR-dependent tubulation in a cell-free system. Nat Cell Biol *12*, 902-908.

Yamada, H., Padilla-Parra, S., Park, S.J., Itoh, T., Chaineau, M., Monaldi, I., Cremona, O., Benfenati, F., De Camilli, P., Coppey-Moisan, M., Tramier, M., Galli, T., and Takei, K. (2009). Dynamic interaction of amphiphysin with N-WASP regulates actin assembly. J Biol Chem *284*, 34244-34256.

Yang, P.T., Lorenowicz, M.J., Silhankova, M., Coudreuse, D.Y., Betist, M.C., and Korswagen, H.C. (2008). Wnt signaling requires retromer-dependent recycling of MIG-14/Wntless in Wnt-producing cells. Dev Cell *14*, 140-147.

Yao, D., Ehrlich, M., Henis, Y.I., and Leof, E.B. (2002). Transforming growth factor-beta receptors interact with AP2 by direct binding to beta2 subunit. Mol Biol Cell *13*, 4001-4012.

Yin, X., Murphy, S.J., Wilkes, M.C., Ji, Y., and Leof, E.B. (2013). Retromer maintains basolateral distribution of the type II TGF-beta receptor via the recycling endosome. Mol Biol Cell *24*, 2285-2298.

Zhang, P., Wu, Y., Belenkaya, T.Y., and Lin, X. (2011). SNX3 controls Wingless/Wnt secretion through regulating retromer-dependent recycling of Wntless. Cell Res *21*, 1677-1690.

Zhang, X., and Zhang, Y. (2012). DBL-1, a TGF-beta, is essential for Caenorhabditis elegans aversive olfactory learning. Proc Natl Acad Sci U S A *109*, 17081-17086.
Zwaagstra, J.C., El-Alfy, M., and O'Connor-McCourt, M.D. (2001). Transforming growth factor (TGF)-beta 1 internalization: modulation by ligand interaction with TGF-beta receptors types I and II and a mechanism that is distinct from clathrin-mediated endocytosis. J Biol Chem *276*, 27237-27245.